1-1-2013

Maximizing Resource Utilization In Video Streaming Systems

Mohammad A. Alsmirat
Wayne State University,

MAXIMIZING RESOURCE UTILIZATION IN VIDEO STREAMING SYSTEMS

by

MOHAMMAD ABDULLAH ALSMIRAT

DISSERTATION

Submitted to the Graduate School

of Wayne State University,

Detroit, Michigan

in partial fulfillment of the requirements

for the degree of

DOCTOR OF PHILOSOPHY

2013

MAJOR: COMPUTER ENGINEERING

Approved by:

_____

Advisor Date

_____

_____

_____

_____

ACKNOWLEDGMENTS

I have taken great efforts in this research. However, it would not have been possible without the kind support and help of many people.

I would like to thank my advisor Dr. Nabil Sarhan for his continuous guidance and support. I also would like to thank my PhD committee Dr. Cheng-Zhong Xu, Dr. Syed Mahmud, and Dr. Nathan Fisher for their valuable input.

I wish to dedicate this work to my beloved parents who always supported me and without their blessings I would not have achieved this work. I also wish to express my love and unlimited gratitude to my beloved family; my wife Hend, my daughter Zainah, and my two sons Hamzah and Amjad, for their understanding, support, motivation, and endless love through the duration of my study. Finally, I would like to thank my brothers, my sisters, and my friends for their continuous support.

TABLE OF CONTENTS

Acknowledgments . . . . . **ii**

List of Tables . . . . . **viii**

List of Figures . . . . . **ix**

CHAPTER 1 **INTRODUCTION** **1**

1.1 Motivation 1

1.2 Overview 1

1.3 Proposed Work on VOD Systems 3

1.4 Proposed Work on AVS Systems 6

CHAPTER 2 **BACKGROUND INFORMATION AND RELATED WORK** **9**

2.1 Main Performance Metrics of Video Streaming Systems 9

2.2 Scalable Delivery of Video Streams with Stream Merging 9

2.3 Request Scheduling of Waiting Video Requests 11

2.4 IEEE 802.11e Standard 13

2.5 Cross-Layer Optimization in Video Streaming Systems 14

2.5.1 Automated Video Surveillance 15

2.6 Effective Airtime Estimation 16

CHAPTER 3 **INCREASING SYSTEM BANDWIDTH UTILIZATION BY USING WAITING-TIME PREDICTION IN VIDEO-ON-DEMAND SYSTEMS** **17**

3.1 Introduction 17

3.2 Providing Time-of-Service Guarantees 19

3.3 Proposed Waiting-Time Prediction Approach 22

3.3.1 Proposed AEC Scheme 23
3.3.2 Proposed Enhancements of AEC 27
3.3.3 Feedback Control of the Prediction Window 28
3.3.4 Proposed Hybrid Prediction Scheme 30
3.4 Evaluation Methodology 31
3.4.1 Workload Characteristics 31
3.4.2 Performance Metrics 32
3.5 Result Presentation and Analysis 33
3.5.1 Waiting-Time Distribution under Various Scheduling Policies 33
3.5.2 Waiting-Time Predictability and Effectiveness of Various Prediction Schemes . . 34
3.5.3 Effectiveness of Further Enhancements 35
3.5.4 Impact of Prediction Window 36
3.5.5 Analysis of Deviation Distributions under Various Prediction Schemes 38
3.5.6 Impact of Workload Parameters on AEC Performance 38
3.5.7 Feedback Control of the Prediction Window in AEC 41
3.5.8 Effectiveness of the Waiting-Time Prediction Approach Compared with GNSTF 42
3.6 Conclusions 44

CHAPTER 4 **INCREASING SYSTEM BANDWIDTH UTILIZATION BY ENHANCING SCHEDULING DECISIONS IN VIDEO-ON-DEMAND SYSTEMS 47**

4.1 Introduction 47
4.2 Analysis of Cost-Based Scheduling 48
4.2.1 Lookahead Scheduling 49
4.2.2 Combinational Scheduling 49
4.3 Proposed Predictive Cost-Based Scheduling 51

4.4 Proposed Adaptive Regular Stream Triggering (ART) 53
4.5 Evaluation Methodology 55
4.5.1 Workload Characteristics 56
4.5.2 Considered Performance Metrics 57
4.6 Result Presentation and Analysis 57
4.6.1 Comparing the Effectiveness of Different Cost-Computation Alternatives 57
4.6.2 Effectiveness of the Proposed PCS Policy 58
4.6.3 Effectiveness of the Proposed ART Enhancement 59
4.6.4 Comparing the Effectiveness of PCS and ART 62
4.6.5 Impact of Workload Parameters on the Effectiveness of PCS and ART 64
4.6.6 Comparing Waiting-Time Predictability with PCS and ART 67
4.6.7 Impact of Flash Crowds on the Effectiveness of PCS and ART 68
4.6.8 Effectiveness of Combining ART with PCS 69
4.7 Conclusions 70

CHAPTER 5 **DISTORTION-BASED CROSS-LAYER OPTIMIZATION FOR WIRELESS VIDEO STREAMING** **72**

5.1 Introduction 72
5.2 Proposed Cross-Layer Optimization Framework 75
5.2.1 Cross-Layer Optimization Problem Formulation 75
5.2.2 Distortion Function Characterization 76
5.2.3 Effective Airtime Estimation 77
5.2.4 Enhanced Effective Airtime Estimation 79
5.2.5 Cross-Layer Optimization Solution 80
5.2.6 Enforcing the Optimization Results 81

5.3 Performance Evaluation Methodology 83
5.4 Results Presentation and Analysis 85
5.4.1 Effectiveness of Using the Cross-Layer Approach in Bandwidth Allocation . . . 85
5.4.2 Analysis of the Enhanced Effective Airtime Estimation Algorithm 85
5.4.3 Analysis of Link-Layer Adaptation 87
5.4.4 Comparing Various Bandwidth Allocation Solutions 88
5.4.5 Impact of Interfering Traffic on the Performance of the Proposed Bandwidth Allocation Solution 89
5.5 Conclusions 91

CHAPTER 6 **ACCURACY-BASED CROSS-LAYER OPTIMIZATION FOR AUTOMATED VIDEO SURVEILLANCE** **95**
6.1 Introduction 95
6.2 Proposed Accuracy-Based Cross-Layer Optimization Framework 96
6.2.1 Optimization Problem Formulation 97
6.2.2 Rate-Accuracy Characterization 98
6.2.3 Effective Airtime Estimation 101
6.2.4 Optimization Solution 102
6.2.5 The Allocation Algorithm 103
6.2.6 Proposed Bandwidth Pruning Mechanism 104
6.3 Performance Evaluation Methodology 104
6.4 Result Presentation and Analysis 106
6.4.1 Effectiveness of the Proposed Effective Airtime Estimation 106
6.4.2 Effectiveness of the Proposed Bandwidth Allocation Solution 107
6.4.3 Effectiveness of the Proposed Bandwidth Pruning Mechanism 108

6.5 Conclusions . . . 108

CHAPTER 7 **SUMMARY AND FUTURE WORK** . . . **117**

7.1 Summary . . . 117

7.1.1 Waiting-time Predictability . . . 117

7.1.2 Scheduling . . . 118

7.1.3 Distortion-based Dynamic Bandwidth Allocation . . . 118

7.1.4 Accuracy-based Dynamic Bandwidth Allocation . . . 119

7.2 Future Work . . . 120

Bibliography . . . **121**

Abstract . . . **131**

Autobiographical Statement . . . **133**

LIST OF TABLES

Table 3.1 Summary of Workload Characteristics 32

Table 3.2 Summary of Deviation Distributions [*ERMT, MCF-P, 300 Channels, Model A*] . . 40

Table 4.1 Summary of Workload Characteristics 56

Table 5.1 Notations Summary 74

Table 5.2 Summary of Simulation Parameters 85

Table 5.3 Impact of the Time Interval Selected to Determine TXOP Limit 87

Table 6.1 Summary of Simulation Parameters 105

Table 6.2 Summary of PID Parameter Tuning 106

LIST OF FIGURES

Figure 1.1 Simplified VOD Streaming Environment 2

Figure 1.2 AVS System Overview 3

Figure 2.1 Patching 10

Figure 2.2 Transition Patching 10

Figure 2.3 ERMT 10

Figure 3.1 Clarification of GNSTF 22

Figure 3.2 Simplified Algorithm for the AEC Scheme 26

Figure 3.3 Clarification of the AEC Scheme 27

Figure 3.4 Controllers of Prediction Accuracy 30

Figure 3.5 Waiting Time Distribution [*Patching, 600 Channels, Model A*] 33

Figure 3.6 Comparing the Accuracy of Prediction Schemes [*MQL,* $W_p = 0.5\mu_{tol}$*, Model A*] . 34

Figure 3.7 Comparing the Accuracy of Prediction Schemes [$W_p = 0.5\mu_{tol}$*, Model A*] 35

Figure 3.8 Comparing the Accuracy of Prediction Schemes 35

Figure 3.9 Effectiveness of the Preferential Treatment of Real Requests Enhancement 36

Figure 3.10 Impact of the Periodic Refinement 36

Figure 3.11 Impact of Prediction Window 37

Figure 3.12 Impact of Prediction Window on Algorithm Computation Time 37

Figure 3.13 Comparing the Deviation Distributions under Various Prediction Algorithms . . . 39

Figure 3.14 Comparing the Distributions of the Deviation Percentage 40

Figure 3.15 Impact of Workload on Average Deviation 41

Figure 3.16 Impact of Workload on PCRE [*AEC, 550 Channels,* $W_p = \mu_{tol}$*, Model A*] 42

Figure 3.17 Impact of Variable-Length Video Workloads 43

Figure 3.18 Impact of the Shape Parameter of Weibull Arrival Distribution 43

Figure 3.19 Effectiveness of PID Controller 44
Figure 3.20 Effectiveness of Exponential Controller 44
Figure 3.21 Comparing GNSTF with Predictive MCF-P [Model B] 45
Figure 3.22 Comparing GNSTF with Predictive MCF-P [Model C] 45
Figure 3.23 Comparing GNSTF with Predictive MCF-P (Two Variants) 46

Figure 4.1 An Illustration of Lookahead Scheduling 50
Figure 4.2 Illustration of Combinational Scheduling 51
Figure 4.3 Simplified Algorithm for Dynamically Computing *freeChannelThresh* 52
Figure 4.4 Simplified Algorithm for PCS-V 53
Figure 4.5 Simplified Algorithm for PCS-L 54
Figure 4.6 Simplified Implementation of ART 54
Figure 4.7 Impact of ART on ERMT Stream Merge Tree 55
Figure 4.8 Effectiveness of Lookahead and Combinational Scheduling [*ERMT*] 58
Figure 4.9 Effectiveness of PCS [*ERMT*] 59
Figure 4.10 Effectiveness of PCS [*Transition Patching*] 59
Figure 4.11 Effectiveness of PCS [*Patching*] 60
Figure 4.12 Effectiveness of ART [*ERMT*] 60
Figure 4.13 Impact of ART on Regular Streams [*ERMT, MCF-P, Server Capacity = 450*] . . . 61
Figure 4.14 Effectiveness of ART [*Transition Patching*] 61
Figure 4.15 Effectiveness of ART [*Patching*] 62
Figure 4.16 Comparing Actual *Wr* 62
Figure 4.17 Comparing the Effectiveness of PCS and ART [*ERMT*] 63
Figure 4.18 Comparing the Effectiveness of PCS and ART [*Transition Patching*] 63
Figure 4.19 Comparing the Effectiveness of PCS and ART [*Patching*] 64
Figure 4.20 Comparing the Impacts of PCS and ART on Cost per Request [*ERMT, MCF-P*] . 64

Figure 4.21 Impact of Request Arrival Rate [*Server Capacity = 500*] 65

Figure 4.22 Impact of Customer Waiting Tolerance [*Server Capacity = 500*] 65

Figure 4.23 Impact of Number of Videos [*Server Capacity = 500*] 66

Figure 4.24 Impact of Video Length [*Server Capacity = 500*] 66

Figure 4.25 Impact of Skew in Video Access [*ERMT, Server Capacity = 450*] 67

Figure 4.26 Comparing the Effectiveness of MCF-P, PCS, and ART 67

Figure 4.27 Impact of the Shape Parameter of Weibull Arrival Distribution [*ERMT, PCS-V*] . 68

Figure 4.28 Comparing MCF-P, PCS-V, and MCF-P with ART 68

Figure 4.29 Waiting-Time Predictability of MCF-P, MCF-P with ART, and PCS-V 69

Figure 4.30 Impact of Flash Crowds 69

Figure 4.31 Comparing MCF-P, PCS-V, and MCF-P with ART with Flash Crowds 70

Figure 4.32 Effectiveness of Combining Art with PCS [*ERMT*] 70

Figure 4.33 Effectiveness of Combining PCS-V and ART [*Patching*] 71

Figure 5.1 Cross Layer Framework Clarification 73

Figure 5.2 Size-Distortion Models 78

Figure 5.3 The Algorithm for Dynamically Estimating the Effective Airtime 79

Figure 5.4 Enhanced Effective Airtime Estimation Algorithm 80

Figure 5.5 Comparing EDCA with Adaptive EDCA [CMU/MIT Image set] 86

Figure 5.6 Enhanced Effective Airtime Estimation Progress [FERET Image Set] 86

Figure 5.7 Calculation Period Impact 86

Figure 5.8 Effect of A_{thresh} on PSNR [EDO, CMU/MIT Image set] 86

Figure 5.9 Comparing Various Bandwidth Allocation Solutions [CMU/MIT Image Set] . . . 88

Figure 5.10 Comparing Various Bandwidth Allocation Solutions [Georgia Tech Image Set] . . 90

Figure 5.11 Comparing Various Bandwidth Allocation Solutions [FERET Image Set] 91

Figure 5.12 Impact of Cross traffic on EDO [Georgia Tech Image Set At 50% Resolution] . . 92

Figure 5.13 Impact of Cross traffic on EDO [FERET Image Set] 92
Figure 5.14 Comparing EDCA, DO, and EDO all with cross traffic 2 [Georgia Tech] 93
Figure 5.15 Comparing EDCA, DO, and EDO all with cross traffic 2 [FERET Image Set] . . 93
Figure 5.16 Comparing EDCA, DO, and EDO all with cross traffic 3 [Georgia Tech] 93
Figure 5.17 Comparing EDCA, DO, and EDO all with cross traffic 3 [FERET Image Set] . . 93
Figure 5.18 Comparing EDCA, DO, and EDO with cross traffic 3 [Georgia Tech] 94
Figure 5.19 Comparing EDCA, DO, and EDO with cross traffic 3 [FERET Image Set] 94

Figure 6.1 MJPEG Rate-Accuracy Characterization 110
Figure 6.2 MPEG-4 Rate-Accuracy and Rate-Distortion Characterization 111
Figure 6.3 Simplified PID Controller for Effective Airtime Estimation 111
Figure 6.4 Simplified PID Algorithm for Dynamically Estimating the Effective Airtime . . . 111
Figure 6.5 Effectiveness of Proposed PID-Based Estimation 112
Figure 6.6 Comparing Various Bandwidth Allocation Solutions in Effective Airtime 112
Figure 6.7 Impact of A_{thresh} with Proposed Weighted Accuracy Optimization 112
Figure 6.8 Comparing the Effectiveness of Various Bandwidth Allocation Solutions [WL1] . 112
Figure 6.9 Comparing the Effectiveness of Various Bandwidth Allocation Solutions [WL2] . 113
Figure 6.10 Comparing the Effectiveness of Various Bandwidth Allocation Solutions [WL3] . 113
Figure 6.11 Comparing the Effectiveness of Various Bandwidth Allocation Solutions [WL4] . 113
Figure 6.12 Comparing the Effectiveness of Various Bandwidth Allocation Solutions [WL5] . 114
Figure 6.13 Comparing the Effectiveness of Various Bandwidth Allocation Solutions [WL6] . 114
Figure 6.14 Effectiveness of Bandwidth Pruning Mechanism [WL1] 114
Figure 6.15 Effectiveness of Bandwidth Pruning Mechanism [WL2] 115
Figure 6.16 Effectiveness of Bandwidth Pruning Mechanism [WL3] 115
Figure 6.17 Effectiveness of Bandwidth Pruning Mechanism [WL4] 115
Figure 6.18 Effectiveness of the Proposed WAO Solution with the Pruning Mechanism [WL1] 116
Figure 6.19 Effectiveness of the Proposed WAO Solution with the Pruning Mechanism [WL2] 116

CHAPTER 1

INTRODUCTION

1.1 Motivation

Video streaming has recently grown dramatically in popularity over the Internet, Cable TV, and wireless networks. Currently, the main applications include Live Webcasting, Web Conferencing, Video-on-Demand (VOD), Distance Learning, Employee Training, Collaborations, Product Announcements, and Automated Video Surveillance (AVS). YouTube, a social video streaming website, is currently ranked as the third most popular Internet website according to Alexa daily traffic ranking [1]. Video surveillance systems have also witnessed a huge growth, with governments spending millions of dollars on installing these systems. For example, the number of installed surveillance cameras in England and Wales increased from 100 in 1990 to 40,000 in 2002 [2], and now the number is estimated to be about 2 million, leading to one camera per 32 persons in UK [3]. Similarly, Chicago city authorities spent at least $60 millions on video surveillance systems [4]. Furthermore, the revenue of video surveillance in China is expected to reach $9.5 billion by 2014 [5].

1.2 Overview

Because of the highly demanding nature of video streaming applications, maximizing resource utilization in any video streaming system is essential for enhancing the scalability and lowering the cost. These resources may include server bandwidth, network bandwidth, energy, and processing resources. In video streaming systems, the consumption of various resources is interdependent. For example, increasing the transmission data rate of a station increases both its power and network bandwidth consumption. As a result, any proposed solution to maximize the utilization of a single resource should take into consideration all other resources in the system.

In this research, we concentrate our work on two video streaming systems: VOD and AVS. In the

VOD system, shown in Figure 1.1, a central video server system streams prerecorded videos to clients upon their requests. The server maintains a waiting queue for every video and routes incoming requests to their corresponding queues. In such a system, *resource sharing* and *request scheduling* are key players in the utilization of the server bandwidth. Besides, enhancing the client perceived quality-of-service (QoS) in these systems is an other important objective.

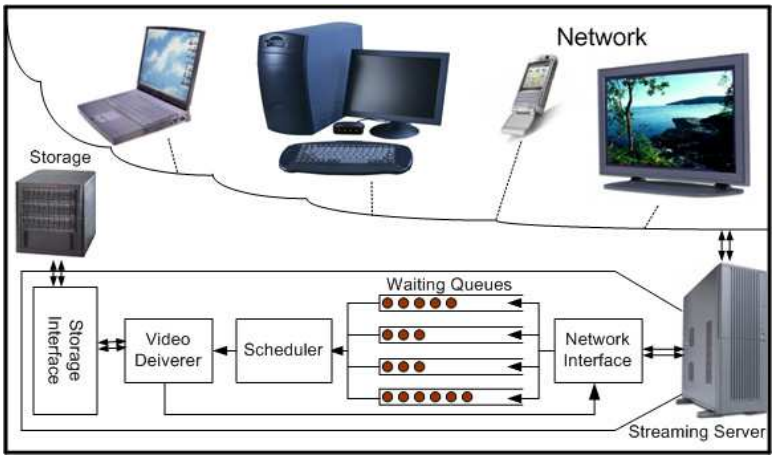

Figure 1.1: Simplified VOD Streaming Environment

In the AVS system under study, depicted in Figure 1.2, a set of wireless video sources stream live videos to a central video processing proxy over a shared wireless medium. The wireless medium can be WLAN, cellular, or WiMAX network. The wireless stations can be battery-powered or outlet-powered. The central processing proxy is connected with a high bandwidth link to the access point (*AP*), which means that this connection is not generally the bottleneck in the system. In this system, maximizing the network bandwidth utilization poses a serious challenge that needs to be addressed.

The main objectives of this research can be summarized as follows:

- To increase the utilization of resources in VOD systems by encouraging customers to wait for service by providing them with accurate expected waiting time for service.
- To propose a new class of scheduling policies that consider not only the current state but also the future state of the VOD system. Current scheduling decisions have a strong effect on future

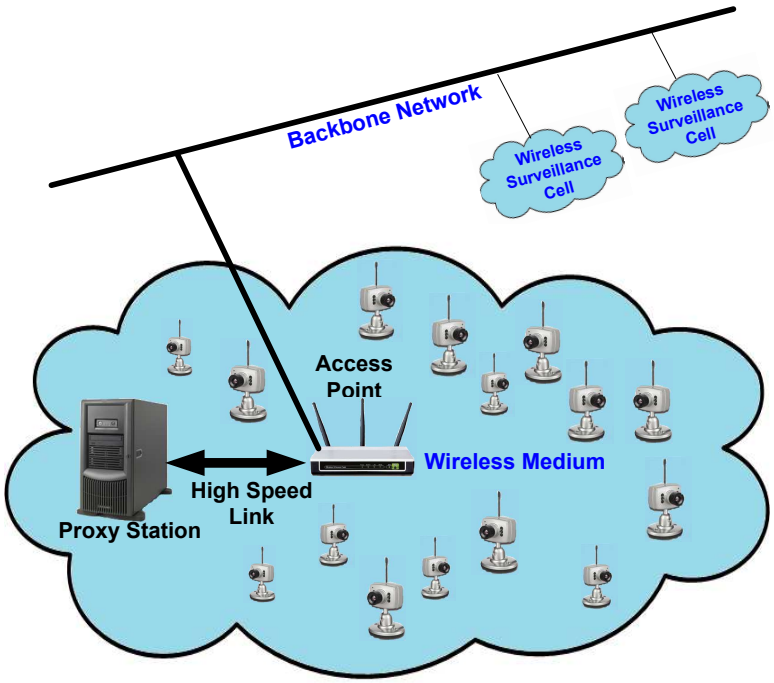

Figure 1.2: AVS System Overview

scheduling and stream delivery decisions in the system. What we seek is a scheduling policy that predicts the future state of the system and takes the prediction results into consideration in the current scheduling decision to achieve maximum system bandwidth utilization.

- To solve the problem of dynamic bandwidth allocation in AVS systems in order to maximize the utilization of network bandwidth. The dynamic bandwidth allocation solution should consider all the characteristics of a typical AVS system.

1.3 Proposed Work on VOD Systems

Unfortunately, the distribution of streaming media by a video streaming system faces a significant scalability challenge due to the high server and network requirements. Hence, numerous techniques have been proposed to deal with this challenge, especially in the areas of *media delivery* (also called *resource sharing*) and *request scheduling*. Scalable video delivery can be achieved using *stream merging* [6, 7, 8, 9, 10, 11, 12] and *periodic broadcasting* [13, 14, 15, 16, 17]. These techniques offer scalable

performance when compared with unicast delivery.

Stream merging techniques reduce the cost by aggregating clients into larger groups that share the same multicast streams. These techniques include *Stream-Tapping/Patching* [6, 18, 19], *Transition Patching* [7, 20], and *Earliest Reachable Merge Target* (ERMT) [8, 21]. The client makes up to one merge with Patching, up to two merges with Transition Patching, and multiple merges with ERMT. Thus, these techniques offer three levels of performance (in terms of the achieved resource sharing and thus the number of customers that can be serviced concurrently) which come at three levels of implementation complexity, with higher performance achievable at higher implementation complexity. For these techniques, request scheduling is an important aspect. A scheduling policy is used to select the requests for service. A cost-based scheduling policy, called *Minimum Cost First* [22], has recently been proposed to capture the significant variation in stream lengths caused by stream merging techniques through selecting the requests requiring the least cost.

While stream merging delivers data in a client-pull fashion, periodic broadcasting techniques deliver data in a server-push fashion by dividing each video into multiple segments and broadcasting each segment periodically on dedicated server channels. Thus, they can be used only for the most popular videos and require the clients to wait until the next broadcast time of the first segment. This part of the proposed research considers the stream merging approach.

Most prior studies focused on only three main performance metrics: server throughput, average waiting time, and unfairness against unpopular videos. Motivated by the rapidly growing interest in human-centered multimedia, we consider other user-oriented metrics, such as the ability to inform users about how long they need to wait for service. Today, even for short videos with medium quality, users of online video websites may experience significant delays. The transition, in the near future, to streaming long videos (such as full-length movies) at high quality (such as HD) may lead to even larger delays. We plan to analyze two approaches for giving waiting-time feedback to users of scalable video streaming. The first approach provides users with hard time-of-service guarantees. By contrast, the second

approach provides expected times of service, or alternatively expected waiting times. Thus, this approach is referred to as the *predictive approach*. Providing users with waiting-time feedback enhances their perceived QoS and encourages them to wait, thereby increasing server utilization by increasing server throughput. In the absence of any waiting-time feedback, users are more likely to defect because of the uncertainty as to when they will start to receive services. The issue of providing time-of-service guarantees has not been analyzed in the context of scalable video delivery techniques.

The achieved resource sharing by stream merging depends greatly on how the waiting requests are scheduled for service. Despite the many proposed stream merging techniques and the numerous possible variations, there has been only a little work on the issue of scheduling in the context of these scalable techniques. The choice of a scheduling policy can be as important as or even more important than the choice of a stream merging technique, especially when the server is loaded. Motivated by the development of cost-based scheduling, we plan to investigate its effectiveness in great detail and discuss opportunities for further tunings and enhancements. In particular, we plan to answer the following two important questions. First, is it better to consider the stream cost only at the current scheduling time or consider the expected overall cost over a future period of time? Second, should the cost computation consider future stream extensions done by advanced stream merging techniques (such as ERMT) to satisfy the needs of new requests? These questions are important because the current scheduling decision can affect future scheduling decisions, especially when stream merging and cost-based scheduling are used. Additionally, we will analyze the effectiveness of incorporating video prediction results into the scheduling decisions. We also plan to study the interaction between scheduling policies and the stream merging techniques and explore new ways for enhancements.

The specific research objectives for this part can be summarized as follows.

- To study how to provide hard time-of-service guarantees in scalable video delivery techniques.
- To propose a waiting-time prediction approach, which provides users with expected waiting times

rather than hard time-of-service guarantees.

- To analyze the effectiveness of incorporating video prediction results into the scheduling decisions.

- To study the interaction between scheduling policies and the stream merging techniques.

1.4 Proposed Work on AVS Systems

Most research on AVS focused on developing robust computer vision algorithms for the detection, tracking, and classification of objects [23, 24, 25, 26, 27, 28, 29] and the detection and classification of unusual events [30, 31, 32, 33, 34, 35]. Much less work, however, considered resource utilization in video surveillance systems. Enhanced resource utilization necessity arises because increasing the coverage through employing additional video sources leads to increasing the required bandwidth and thus the computational capability to process all these video streams. (The fact that increasing the bandwidth also increases the computational cost applies to most practical circumstances.) Even when a distributed processing architecture is used to increase scalability, the cost of such a system can still be a big concern as computer vision algorithms are computationally intense. Power consumption is another major problem, especially in battery-powered (wireless) video sources. Considering that video sensors consume orders of magnitude more resources than scalar sensors, reducing power consumption is essential even when the power is available [36].

Enhanced resource utilization in AVS systems can be achieved by controlling the sending rate of a video source according to the state of that video source. The state of the video source may include the network channel conditions, the video source power constrains, the potential threat level at the video source location, the placement of the video source, the source location importance, and the lighting conditions in the source environment. This controlling process can be achieved by dynamic network bandwidth management and allocation. With the introduction of 802.11e standard, the provision of

deferential bandwidth allocation is now possible among different traffic categories in the same station. Unfortunately, bandwidth management and providing differential bandwidth allocation among different stations within the same access category is not yet provided by the standard and needs further investigation.

As depicted in Figure 1.2, AVS systems usually have $S \geq 1$ video sources. Each video source s streams a different encoded video stream of rate (R_s). These video streams are being sent to a central processing proxy that is linked to the AP. Each video source s has a physical rate (y_s) and a weight factor (w_s). The weights can be assigned based on many factors, including the potential threat level, placement of video sources, and location importance. The wireless network in the system has limited available bandwidth that have to be estimated accurately and distributed efficiently among the video sources to achieve the best results in terms of some objective function.

In prior bandwidth management studies [37, 38, 39, 40, 41, 42, 43, 44], maximizing the overall perceived video quality or minimizing overall video distortion is the main objective. In some of these studies, the problem was formulated as an optimization problem using a rate-distortion function. This function characterizes the relationship between video bit rate and video distortion. In AVS systems, however, computer vision algorithms are utilized to produce automatic alerts when any event of interest, such as object detection, happens in the surveillance area. Consequently, it is more intuitive to consider maximizing the accuracy of the computer vision algorithm as the objective of the network bandwidth management. This can be done by formulating the bandwidth management problem as an optimization problem using a rate-accuracy function. This function characterizes the relationship between the video bit rate and the accuracy of the used computer vision algorithm.

Another motivation behind using a rate-accuracy function instead of a rate-distortion function is that computer vision algorithm accuracy is less sensitive to the reduction of the video bit rate when compared to video quality [45, 46, 47].

In this research, the main idea is to formulate the bandwidth allocation problem as a cross-layer

optimization problem of the sum of the weighted event detection accuracy (or alternatively the sum of the weighted detection error), subject to the constraint in the total available bandwidth.

The specific research objectives for this part can be summarized as follow.

- To build a cross-layer framework for managing the network bandwidth in AVS systems.
- To develop an online and dynamic approach for estimating the effective airtime of the network.
- To develop accurate models that characterize the relationship between video bit rate and the accuracy of a computer vision algorithm.

CHAPTER 2

BACKGROUND INFORMATION AND RELATED WORK

2.1 Main Performance Metrics of Video Streaming Systems

The main performance metrics of video streaming servers are *user defection probability*, *average waiting time*, and *unfairness*. The defection probability is the probability that a new user leaves the server without being serviced because of a waiting time exceeding the user's tolerance. It is the most important metric, followed by the average waiting time, because it translates directly to the number of users that can be serviced concurrently and to server throughput. Unfairness measures the bias of a scheduling policy against unpopular videos and can be computed as the standard deviation of the defection probability among the videos:

$$Unfairness = \sqrt{\sum_{i=1}^{n}(d_i - \bar{d})^2/(n-1)}, \tag{2.1}$$

where d_i is the defection probability for video i, $\bar{d}$ is the mean defection probability across all videos, and n is the number of videos.

2.2 Scalable Delivery of Video Streams with Stream Merging

Stream merging techniques aggregate users into larger groups that share the same multicast streams. In this subsection, we discuss three main stream merging techniques: Patching [18, 6, 19], Transition Patching [7, 20], and ERMT [8, 21]. Each of these techniques requires two download channels at the client.

In Patching, a new request joins immediately the latest full-length multicast stream for the video and receives the missing portion as a *patch* using a unicast stream. A full-length multicast stream is called *regular stream*. Both the regular and patch streams are delivered at the video playback rate. The length

of a patch stream and thus its delivery cost are proportional to the temporal skew from the latest regular stream. The playback starts using the data received from the patch stream, whereas the data received from the regular stream is buffered locally for use upon the completion of the patch stream. Because patch streams are not sharable with later requests and their cost increases with the temporal skew from the latest regular stream, it is cost-effective to start a new regular stream when the patch stream length exceeds a certain value, called *regular window* (Wr). Figure 2.1 further explains the concept. Initially, one regular stream (first solid line) is delivered, followed by two patch streams (next two dashed lines) to service new requests. Note that the length of the patch stream is the temporal skew to the regular stream. Subsequently, another regular stream (second solid line) is initiated followed by two other patch streams.

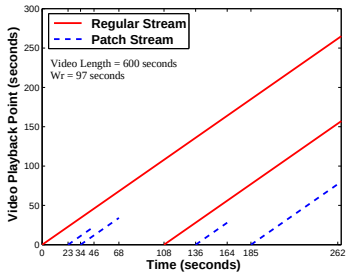

Figure 2.1: Patching

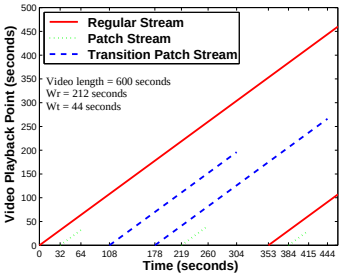

Figure 2.2: Transition Patching

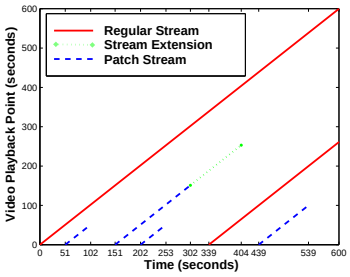

Figure 2.3: ERMT

Transition Patching allows some patch streams to be sharable by extending their lengths. Specifically, it introduces another multicast stream, called *transition stream*. The threshold to start a regular stream is Wr as in Patching, and the threshold to start a transition stream is called *transition window* (Wt). Figure 2.2 further illustrates the concept. For example, the client at time 219 seconds starts listening to its own patch stream (second dotted line) and the closest preceding transition patch stream (second dashed line), and when its patch is completed, it starts listening to the closest preceding regular stream (first solid line).

ERMT is a near optimal hierarchical stream merging technique. Whereas a stream can merge at most once in Patching and at most twice in Transition Patching, ERMT allows streams to merge multiple

times, thereby leading to a dynamic merge tree. In particular, a new user or a newly merged group of users snoops on the closest stream that it can merge with if no later arrivals preemptively catch them [8]. To satisfy the needs of the new user, the target stream may be extended, and thus its own merging target may change. Figure 2.3 illustrates the operation through a simple example. We can see that the third stream length got extended after the fourth stream had merged with it. Extensions are shows as dotted lines. ERMT performs better than other hierarchical stream merging alternatives and close to the optimal solution, which assumes that all request arrival times are known in advance [8, 48, 49].

Patching, Transition Patching, and ERMT differ in complexity and performance. Both the implementation complexity and performance increase from Patching to Transition Patching to ERMT. Patching is the simplest to implement since it allows only one merge during the client's service period and allows only regular streams to be shared. Hence, it enables the client to know the streams it will listen to in advance. Transition Patching also informs the client about all the streams to listen to in advance, but it allows up to two merges per client. ERMT is the most complex because it allows any number of merges that can help in maximizing resource sharing. The client needs to be continuously informed about all previous streams for the same video, and the client (or the server) needs to perform frequent calculations to decide on the next merge target when a merge occurs. Selecting the most appropriate stream merging technique depends on a tradeoff between the required implementation complexity and the achieved performance.

2.3 Request Scheduling of Waiting Video Requests

A scheduling policy selects an appropriate video for service whenever it has an available *channel*. A channel is a set of resources (network bandwidth, disk I/O bandwidth, etc.) needed to deliver a multimedia stream. All waiting requests for the selected video can be serviced using only one channel. The number of channels is referred to as *server capacity*.

All scheduling policies are guided by one or more of the following primary objectives: (i) minimize

the overall customer defection (turn-away) probability, (ii) minimize the average request waiting time, and (iii) minimize unfairness. Let us now discuss the main scheduling policies.

- *First Come First Serve* (FCFS) [50] selects the video with the oldest waiting request.
- *Maximum Queue Length* (MQL) [50] maximizes the number of request that can be serviced at any time by selects the video with the largest number of waiting requests.
- *Maximum Factored Queue Length* (MFQL) [51] - This policy attempts to minimize the mean request waiting time by selecting the queue with the *largest factored length*. The factored length of a queue is defined as its length divided by the square root of the relative access frequency of its corresponding video. MFQL reduces the average waiting time optimally only if the server is fully loaded and customers always wait until they receive service (i.e., no defections).
- *Next Schedule Time First* (NSTF) [52] – This policy assigns schedule times to incoming requests, and it guarantees that they will be serviced no later than scheduled. In addition, it ensures that these schedule times are very close to the actual times of service. NSTF, therefore, improves both QoS and server throughput. Improving throughput is attained by enhancing the waiting tolerance of customers. In the absence of any time of service guarantees, customers are more likely to defect because of the uncertainty of when they will start to receive services. Another desirable feature of NSTF is the ability to prevent starvation (as FCFS).
- *Minimum Cost First* (MCF) [22] policy has been recently proposed to exploit the variations in stream lengths caused by stream merging techniques. It gives preference to the videos whose requests require the least cost in terms of the amount of video data (measured in bytes) to be delivered. The length of the stream (in time) is directly proportional to the cost of servicing that stream since the server allocates a channel for the entire time the stream is active. Please note the distinction between video lengths and required stream lengths. Due to stream merging, even the requests for the same video may require different stream lengths. *MCF-P* (P for “Per”), the preferred implementation of

MCF, selects the video with the least cost per request. The objective function here is

$$F(i) = \frac{L_i \times R_i}{N_i}, \tag{2.2}$$

where L_i is the required stream length for the requests in queue i, R_i is the (average) data rate for the requested video, and N_i is the number of waiting requests for video i. To reduce the bias against videos with higher data rates, R_i can be removed from the objective function (as done in this study). MCF-P has two variants: *Regular as Full* (RAF) and *Regular as Patch* (RAP). RAP treats regular and transition streams as if they were patches, whereas RAF uses their normal costs. MCF-P performs significantly better than all other scheduling policies when stream merging techniques are used. In this study, we simply refer to MCF-P (RAP) as MCF-P unless the situation calls for specificity.

2.4 IEEE 802.11e Standard

The 802.11e standard enables the provision of different quality-of-service (QoS) levels among different access categories (AC) in the same station, thereby enhancing the support of multimedia applications. These access categories include Voice, Video, Best Effort, and Background. The IEEE 802.11e MAC layer provides two methods for managing the access to the wireless channel: *Hybrid Coordination Function Controlled Channel Access* (HCCA) and *Enhanced Distributed Channel Access* (EDCA). In contrast with HCCA, EDCA provides reduced complexity and better flexibility by providing a distributed coordination function [44, 53].

With EDCA, priorities are implemented using four EDCA parameters: *Arbitration Inter Frame Space (AIFS)*, *Minimum Contention Window (CW_{min})*, *Maximum Contention Window (CW_{max})*, and *Transmission Opportunity Time (TXOP)*. AIFS controls the waiting time before an AC starts the transmission when the medium is not busy. In case of a collision, the AC will back off for a random time between 0 and CW, where CW is a variable that is initialized to CW_{min}, is incremented after every

transmission failure until it reaches CW_{max}, and is reset to CW_{min} after a successful transmission. The backoff timer is decremented every time the medium is sensed to be idle for at least $AIFS$ seconds. Finally, the TXOP limit controls the time period during which the AC keeps transmitting when it gains access to the medium.

2.5 Cross-Layer Optimization in Video Streaming Systems

Numerous studies have discussed cross-layer optimization in video streaming over wireless networks. Studies [37, 38, 39] (and references within) consider a system in which only one station streams a video at a time, whereas studies [40, 41, 42] (and references within) consider a system in which multiple stations receive video streams form a central video server, and studies [43, 44] consider systems in which multiple stations deliver video streams to a central station. The latter studies are more related to this work.

Study [43] optimizes video streaming over a 2G wireless network. The solution proposed in this study adapts the video streams by using video summarization techniques, such as frame skipping, which are not applicable to video surveillance because of the system's sensitivity for losing video frames.

Study [44] formulates and solves an optimization problem that minimizes the sum of distortion in all video streams. That paper used the formulation in [54] to develop an analytical model for the effective airtime. The model, however, is incorrect as will be discussed in Subsection 2.6. In addition, that paper assumes *p*-persistent EDCA, which differs from the standard EDCA in the backoff timer selection process. Moreover, it ignored the packetization overhead of the transport and application layers when determining the optimal application rate and link layer parameters. In this study, we address the problems of that study, and we also improve its link-layer adaptation model, which was based on the formulation in [55, 53].

2.5.1 Automated Video Surveillance

Major prior work on surveillance systems can be summarized as follows.

- In [56], a prototype for an urban surveillance system is proposed. This prototype, called *Detection of Events for Threat Evaluation and Recognition* (DETER), targets the high-end of the security market and uses a dedicated network for high-quality streaming.
- Studies [30, 25] reduce the bandwidth requirements by proposing systems that send still images periodically from the video source to the user.
- Knight [57] is a wide-area surveillance system that detects, tracks, and classifies moving objects across multiple cameras. It transmits videos with fixed encoding parameters to a centralized server.
- SfniX [58] is a surveillance system that supports realtime monitoring and storage of all the video streams, performs video analysis, and answers semantic database queries. Like Knight [57], it transmits videos with fixed encoding parameters to a central server for processing.
- VSAM [23] uses multiple video sensors to provide continuous coverage of people and vehicles in a cluttered area. Basically, it facilitates the tracking of people and vehicles in such areas. VSAM sends one low quality video at a time and relies on dedicated workstations for the detection, tracking, and classification of events. Some of the technologies developed by the VSAM project have been commercialized by companies, such as ObjectVideo.
- Studies [45, 46, 47] generated rate-accuracy curves for face detection and face tracking algorithms. They simply limited the video rates of all video sources to one value, referred to as the “sweet point”. In this study, we develop a comprehensive cross-layer optimization solution. We also develop an accurate rate-accuracy model using multiple datasets.

2.6 Effective Airtime Estimation

The effective airtime is the fraction of the network time that is used for delivering useful data. As will be discussed later, solving the optimization problem requires an accurate estimation of the effective airtime. In [53], the effective airtime for ad-hoc networks was simply determined as the total throughput divided by the physical rate, assuming that all stations in the network have the same physical rate. Study [44] developed an analytical model for the effective airtime for video streaming from multiple stations to a proxy, based on the formulation in [54]. These two studies involve significant simplifications, approximations, and assumptions. The developed airtime model was simply given in terms of only CW_{min} and the number of stations in the network. Furthermore, according to the model, the effective airtime increases with the number of nodes and yields a value close to 1 ($i.e.$, 100%) in networks with 30 stations or more. Such behavior is logically and empirically incorrect. As will be shown in Section 5.4, this model leads to significant dropping after the optimization and gives relatively high distortion.

Other studies [59, 60, 61, 62, 63, 64] sought to determine other related parameters, such as the saturation bandwidth and network capacity for ad-hoc networks. None of these studies is directly applicable to finding the effective airtime in our considered system.

CHAPTER 3

INCREASING SYSTEM BANDWIDTH UTILIZATION BY USING WAITING-TIME PREDICTION IN VIDEO-ON-DEMAND SYSTEMS

3.1 Introduction

In this part of the dissertation, we analyze waiting-time predictability in scalable video streaming services. In particular, we seek to assess through an extensive analysis whether the waiting times can be accurately predicted when stream merging techniques are employed. Moreover, we investigate the impacts of stream merging techniques, scheduling policies, and numerous workload and design parameters. Providing users with waiting-time feedback enhances their perceived quality-of-service (QoS) and encourages them to wait (given that the waiting times are not too long), thereby increasing server throughput. In the absence of any waiting-time feedback, users are more likely to defect because of the uncertainty as to when they will start to receive services. The proposed waiting-time prediction approach provides users with expected times of service, or alternatively expected waiting times.

To assess the effectiveness of the waiting-time prediction approach, we present and analyze two alternative prediction schemes. The first, called *Assign Expected Stream Completion Time* (AEC), is highly intelligent and adaptive to server workload by utilizing detailed information about the current state of the server and considering the specific dynamic nature of the applied scheduling policy. This information includes the current queue lengths, the completion times of running streams, and regularly-updated statistics, such as the average request arrival rate for each video. AEC uses the completion times of running streams to know when server channels will become available, and thus when waiting requests can be serviced. The main idea of AEC is to predict the future scheduling decisions over a certain period, called *prediction window*. As the prediction window increases, the percentage of users receiving expected times increases, but at the expense of increasing the implementation complexity and more importantly reducing the prediction accuracy. The prediction accuracy is an essential QoS metric that

also contributes to establishing the users' trust and confidence in the provided expected times, and thus should not be significantly reduced to provide an expected time to each user. We utilize feedback control theory to tune the value of the prediction window to allow a pre-specified tolerance in the accuracy. The inability of AEC to provide an expected time to each user is addressed by the second scheme, called *Hybrid Prediction*. This scheme employs two predictors.

We also compare the effectiveness of the waiting-time prediction approach with another approach that provides users with time-of-service guarantees. The issue of providing time-of-service guarantees has not been analyzed in the context of scalable video delivery techniques. A policy, called *Next Schedule Time First* (NSTF) [65], was proposed for Batching. This policy provides users with schedule times and guarantees that they will be serviced no later than scheduled. We show that NSTF can be extended to stream merging but has two inherent shortcomings. First, it performs significantly worse in throughput and average waiting time than the recently proposed MCF policy, which utilizes aggressive cost-based scheduling but cannot provide time-of-service guarantees. Second, NSTF cannot work with hierarchical stream merging techniques (such as *Earliest Reachable Merge Target* (ERMT) [8, 21]), which achieve the most scalable performance, because they may extend streams to satisfy the needs of new requests. We refer to the extended version of NSTF as *Generalized NSTF* (GNSTF) throughout this chapter.

The proposed waiting-time prediction approach eliminates the shortcomings of NSTF by providing expected waiting times of service (or approximate times of service) rather than hard time-of-service guarantees. This approach can be applied with MCF and hierarchical stream merging to ensure the highest performance.

The results show that the waiting-time prediction approach is highly accurate and leads to outstanding performance benefits.

The rest of the chapter is organized as follows. Section 3.2 discusses how to provide time-of-service guarantees in scalable video streaming, and Section 3.3 presents the proposed prediction schemes. Subsequently, Section 3.4 discusses the performance evaluation methodology and Section 3.5 presents and

analyzes the main results.

3.2 Providing Time-of-Service Guarantees

For Batching, a scheduling policy, called *Next Schedule Time First* (NSTF), was proposed in [65] to provide time-of-service guarantees. In this study, we extend NSTF to work with stream merging techniques and analyze its effectiveness in this environment.

Let us start by discussing how (NSTF) works. NSTF assigns schedule times to incoming requests and guarantees that they will be serviced no later than scheduled. In addition, it ensures that these schedule times are very close to the actual times of service. Note that the completion times of running streams (i.e., currently being serviced streams) represent when channels will become available and thus when new requests can be serviced. When a new request calls for the playback of a video with no waiting requests, NSTF assigns the request a new schedule time that is equal to the closest unassigned completion time of a running stream. If the new request, however, is for a video that has already at least one waiting request, then NSTF assigns it the same schedule time assigned to the other waiting request(s) because all these requests can be serviced together using only one stream. NSTF eliminates some potential problems when the basic FCFS is used to provide time-of-service guarantees as done in [66].

When all waiting requests for a video are canceled, their schedule time becomes available and can be used by other requests. This leads to two variants of NSTF: *NSTFn* and *NSTFo*. NSTFn assigns the freed schedule times to incoming requests, whereas NSTFo assigns them to existing requests that will wait beyond a certain threshold, and thus are likely to defect without being assigned better schedule times. Hence, requests that are assigned schedule times that require them to wait beyond a certain threshold should be notified that they may be serviced earlier.

NSTFo assigns each freed schedule time to an appropriate waiting queue that meets the following three conditions: (i) it is nonempty, (ii) its assigned schedule time is worse than the freed schedule time,

and (iii) the expected waiting time for each request in it is beyond a certain threshold. If no candidate is found, NSTFo grants the freed schedule time to a new request. In contrast, if more than one queue meet these conditions, it selects the most appropriate one. The *NSTFo-MQL* implementation (which was shown to provide the best overall performance) selects the longest queue among the candidates. NSTFo-MQL combines the benefits of FCFS and MQL by assigning schedule times on a FCFS basis and reassigning freed schedule times on a MQL basis.

We present next an efficient generalized implementation of NSTF, called *Generalized NSTF* (GNSTF), which can be applied for Batching as well as some stream merging techniques, including Patching and Transition Patching. The server maintains a running queue (RQ), which keeps track of all currently running streams. These streams are stored in an decreasing order of their completion times. To provide time-of-service guarantees, the server needs to maintain an index, $RQIndex$, which points to the next stream in RQ whose completion time has not been assigned yet. $RQ[0]$ is the first element of RQ, and it corresponds to the stream with the furthest completion time. $RQIndex$ is incremented when a video is selected for service and the location of its stream completion time in RQ precedes $RQIndex$. In contrast, $RQIndex$ is decremented every time a schedule time is assigned from RQ. In addition, the server needs to maintain a free pool of freed schedule times. Any assigned schedule time that is freed (due to request defection for instance) and thus can be used by later requests will be inserted in this pool. This pool can be implemented using a priority queue, where schedule times are placed in an ascending order. When a request for a video with no waiting requests arrives, the server first tries to assign it a schedule time from the top of the free pool. If the pool does not contain any live schedule times (i.e., schedule times that are further than the current time), then the server assigns it a new schedule time that corresponds to the next unassigned completion time.

For an efficient operation of GNSTF when used with stream merging, we propose and utilize two enhancements. First, GNSTF triggers a schedule-time reassignment not only when a schedule time is freed but also when a new running stream has a closer completion time than an earlier stream whose

completion time has already been assigned. The latter situation does not happen when Batching is applied because all streams are of the same length. In stream merging techniques, however, streams vary significantly in length, and thus the completion time of a new stream may be closer than that of an old stream. Assigning the new completion time to existing requests with significantly long expected waiting times enhances performance and increases fairness. Second, we improve the performance of NSTFo by utilizing the old schedule times that have been reassigned with better schedule times. When the requests for a certain video receive a new schedule time, their old schedule time can be assigned to the requests for the video with a worse schedule time. This enhancement, called *schedule-times cascading*, is valid because the reassignment of schedule times in NSTFo is highly constrained and the freed schedule times may not be assigned to the requests with the worst schedule time. This enhancement can also be used with Batching but is likely to be more effective with stream merging techniques.

Figure 3.1 clarifies the general operation of GNSTF. The figure shows three request waiting queues (WQs) (one for each video) and the stream running queue (RQ). The stream running queue holds information for each stream that is currently being delivered. This information contains the video number, the stream completion time, and the waiting request to which this completion time is assigned as the schedule time. Note that $RQ[0]$ corresponds to the bottom of RQ. At time T_6, request R_6 for video V_2 is made. Since the free pool is empty, this request will be assigned the completion time of the stream pointed to by $RQIndex$, and subsequently $RQIndex$ will be decremented by 1. At time T_7, request R_5 is canceled (request defection) and because it is the only request in the waiting queue, its schedule time (T_9) will become available and can be used by other requests. Request R_6 has a further schedule time and thus will be assigned this schedule time, releasing its own schedule time (T_{15}) to the free pool. At time T_8, request R_7 for video V_1 is made. Since a schedule time (T_{15}) is available in the free pool, this request will receive T_{15} as the assigned schedule time. Finally, at time T_9, R_6 is serviced, and thus a new completion time (T_{24}) becomes available and thus $RQIndex$ will be incremented by 1.

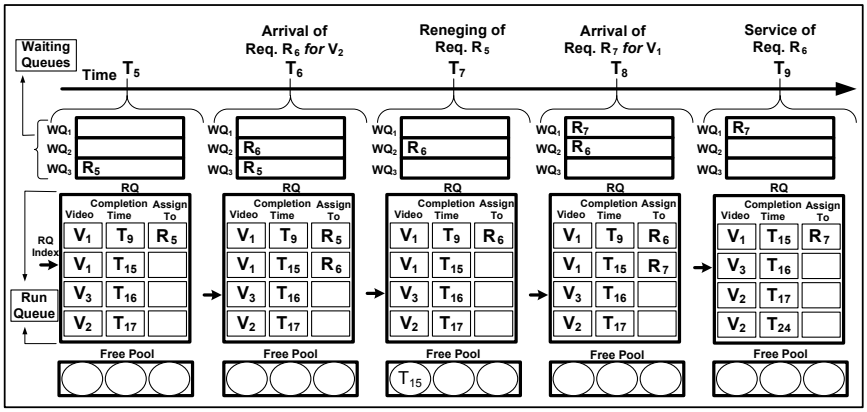

Figure 3.1: Clarification of GNSTF

3.3 Proposed Waiting-Time Prediction Approach

Unfortunately, the NSTF/GNSTF approach has two main inherent shortcomings. First, it may not perform well in terms of server throughput (or defection probability) and waiting times compared with other aggressive scheduling approaches, such as MCF-P. The cost-based approach is indeed hard to be outperformed in terms of defection probability, especially by a policy whose main objective is to provide hard time-of-service guarantees and in which the initial assignment of schedule times is done on a FCFS basis. Second, NSTF/GNSTF cannot work with hierarchical stream merging techniques (such as ERMT) which achieve the highest performance. NSTF/GNSTF is incompatible with these techniques because in hierarchical stream merging, streams may be extended to satisfy the needs of new users, thereby violating some time-of-service guarantees.

To overcome both these shortcomings, we propose the *waiting-time prediction* approach. This approach provides users with expected waiting times for service (or alternatively, approximate times of service) rather than hard time-of-service guarantees. The main advantage of this approach is that the server can use hierarchical stream merging techniques and aggressive scheduling policies (such ERMT and MCF-P, respectively) while improving user-perceived QoS by informing users with their expected waiting times. The success of the waiting-time prediction approach depends on whether the waiting times can be accurately predicted when such scheduling policies are used. If the predictions are accu-

rate, users will appreciate the service, trust the service provider, and feel motivated to wait. Encouraging users to wait further improves the server throughput.

We present two schemes for predicting the waiting times: *Assign Expected Stream Completion Time* (AEC) and *Hybrid Prediction*. These two schemes are compared with a straightforward approach that dynamically computes the average waiting time for each video and provides the average value as the predicted waiting time for the new requests for the corresponding video. This scheme is referred to as *Assign Per-Video Average Waiting Time* (APW). In contrast with APW, the proposed AEC scheme exhibits high intelligence. It predicts the future scheduling decisions over a certain period of time and uses the completion times of running streams to know when channels will become available, and thus when waiting requests can be serviced. The hybrid scheme combines AEC with APW to provide an expected time to each user.

3.3.1 Proposed AEC Scheme

Let us now discuss the proposed AEC scheme in more detail. Basically, this scheme predicts the waiting times (or times of service) by "simulating" the future behavior of the server. It utilizes detailed information about the current state of the server to predict the waiting time and considers the applied scheduling policy. This information includes the current queue lengths, the completion times of running streams, and statistics, such as the average request arrival rate for each video (which is to be updated periodically).

As discussed earlier, a stream's completion time indicates when a server channel will be free and can be used by new requests. Thus, the server knows when each channel will be available. The server can use these times as expected times of service for new requests. The assignment of a completion time to a new request is done by predicting the future scheduling decisions.

The basic idea of AEC can be explained as follows. When a new request arrives, the server determines the closest stream completion time that can be assigned to that request as the expected time of

service. The server examines the completion times in the order of their closeness from the current time and finds the expected video to be serviced at that completion time. The process continues until the expected video to be serviced is the same as the currently requested video. To predict the scheduling outcome at a certain completion time, the server needs to estimate the video queue lengths at that completion time if the scheduling policy requires so (such as MQL, MFQL, and MCF) based on the video arrival rates, which are to be computed periodically, but not frequently. The expected queue length for video v at completion time T is given by

$$expected\_qlen[v] = (qlen[v] + \lambda[v] \times (T - T_{Now})) \times def\_rate[v], \tag{3.1}$$

where $qlen[v]$ is the queue length of video v at the current time (T_{Now}), $\lambda[v]$ is the arrival rate for video v, and $def\_rate[v]$ is the defection rate of video v. The video waiting queues are likely to experience some defections, and these defections will become more significant during longer periods. Accounting for these defections is effective, especially for large prediction windows. Thus, the expected queue length is adjusted by the current video defection rate. Note that the waiting tolerance distribution is generally a memoryless process. Therefore, it is not advantageous to use the current waiting times in determining when users will actually defect.

Note that the same video may be serviced again at later completion times. Equation (3.1) assumes that video v has not been identified before (while running the AEC algorithm to find the expected time of service for the new request) as the expected video to be serviced at an earlier stream completion time. Otherwise, the expected arrivals will have to be found during the time interval between the latest completion time (T_l) at which video v is expected to be serviced and T. In that case, the expected queue length for video v at completion time T is given by

$$expected\_qlen[v] = \lambda[v] \times (T - T_l) \times def\_rate[v]. \tag{3.2}$$

Note that $qlen$ is not part of the equation because all existing requests (as of time T_{Now}) for video v are expected to be serviced at time T_l. To predict the scheduling decisions of MCF-P, AEC considers the expected stream lengths required by various videos in addition to the expected queue lengths.

To reduce the implementation complexity in terms of algorithm computation time, AEC predicts the future scheduling decisions only during certain duration of time, called *prediction window* (W_p). Thus, it needs to examine only the next stream completion times within W_p seconds from the arrival of the new request. Therefore, AEC may not give an expected time of service for each request. The prediction window introduces a tradeoff between the percentage of requests receiving expected times of service and prediction accuracy. Subsection 3.3.3 provides additional details on the implications of the value of the prediction window.

Figure 3.2 shows a simplified algorithm of AEC. This algorithm is performed upon the arrival of request R_i to video v_j when the server is fully loaded. If the server is not fully loaded, the request can be serviced immediately. The assigned time for video v ($assigned\_time[v]$) corresponds to the latest completion time (T_l) at which video v is expected to be serviced in Equation (3.2).

Figure 3.3 demonstrates the general idea of AEC. A new request for video 2 ($v2$) arrives at time T_{Now}. The server finds that video 1 ($v1$) is the expected video to be serviced at stream completion time $T1$. Then, the server examines the next completion time $T2$ (which is still within the prediction window) and determines that $v2$ is the most likely to be serviced at that time. Because $v2$ is the requested video for which we need to find the expected time of service, the prediction algorithm terminates by assigning $T2$ as the expected time of service to the new request.

The proposed AEC algorithm involves another important aspect: *prediction of stream completion times*. The server here uses aggressive prediction. It not only predicts how the completion times will be assigned to incoming requests but also predicts new stream completion times and assigns them if possible to new requests. When AEC assigns a stream completion time to a request as the expected time of service, it adds the expected completion time of the new stream to the set of the to-be examined

```
for (v = 0; v < N_v; v++) // Initialize the assigned time for each video
    assigned_time[v] = −1;
T = closest completion time; // Start with closest completion time
while (T < T_Now + W_p) { // Loop till prediction window is exceeded
    // Find expected video queue lengths
    for (v = 0; v < N_v; v++){
        if ( assigned_time[v] == −1) // video v has not been assigned an expected time
            expected_qlen[v] = (qlen[v] + λ[v] × (T − T_Now)) × def_rate[v];
        else // video v has been assigned an expected time
            expected_qlen[v] = λ[v] × (T − assigned_time[v]) × def_rate[v];
        Compute scheduling objective function for video v;
    } //for
    // Find the expected video to be served at time T
    expected_video = find video with the minimum objective function;
    if (expected_video == v_j){
        Assign T to request R_i as the expected service time;
        break; // Done
    }
    else
        assigned_time[expected_video] = T;
    T = next completion time; // Try again for this new completion time
} //while
```

Figure 3.2: Simplified Algorithm for the AEC Scheme [performed upon the arrival of request R_i to Video v_j]

completion times if its completion time falls within the prediction window. This aspect is challenging to implement efficiently, especially with ERMT, because the impacts of these new "predicted" streams on stream merging decisions should be considered in order to achieve accurate predictions. To isolate the actual request scheduling from prediction, the implementation creates a virtual running queue by duplicating the portion of the running stream queue containing all streams within the current prediction window. When a new stream is predicted to be scheduled at a certain completion time, its own completion time is inserted in the proper position in the virtual queue. Proper stream merging and potential stream extensions are performed on the virtual queue.

The following points serve as further clarifications of AEC. (1) The assignment of times of service is done based on predicting scheduling decisions, but the actual scheduling is kept totally isolated from prediction. Thus, scheduling is performed based on only the scheduling criterion and does not consider

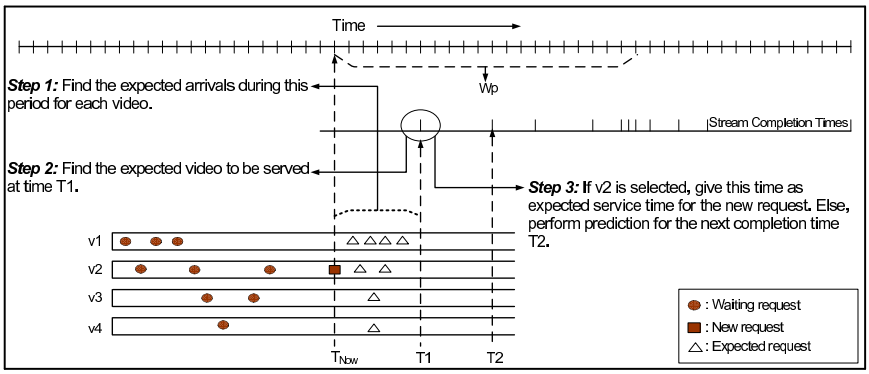

(a) Assignment of Completion Time T1

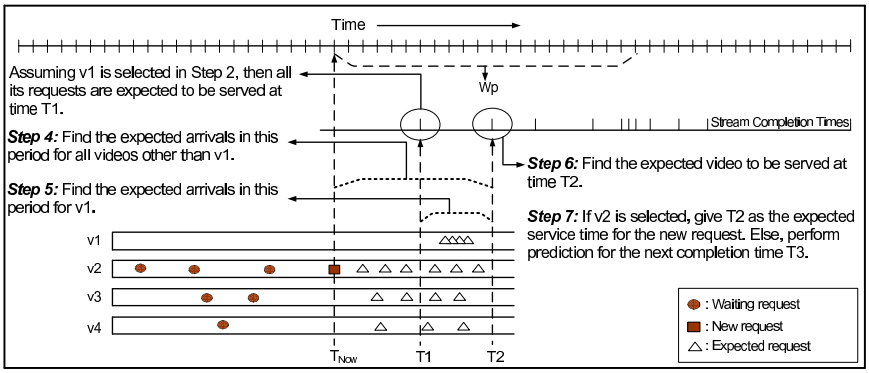

(b) Assignment of Completion Time T2

Figure 3.3: Clarification of the AEC Scheme

the assigned expected times of service in any way. (2) AEC may assign the same expected time to requests for different videos because the assignments are based on the current server state and workload, which vary with time. Similarly, the requests for the same video that are currently together in the waiting queue may have received different expected waiting times although they will be serviced together. Later requests in the queue are more likely to receive more accurate predictions. (3) Because of the prediction window constraint, AEC may not give an expected time for each user. As will be discussed in Subsection 3.3.4, the proposed hybrid scheme addresses this limitation.

3.3.2 Proposed Enhancements of AEC

We propose the following two enhancements of AEC: *Preferential Treatment of Real Requests* and *Refine Assigned Expected Times*.

Preferential Treatment of Real Requests

With AEC, the expected queue lengths are computed and used to predict future scheduling decisions. An expected queue length includes a number of real requests and a number of expected requests. This enhancement values real requests more than expected requests. One interesting way to implement this enhancement is to truncate the expected queue lengths in Equations (3.1) and (3.2). Thus, if a video has an expected queue length less than one, it will not be selected as an expected video to be serviced at any stream completion time.

Periodic Refinement of Assigned Expected Times

With this enhancement, the server periodically attempts to provide users with updated expected times of service. For a waiting request already assigned an expected time of service, a new time of service becomes available whenever a new request for the same video arrives and receives an expected time because all requests for the same video will be serviced concurrently using only one stream. The new expected time will most likely be more accurate than the old one because it is estimated based on the latest system state. To avoid unnecessary updates, this enhancement provides updated expected times only when a considerable difference exists between the new and old expected times. With the periodic refinement, some requests that never received expected times before may be able to get expected times later on as updates. Therefore, this enhancement is expected to improve both the prediction accuracy and the percentage of users receiving expected times. Unless otherwise indicated, the reported accuracy is determined based on the deviation of the initial expected service time and the actual time of service.

3.3.3 Feedback Control of the Prediction Window

In addition to limiting the implementation complexity, the prediction window introduces a tradeoff between the percentage of requests receiving expected times of service and the prediction accuracy. In particular, as the prediction window increases, the number of requests receiving expected times increases

at the expense of reducing the prediction accuracy as well as increasing the implementation complexity. The AEC algorithm computation time is proportional to the prediction window and can be shown to be $O(N_v \times W_p)$, where N_v is the number of videos. Subsection 3.5.4 analyzes the impact of the prediction window based on actual runs of the algorithm. Large prediction windows have negative impacts on the algorithm computation time and more importantly the prediction accuracy. The reduced prediction accuracy may have a serious impact on the user-perceived quality of service and the confidence of users in the provided expected waiting times. The prediction window in AEC is constrained because the proposed AEC algorithm does not predict the waiting times accurately beyond a certain value of the prediction window, and it is better to provide no prediction than to provide misleading or inaccurate waiting times.

We utilize feedback control theory to tune W_p to allow a pre-specified tolerance in the accuracy. Here, the administrator sets the minimum value of accuracy that can be tolerated. This value, called *setpoint*, can be specified in the form of the tolerable average deviation between the actual and expected times of service. Ideally, W_p should be set to the largest possible value that satisfies the setpoint in order to maximize the number of users receiving expected times. The loop control is driven by the *error* ($e(t)$), which is the difference between the setpoint and the actual average deviation (called the *process variable*).

For stable and accurate control, we use a *Proportional Integral Differential* (PID), as depicted in Figure 3.4(a), to adjust W_p based on the history and rate of change of the error. It has three components: proportional, integral, and differential. Each component is weighted by a constant. The proportional component changes W_p based on the immediate value of the error. The integral component considers the past values of the error, whereas the differential component anticipates the future, and thus they help reduce the steady state error and the overshoot, respectively.

To eliminate the problem of optimizing three constants in the PID Controller, we propose another controller, called *Exponential Controller*, which uses the power of the error, as shown in Figure 3.4(b).

The power of the error is used because when the error is small, W_p should be changed slightly to minimize overshooting and undershooting. When the error however, is large, W_p should be changed by large values to expedite the convergence to the desired setpoint. By extensive analysis, we found that the best function is $sign(e(t)) \times 2^{|e(t)|}$.

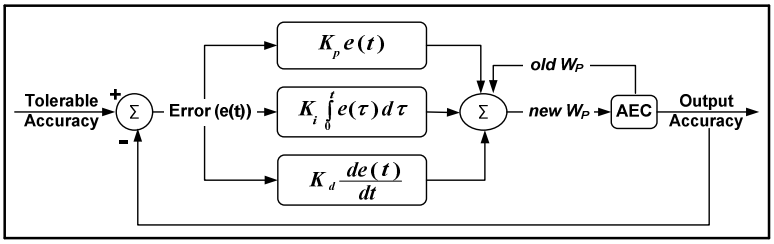

(a) PID Controller

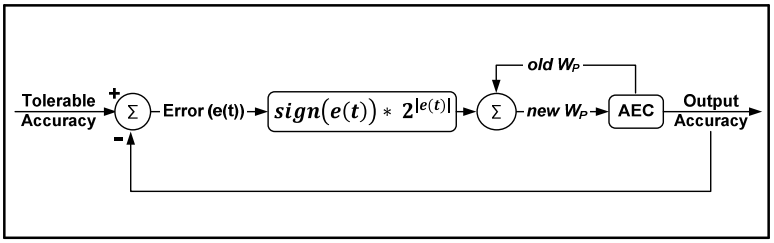

(b) Proposed Exponential Controller

Figure 3.4: Controllers of Prediction Accuracy

3.3.4 Proposed Hybrid Prediction Scheme

The main problem with the AEC scheme is that not all users may receive an expected time of service. To address this problem, we propose and analyze an alternative scheme, called *Hybrid Prediction,* which can give an expected time to each user. The hybrid scheme first uses AEC to predict the waiting time, and if no prediction is made, it provides the user with the average per-video waiting time. Thus, it can be thought of as a hybrid of AEC and APW. The use of APW enables the hybrid scheme to provide a predicted waiting times for each request at the expense of lower prediction accuracy. The prediction windows has an important impact on the accuracy of this hybrid predictor. As the prediction window increases, a larger fraction of users will receive expected times using AEC, which is more accurate than APW for small values of the prediction window.

3.4 Evaluation Methodology

We analyze the effectiveness of the proposed schemes through extensive simulation.

3.4.1 Workload Characteristics

Table 5.2 summarizes the workload characteristics used. Like most prior studies, we generally assume that the arrival of the requests to the server follows a Poisson Process with an average arrival rate λ. We also experiment with the Weibull distribution with two parameters: shape and scale [67] . We analyze the impact of the shape (k), while adjusting the scale so that the desired average request arrival rate is reached. Additionally, we assume that the access to videos is highly localized and follows a Zipf-like distribution. With this distribution, the probability of choosing the n^{th} most popular video is $C/n^{1-\theta}$ with a parameter θ and a normalized constant C. The parameter θ controls the skew of video access. Note that the skew reaches its peak when $\theta = 0$, and that the access becomes uniformly distributed when $\theta = 1$. We analyze the impact of this parameter, but we generally assume a value of 0.271 [66, 65].

We characterize the waiting tolerance of users by three models. In *Model A*, the waiting tolerance follows an exponential distribution with mean μ_{tol} [66, 65]. In *Model B*, users with expected waiting times less than μ_{tol} will wait, and the others exhibit the same waiting tolerance as Model A [66, 65]. We introduce *Model C* to capture situations in which users either wait or defect immediately depending on the expected waiting times. The user waits if the expected waiting time is less than μ_{tol} and defects immediately if the waiting time is greater than $2\mu_{tol}$. Otherwise, the defection probability increases linearly from 0 to 1 for the expected waiting times between μ_{tol} and $2\mu_{tol}$. In all these models, defections happen only while users are waiting for service.

We generally study a server with 120 videos, each of which is 120 minutes long. We examine the server at different loads by fixing the request arrival rate at 40 requests per minute and varying the number of channels (server capacity) generally from 300 to 750. In addition to the fixed-length video workload (in which all videos have the same length), we experiment with two variable-length video

workloads. Moreover, we study the impacts of arrival rate, user's waiting tolerance, number of videos, and video length (in the fixed-length workload).

Table 3.1: Summary of Workload Characteristics

Parameter	**Model/Value(s)**
Request Arrival	Poisson Process (Default) Weibull Distribution with shape k = 0.6 to 0.9
Request Arrival Rate (λ)	10 to 70 Requests/min, Default = 40 Requests/min
Server Capacity	300 to 750 channels
Video Access	Zipf-Like
Video Skew (θ)	0.1 to 0.6, Default = 0.271
Number of Videos	60 to 240, Default = 120
Video Length	Fixed-Length Video Workload (Default) with length of 30 to 120 min (same for all videos), Default = 120 min Variable-Length Video Workload 1: with lengths randomly in the range: 30 to 120 min Variable-Length Video Workload 2: with lengths randomly in the range: 100 to 200 min
Waiting Tolerance Model	A, B, and C
Waiting Tolerance Mean (μ_{tol})	15 to 90 sec, Default = 30 sec

3.4.2 Performance Metrics

We use two performance metrics to compare the effectiveness of various prediction schemes: *waiting-time prediction accuracy* and *percentage of clients receiving expected times of service* (PCRE). The *average deviation* between the expected and actual times of service is used as a measure of accuracy. The accuracy decreases with the deviation.

We compare the effectiveness of the predictive and GNSTF approaches in terms of the user defection probability, average waiting time, and unfairness against unpopular videos.

3.5 Result Presentation and Analysis

3.5.1 Waiting-Time Distribution under Various Scheduling Policies

Let us start by comparing the waiting-time distributions of requests resulting from various scheduling policies: FCFS, MQL, MCF-P (RAF), and MCF-P (RAP). Figure 3.5 depicts the overall waiting time distributions (considering all videos), and the waiting distributions of two individual videos with significantly varying popularities. Only the results for Patching with 600 server channels are shown. The results for Transition Patching and ERMT are similar, and thus not shown. The waiting times are distributed between 0 and 30 seconds because the waiting tolerance is set to 30 seconds. The waiting times with MCF-P (RAP) and MCF-P (RAF) are concentrated around 0 to 5 seconds in this example and decay quickly as we approach large values, in a manner similar to an exponential distribution. (Note that the numbers vary with the stream merging technique and server capacity but with similar behavior.) Moreover, the decay is faster for more popular videos. The waiting times with MQL follow the same pattern, but the decay happens less quickly. By contrast, FCFS produces a bell-shaped distribution. These results suggest that using the average value to predict the waiting time leads to the lowest accuracy in FCFS and the highest accuracy in MCF-P (RAF) and MCF-P (RAP).

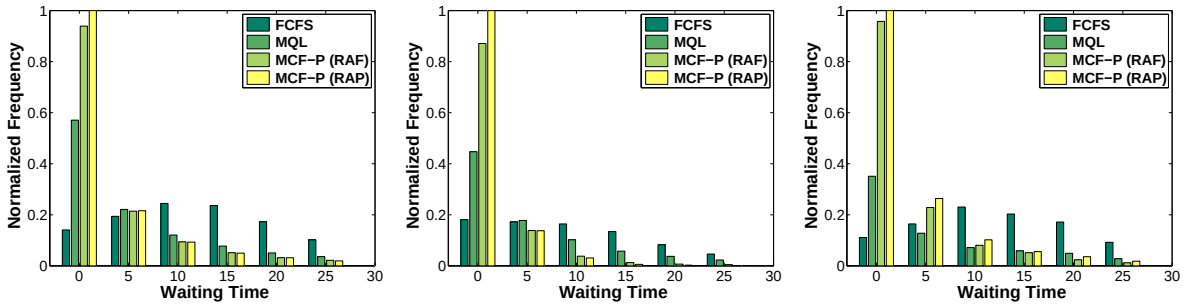

(a) All Videos (b) Video 1 (c) Video 10

Figure 3.5: Waiting Time Distribution [*Patching, 600 Channels, Model A*]

3.5.2 Waiting-Time Predictability and Effectiveness of Various Prediction Schemes

Let us now compare the effectiveness of the proposed prediction schemes in terms of accuracy, which is the most important metric in this case. Figures 3.6, 3.7, and 3.8 depict the average deviation results for ERMT, Transition Patching, and Patching under three different scheduling policies: MQL, MCF-P (RAF), and MCF-P (RAP). (FCFS, in the form of NSTF/GNSTF, is more suited for providing hard time-of-service guarantees than prediction. Subsection 3.5.8 analyzes the performance of GNSTF.) These figures demonstrate that AEC performs significantly better than APW and the results are better with more scalable stream merging. The deviation with AEC is within only two seconds. APW has the advantage of giving an expected time of service to each user, but the accuracy of these expectations is a more important factor. The hybrid scheme serves as a compromise between AEC and APW.

The two variants of MCF-P (RAF and RAP) perform very close to each other in accuracy. MCF-P, however, is more predictable than MQL because the scheduling decisions of MCF-P are based on both the queue lengths and the required stream costs, whereas MQL uses only the queue lengths. The required stream cost for a video can be determined precisely, but the queue lengths in the future require prediction, as done in Equations (3.1) and (3.2). Fortunately, MCF-P is not only more predictable than MQL but also achieves better performance (as shown in [22]) in terms of defection probability, average waiting time, and unfairness. From this point on, we consider only MCF-P (RAP) and refer to it simply as MCF-P.

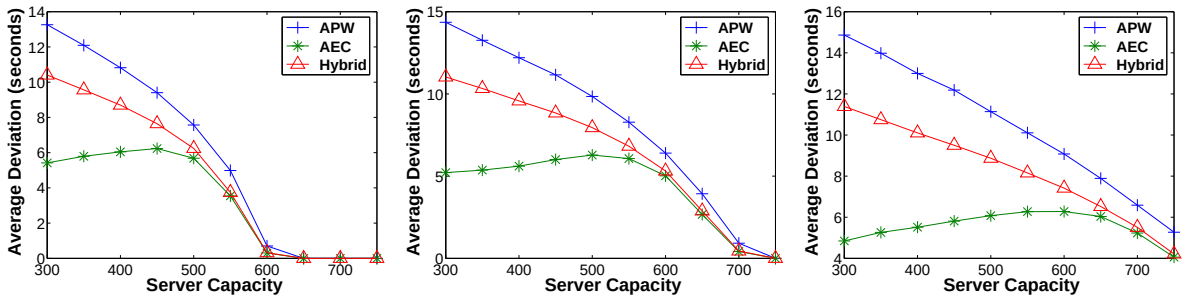

(a) ERMT (b) Transition Patching (c) Patching

Figure 3.6: Comparing the Accuracy of Prediction Schemes [*MQL*, $W_p = 0.5\mu_{tol}$, *Model A*]

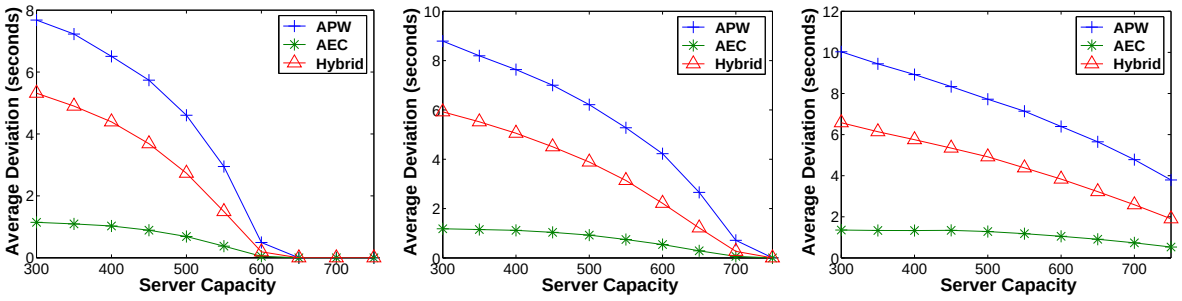

(a) ERMT, MCF-P (b) Transition Patching, MCF-P (RAF) (c) Patching, MCF-P (RAF)

Figure 3.7: Comparing the Accuracy of Prediction Schemes [$W_p = 0.5\mu_{tol}$, *Model A*]

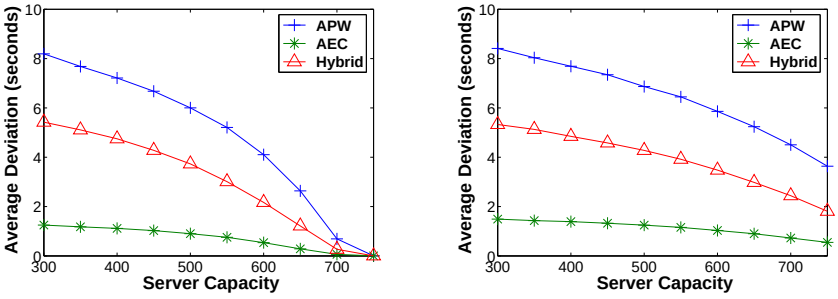

(a) Transition Patching (b) Patching

Figure 3.8: Comparing the Accuracy of Prediction Schemes [*MCF-P (RAP)*, $W_p = 0.5\mu_{tol}$, *Model A*]

3.5.3 Effectiveness of Further Enhancements

The effectiveness of the Preferential Treatment of Real Requests Enhancement is illustrated in Figure 3.9, which shows that this enhancement significantly improves PCRE, but at the expense of accuracy. It may be a good choice in certain situations, primarily because the deviation is within 3 seconds.

Figure 3.10 illustrates the effectiveness of the Periodic Refinement of Assigned Expected Times Enhancement in terms of the average deviation when the hybrid prediction scheme is used under the three stream merging techniques. The results are similar when AEC is used and thus not shown. The figure shows that the enhancement reduces the average deviation in Patching, Transition Patching, and ERMT by up to 24%, 18%, and 11%, respectively.

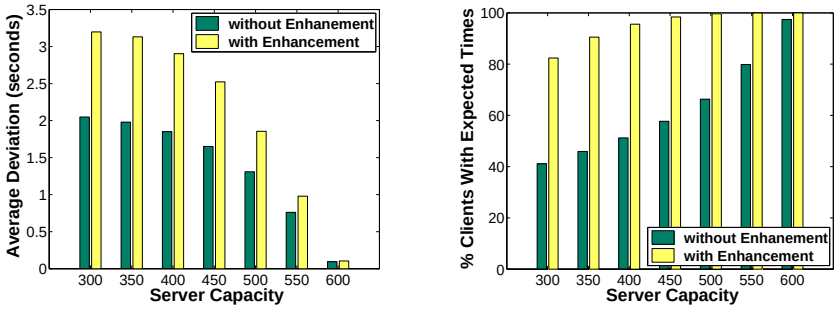

(a) Deviation (b) PCRE

Figure 3.9: Effectiveness of the Preferential Treatment of Real Requests Enhancement [*ERMT, MCF-P, AEC,* $W_p = \mu_{tol}$*, Model A*]

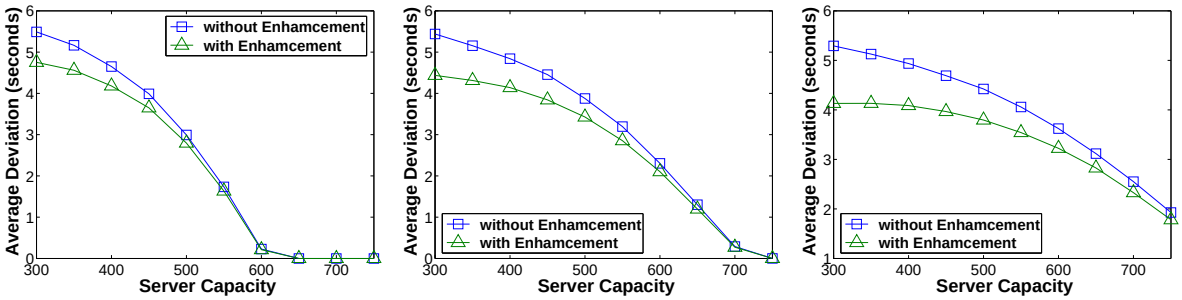

(a) ERMT, MCF-P (b) Transition Patching, MCF-P (RAP) (c) Patching, MCF-P (RAP)

Figure 3.10: Impact of the Periodic Refinement of Assigned Expected Times Enhancement on the Hybrid Prediction Scheme [$W_p = \mu_{tol}$*, Model A*]

3.5.4 Impact of Prediction Window

Figure 3.11(a) plots the impact of prediction window (W_p) in AEC on the prediction accuracy and PCRE for the three stream merging techniques. As expected, both the deviation and PCRE increase with W_p. PCRE significantly increases with W_p up to a certain point, after which it starts to increase slightly. Both these metrics generally improve with more scalable stream merging, except for large values of W_p. When the Preferential Treatment of Real Requests Enhancement is used, a significantly different behavior is observed, especially in the deviation, as shown in Figure 3.11(b). The deviation increases with W_p up to a certain point, after which it reaches a steady value. The impact of W_p in the case of the hybrid prediction scheme is shown in Figure 3.11(c). The accuracy increases with W_p up to a certain value and then starts to decrease. (Recall that the accuracy decreases with the deviation.) The increase

is due to increasing the fraction of clients receiving expected times by AEC (which is more accurate) rather than APW. After a certain value, the reduced accuracy of AEC with W_p becomes more dominant.

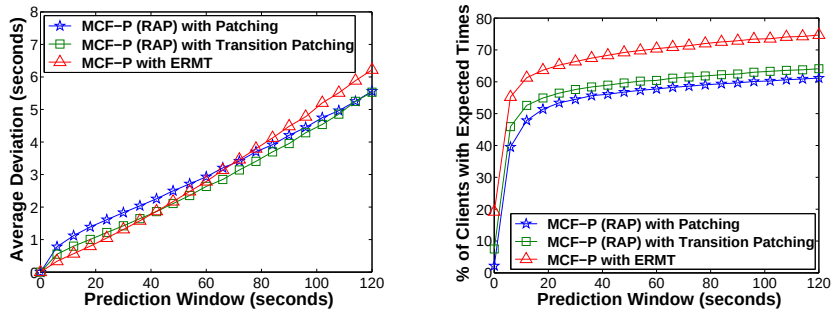

(a) AEC without Enhancement

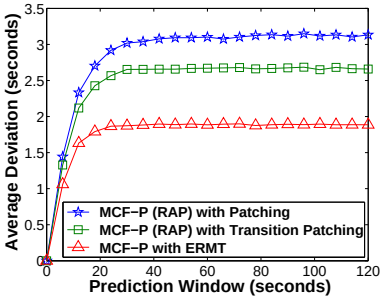

(b) AEC with Enhancement

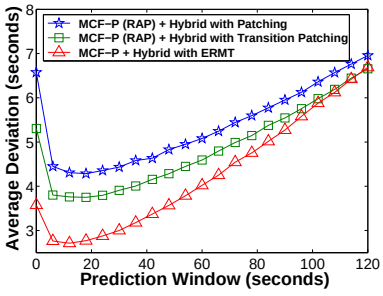

(c) Hybrid without Enhancement

Figure 3.11: Impact of Prediction Window without and with the Preferential Treatment of Real Requests Enhancement [*MCF-P, 500 Channels, Model A*]

Figure 3.12 demonstrates the impact of the prediction window on the average computation time of the AEC algorithm. The results are obtained by averaging the computation time values during the entire lifetime of the simulation. The figure illustrates the increased implementation complexity with the prediction window and indicates a linear relationship.

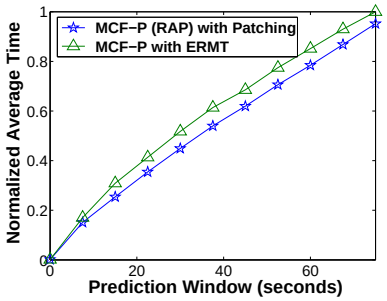

Figure 3.12: Impact of Prediction Window on Algorithm Computation Time [*AEC, 500 Channels, Model A*]

3.5.5 Analysis of Deviation Distributions under Various Prediction Schemes

So far, we compared various prediction schemes in only the average deviation. In this subsection, we discuss the distributions of the deviation results, so that we can compare various schemes in the range, standard deviation (σ), and confidence interval (CI). Figure 3.13 shows the distributions of the deviation for the three prediction schemes. The results for AEC and Hybrid are shown for two and three values of the prediction window, respectively. Table 3.2 shows the means, standard deviations, and the 90% confidence intervals for various schemes. As expected, AEC provides the smallest standard deviation, and the shortest confidence interval, and these values increase with the prediction window. Although the hybrid scheme performs better than APW in the average accuracy (as shown in Subsection 3.5.2), it provides comparable results to APW in terms of the standard deviation and the confidence interval. Note that the means of the distribution can be positive or negative. A negative value indicates a stronger negative deviation component, whereas a positive value indicates a stronger positive deviation component. A negative deviation means that a user waits shorter than expected, while a positive deviation means waiting longer than expected. It is possible to assign different weights for negative and positive deviations, but in this study we treat them equally. Accurate waiting times help users wait accordingly, so it may not be beneficial if the user waits less than expected because the user may be doing something else meanwhile. Finally, it is useful to study the relative deviation compared to the actual waiting time. Figure 3.14 compares the distributions of the deviation percentage of the three prediction algorithms. These results illustrate that the benefits of AEC, especially compared to APW, are more outstanding in terms the percentage deviation.

3.5.6 Impact of Workload Parameters on AEC Performance

Figures 3.15 and 3.16 show the impacts of request arrival rate, user's waiting tolerance, skew in video access (θ), number of videos, and video length on the effectiveness of AEC in terms of accuracy and PCRE, respectively. The deviation increases with the arrival rate but remains with 2 seconds even

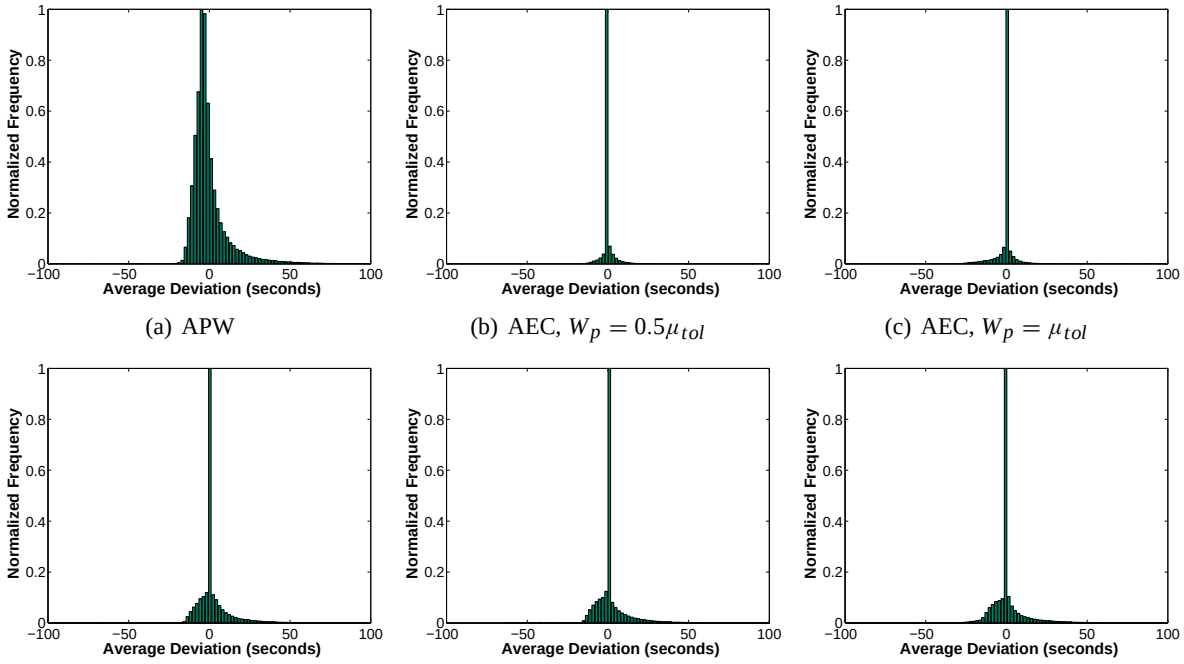

(a) APW (b) AEC, $W_p = 0.5\mu_{tol}$ (c) AEC, $W_p = \mu_{tol}$

(d) Hybrid,$W_p = 0.25\mu_{tol}$ (e) Hybrid, $W_p = 0.5\mu_{tol}$ (f) Hybrid, $W_p = \mu_{tol}$

Figure 3.13: Comparing the Deviation Distributions under Various Prediction Algorithms [*ERMT, MCF-P, 300 Channels, Model A*]

for up to 70 requests/minute. The deviation also increases at a relatively high rate with the waiting tolerance because requests stay longer in the waiting queue and queue lengths become harder to predict. We believe that smaller values of the mean waiting tolerance are more realistic because the expectations of users these days are getting much higher and their waiting tolerance is getting lower. PCRE decreases with the arrival rate but does not change much with the waiting tolerance.

The skew in video access has significant impacts on the average deviation and PCRE. Recall that as θ increases, the skew in video access decreases. Both the prediction accuracy and PCRE are worsen by the reduction in the skew. This is due to the reduced predictability of which video can be serviced at any particular time as the video access approaches the uniform distribution.

Finally, both the accuracy and PCRE also decrease with the number of videos and video length, primarily due to the increased load on the server, as can be noted by the increase in the user defection rate (not shown for space limitation). This behavior is consistent with the results in Subsection 3.5.2.

Table 3.2: Summary of Deviation Distributions [*ERMT, MCF-P, 300 Channels, Model A*]

Scheme	**Mean** (sec)	**Standard Deviation** (sec)	90% **Confidence Interval** (sec)
APW	-0.027	12.5604	[-14.0396,14.0104]
AEC, $W_p = 0.25\mu_{tol}$	0.4537	2.6762	[-1.5707,2.4793]
AEC, $W_p = 0.5\mu_{tol}$	0.2367	3.3914	[-3.8063,4.2437]
AEC, $W_p = \mu_{tol}$	-0.6131	5.2066	[-7.8732,6.6768]
Hybrid, $W_p = 0.25\mu_{tol}$	2.4055	11.7448	[-11.7366,16.5134]
Hybrid, $W_p = 0.5\mu_{tol}$	2.0781	11.6507	[-11.8441,16.0059]
Hybrid, $W_p = \mu_{tol}$	1.3027	11.8306	[-13.5439,16.1061]

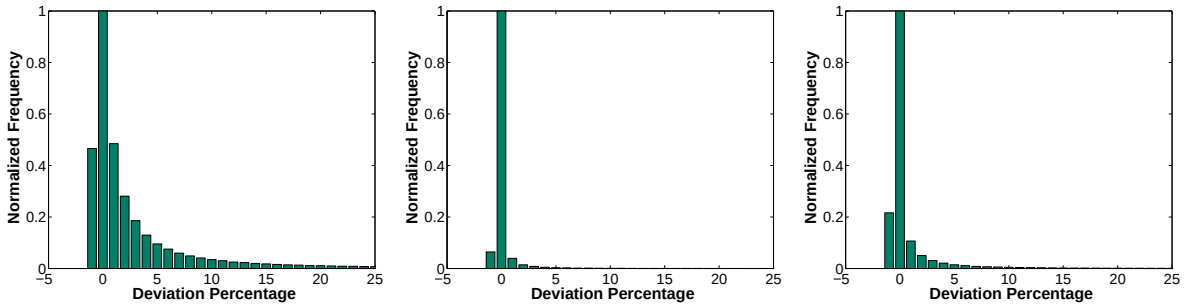

(a) APW (b) AEC (c) Hybrid

Figure 3.14: Comparing the Distributions of the Deviation Percentage [*ERMT, MCF-P,* $W_p = 0.5\mu_{tol}$*, 300 Channels, Model A*]

The increase in the server load as the number of videos increases happens as a result of the reduction in data sharing. Although the deviation increases with the number of videos, it remains with 2 seconds even for up to 240 supported videos.

The results so far are for a video workload of a fixed video length. Figure 3.17 shows the average deviation and PCRE results for two different variable-length workloads. The first is comprised of videos with lengths in the range of 30 to 120 minutes, whereas the lengths in the second range from 100 to 200 minutes. The length of each video is generated randomly within the specified range. The results for each workload are obtained by averaging the values of three runs. The AEC algorithm also works well in these workloads, with an average deviation within only 2.5 seconds. For workloads with longer videos, the server load becomes larger (as indicated in Figure 3.17(c)), and thus both the average deviation and PCRE become worse.

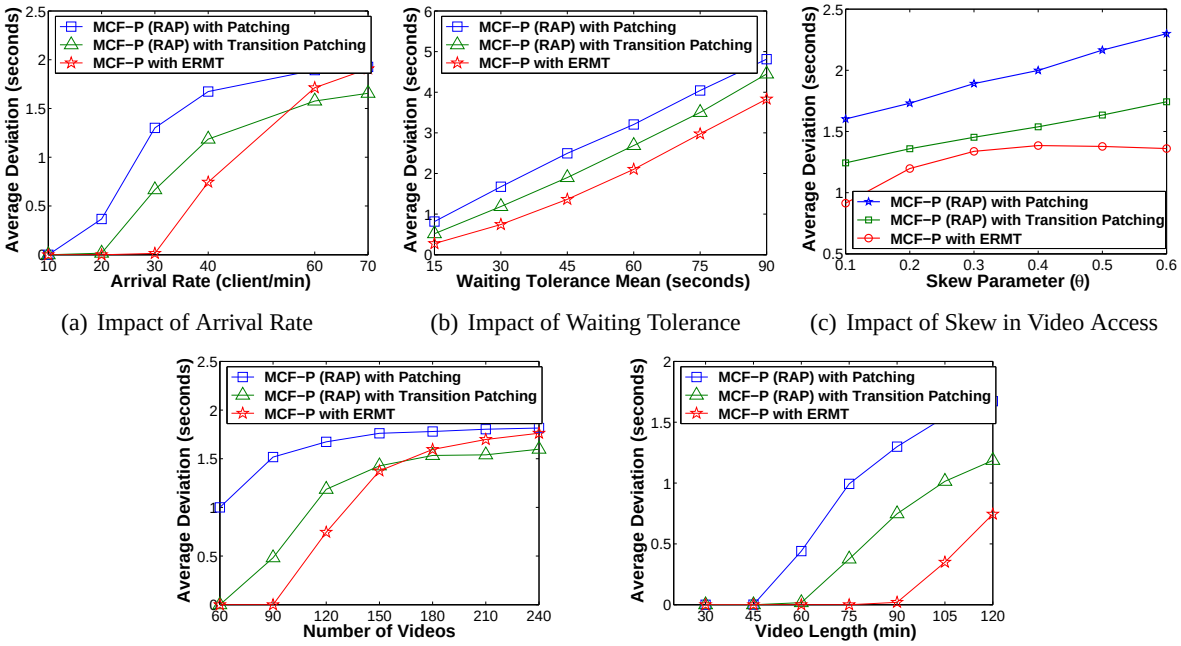

(a) Impact of Arrival Rate (b) Impact of Waiting Tolerance (c) Impact of Skew in Video Access

(d) Impact of Number of Videos (e) Impact of Video Length

Figure 3.15: Impact of Workload on Average Deviation [*AEC, 550 Channels,* $W_p = \mu_{tol}$*, Model A*]

The results so far assume a Poisson request arrival process. Let us now examine the behavior under Weibull distribution with different shape (k) values. Figure 3.18 demonstrates that the waiting times can still be predicted accurately with the AEC algorithm. The shape has a little impact, especially when the prediction window is smaller than 35 seconds.

3.5.7 Feedback Control of the Prediction Window in AEC

Let us now discuss the effectiveness of using the proposed controller of the prediction window, when the AEC scheme is used. Figure 3.19 demonstrates how the PID Controller can effectively achieve five desired accuracy values (setpoints): 0.5, 1.5, 2.5, 3.5, and 4.5 seconds with different stream merging techniques. By dynamically tuning W_p to the largest possible value that satisfies the setpoint, the PID Controller ensures the largest possible value of PCRE. As the tolerable accuracy increases from 0.5 to 4.5, PCRE increases by more than 39%, 46%, and 93% with ERMT, Transition Patching, and Patching respectively. The system administrator should consider this significant implication of the setpoint on PCRE. Figure 3.20 shows how that the Exponential Controller behaves close to the PID Controller. The

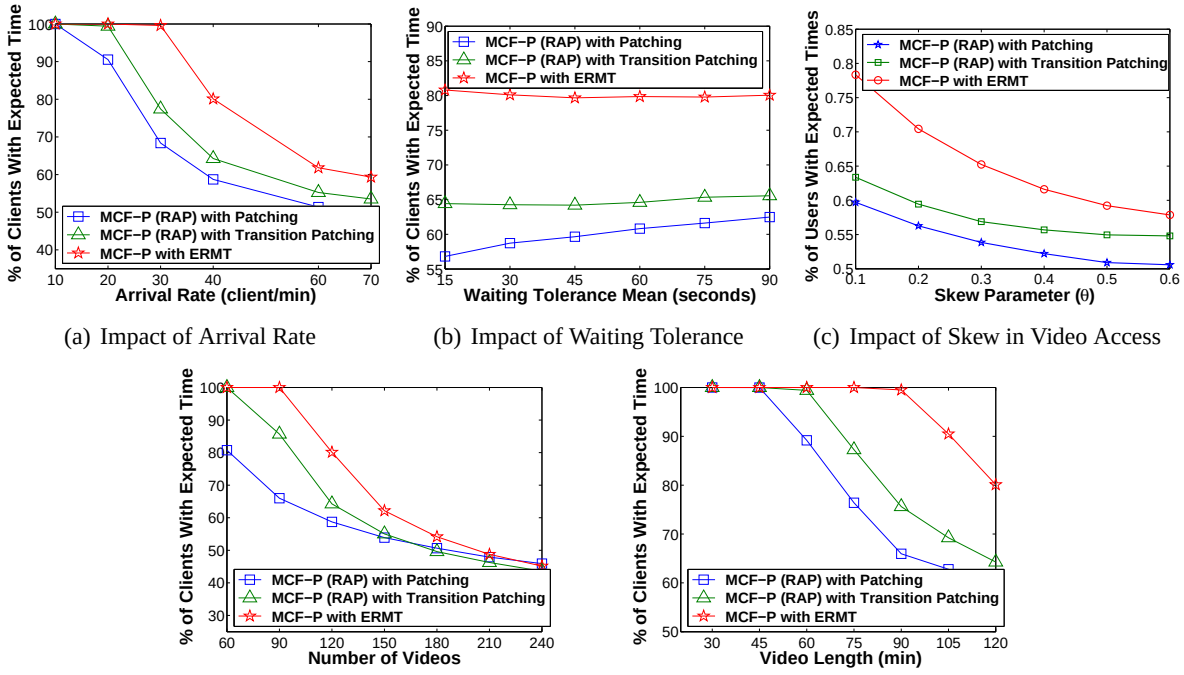

(a) Impact of Arrival Rate (b) Impact of Waiting Tolerance (c) Impact of Skew in Video Access

(d) Impact of Number of Videos (e) Impact of Video Length

Figure 3.16: Impact of Workload on PCRE [*AEC, 550 Channels,* $W_p = \mu_{tol}$*, Model A*]

PID Controller has a little advantage over the Exponential for small setpoints, where it achieves larger PCRE because it has a slightly larger overshoot and is a little faster in reaching the desired setpoint.

3.5.8 Effectiveness of the Waiting-Time Prediction Approach Compared with GNSTF

As discussed earlier, GNSTF is a scheduling policy that performs request scheduling based on the schedule times, which are initially assigned on a FCFS basis. The proposed waiting-time prediction approach allows the application of aggressive cost-based scheduling policies and hierarchical stream merging techniques (such as MCF-P and ERMT, respectively). In this subsection, we demonstrate the implications of the predictive approach on improving system performance in terms of the overall user defection rate and average waiting time. The prediction approach here is applied with MCF-P and this combination is referred to as "Predictive MCF-P". Figures 3.21 and 3.22 compare the two approaches in user defection probability, average waiting time, and unfairness for Model B and C of the waiting tolerance, respectively. Three variants of Predictive MCF-P are analyzed. The first two apply

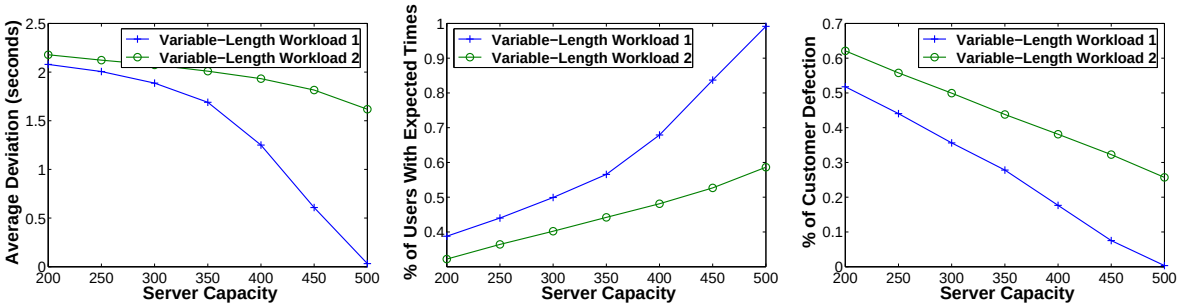

(a) Average Deviation (b) PCRE (c) User Defection Rate

Figure 3.17: Impact of Variable-Length Video Workloads [*AEC, ERMT, MCF-P,* $W_p = \mu_{tol}$*, Model A*]

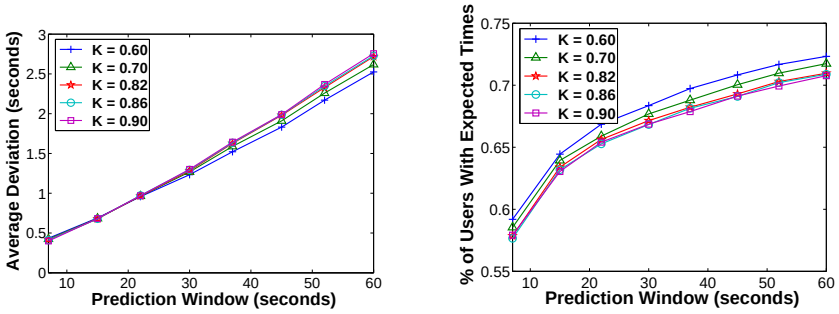

(a) Average Deviation (b) PCRE

Figure 3.18: Impact of the Shape Parameter of Weibull Arrival Distribution [*AEC, ERMT, MCF-P,* $W_p = \mu_{tol}$*, 500 Channels, Model A*]

AEC prediction scheme, whereas the third applies the hybrid. The best implementation of GNSTF (GNSTFo-MQL) is used to ensure a fair comparison. These results demonstrate that predictive MCF-P performs significantly better than GNSTF under both tolerance models in terms of the two most important performance metrics. The relative performance among the different predictive MCF-P variants depends on the tolerance model. Under Model B, the hybrid scheme leads to the least defection rate and the longest waiting time among various variants. With model C, however, it leads to the shortest waiting time and the highest defection rate. Under both models, the RAP and RAF variants perform very close to each other in the two most important metrics

Finally, Figure 3.23 captures the fact that GNSTF cannot be applied with ERMT, whereas the waiting-time prediction approach can. The figure compares GNSTF and two variants of predictive

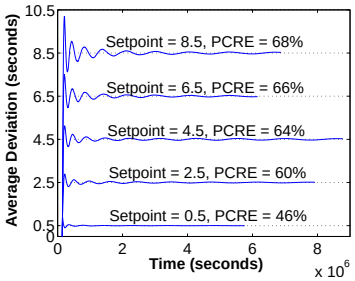

(a) *ERMT*, MCF-P, 450 Channels

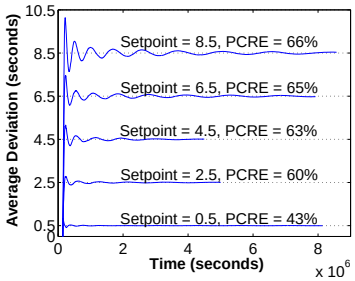

(b) *Transition Patching*, MCF-P (RAP), 500 Channels

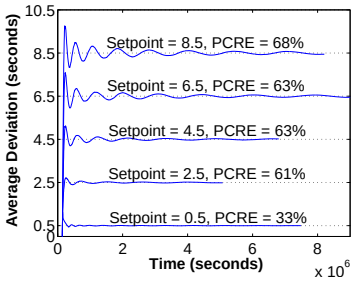

(c) *Patching*, MCF-P (RAP), 550 Channels

Figure 3.19: Effectiveness of PID Controller using different Average Deviation Setpoints [*AEC, Model A*, $K_p = 7$, $K_i = 1$, $K_d = 0.1$]

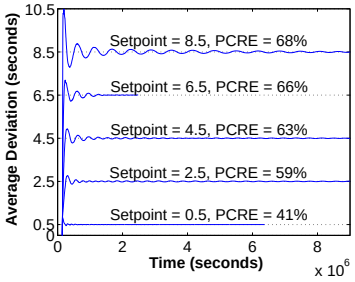

(a) *ERMT*, MCF-P, 450 Channels

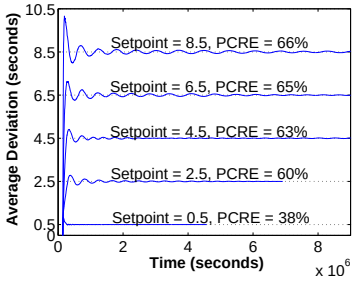

(b) *Transition Patching*, MCF-P (RAP), 500 Channels

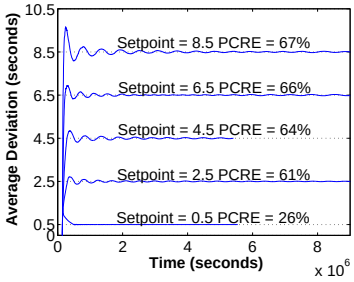

(c) *Patching*, MCF-P (RAP), 550 Channels

Figure 3.20: Effectiveness of Exponential Controller using different Average Deviation Setpoints [*AEC, Model A*]

MCF-P (AEC and Hybrid), when each is applied with the most scalable stream merging technique that is applicable to it. Here, only the results under Model C (which is more realistic) are shown. Model B exhibits a similar behavior. The results demonstrate the outstanding performance gains achieved by applying the prediction approach in terms of the two most important performance metrics. The two variants perform generally close to each other.

3.6 Conclusions

We have analyzed the waiting-time predictability in scalable video streaming and have presented two prediction schemes: *Assign Expected Stream Completion Time* (AEC) and *Hybrid Prediction*. AEC utilizes detailed information about the server state and considers the applied scheduling policy to predict

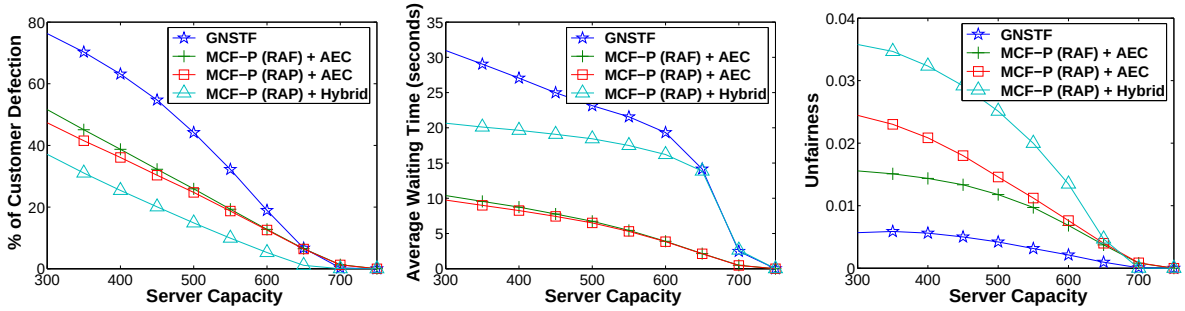

(a) Defection Rate (b) Waiting Time (c) Unfairness

Figure 3.21: Comparing GNSTF with Predictive MCF-P (Three Variants) [*Transition Patching*, $W_p = 0.5\mu_{tol}$, *Model B*]

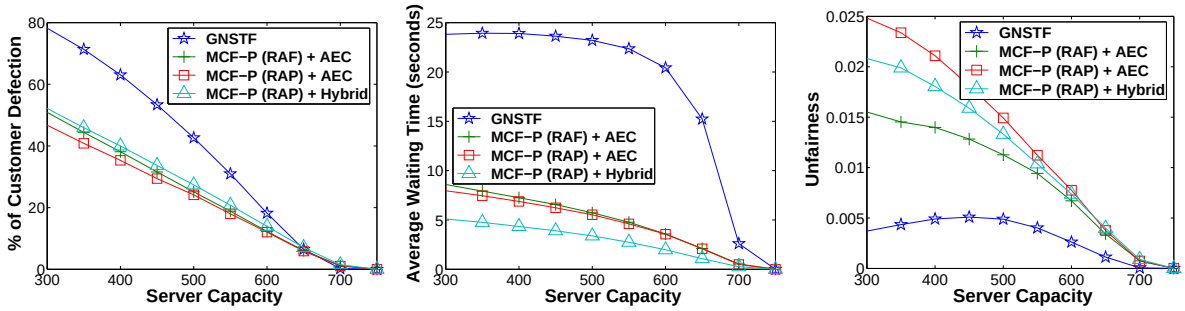

(a) Defection Rate (b) Waiting Time (c) Unfairness

Figure 3.22: Comparing GNSTF with Predictive MCF-P (Three Variants) [*Transition Patching*, $W_p = 0.5\mu_{tol}$, *Model C*]

the future scheduling decisions over a certain period, called *prediction window*. This window introduces a tradeoff between the prediction accuracy and the number of users receiving expected waiting times. The hybrid scheme uses AEC and then assigns the average video waiting time for those requests that did not obtain a predicted time by AEC.

We have analyzed the effectiveness of the two prediction schemes when applied with various stream merging techniques and scheduling policies. We have also compared the effectiveness of the waiting-time prediction approach with the approach that provides time-of-service guarantees. The latter is represented by an extended policy, called *Generalized Next Schedule Time First* (GNSTF). In addition, we have studied the impacts of prediction window, server capacity, user's waiting tolerance, arrival rate, skew in video access, video length, and number of videos.

The main results can be summarized as follows.

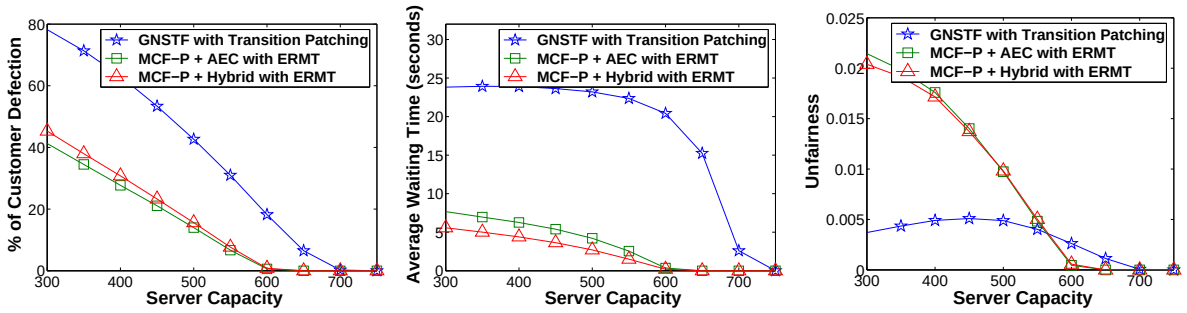

(a) Defection Rate (b) Waiting Time (c) Unfairness

Figure 3.23: Comparing GNSTF and Predictive MCF-P (Two Variants), Each with Its Most Scalable Stream Merging Technique [$W_p = \mu_{tol}$, *Model C*]

- The waiting time can be predicted accurately, especially with AEC and when MCF-P is used. MCF-P is not only highly predictable (in terms of user waiting time) but also achieves the best performance in server throughput and average waiting time.
- In contrast with AEC, the hybrid prediction scheme provides expected times to each user but achieves lower accuracy and a longer confidence interval.
- Combining AEC or the hybrid scheme with MCF-P leads to outstanding performance benefits, compared with GNSTF.
- This combination, called *Predictive MCF-P*, can be applied with hierarchical stream merging techniques (such as ERMT) to improve performance further, whereas GNSTF cannot.

CHAPTER 4

INCREASING SYSTEM BANDWIDTH UTILIZATION BY ENHANCING SCHEDULING DECISIONS IN VIDEO-ON-DEMAND SYSTEMS

4.1 Introduction

Motivated by the development of cost-based scheduling, we investigate its effectiveness in detail and discuss opportunities for further tunings and enhancements. In particular, we initially seek to answer the following two important questions. First, is it better to consider the stream cost only at the current scheduling time or consider the expected overall cost over a future period of time? Second, should the cost computation consider future stream extensions done by advanced stream merging techniques (such as ERMT) to satisfy the needs of new requests? These questions are important because the current scheduling decision can affect future scheduling decisions, especially when stream merging and cost-based scheduling are used.

Additionally, we analyze the effectiveness of incorporating video prediction results into the scheduling decisions. The prediction of videos to be serviced and the prediction of waiting times for service have recently been proposed in chapter 3. These prediction results, however, were not used to alter the scheduling decisions. We propose a scheduling policy, called *Predictive Cost-Based Scheduling* (PCS). Like MCF, PCS is cost-based, but it predicts future system state and uses the prediction results to potentially alter the scheduling decisions. It delays servicing requests at the current scheduling time (even when resource are available) if it is expected that shorter streams will be required at the next scheduling time. We present two alternative implementations of PCS.

We also propose an enhancement technique, called *Adaptive Regular Stream Triggering* (ART), which can be applied with any scheduling policy to enhance stream merging. The basic idea of ART is to selectively delay the initiation of full-length video streams.

We study the effectiveness of various strategies and design options through extensive simulation in terms of performance effectiveness as well as waiting-time predictability. The analyzed metrics include customer defection (i.e. turn-away) probability, average waiting time, unfairness against unpopular videos, average cost per request, waiting-time prediction accuracy, and percentage of clients receiving expected waiting times. The waiting-time prediction accuracy is determined by the average deviation between the expected and actual waiting times. We consider the impacts of customer waiting tolerance, server capacity, request arrival rate, number of videos, video length, and skew in video access. We also study the impacts of different request arrival processes and video workloads. Furthermore, in contrast with prior studies, we analyze the impact of flash crowds, whereby the arrival rate experiences sudden spikes.

The results demonstrate that the proposed PCS and ART strategies significantly enhance system throughput and reduces the average waiting time for service, while providing accurate predicted waiting times.

The rest of the chapter is organized as follows. Section 4.2 analyzes cost-based scheduling and explores alternative ways to compute the cost. Sections 4.3 and 4.4 present the proposed PCS and ART strategies, respectively. Section 4.5 discusses the performance evaluation methodology and Section 4.6 presents and analyzes the main results.

4.2 Analysis of Cost-Based Scheduling

We seek to understand the behavior of cost-based scheduling and its interaction with stream merging. Understanding this behavior helps in developing solutions that optimize the overall performance. One of the issues that we explore in this study is determining the duration over which the cost should be computed. In particular, we seek to determine whether the cost should be computed only at the current scheduling time (T_{Now}) or over a future duration of time, called *prediction window* (W_p). In other words, should the system select the video with the least cost per request at time T_{Now} or the least cost per request

during W_p. The latter requires prediction of the future system state. We devise and explore two ways to analyze the effectiveness of computing the cost over a period of time: *Lookahead* and *Combinational* scheduling.

4.2.1 Lookahead Scheduling

In Lookahead Scheduling, the service rate (which is the rate at which a video gets serviced) is computed dynamically for each video that has waiting requests. The total cost for servicing each one of these videos is computed during the time interval W_p. Lookahead Scheduling selects the video j that minimizes the expected cost per request. Thus, the objective function to minimize is

$$F(j) = \frac{\sum_{i=1}^{n} C_i}{\sum_{i=1}^{n} N_i}, \tag{4.1}$$

where n is the number of expected service times for video j during W_p, C_i is the cost required to service the requests for video j at service time i, and N_i is the number of requests expected to be serviced at service time i. The number of requests at future service times is predicted by dynamically computing the arrival rate for each video. Figure 4.1 further illustrates the idea. As discussed earlier, ERMT may extend streams to satisfy the needs of new requests. MCF-P, however, does not consider later extensions in computing the cost. In analyzing cost-based scheduling, we also need to consider whether it is worthwhile to predict and consider these later extensions. Hence, we consider a variant of Lookahead Scheduling that considers these extensions. (In Figure 4.1, the term “virtual time” means the the future time imagined or simulated by Lookahead Scheduling, as opposed to the actual system time.)

4.2.2 Combinational Scheduling

In contrast with Lookahead Scheduling, Combinational Scheduling predicts the best sequence in which various videos should be serviced and performs scheduling based on this sequence. Thus, it

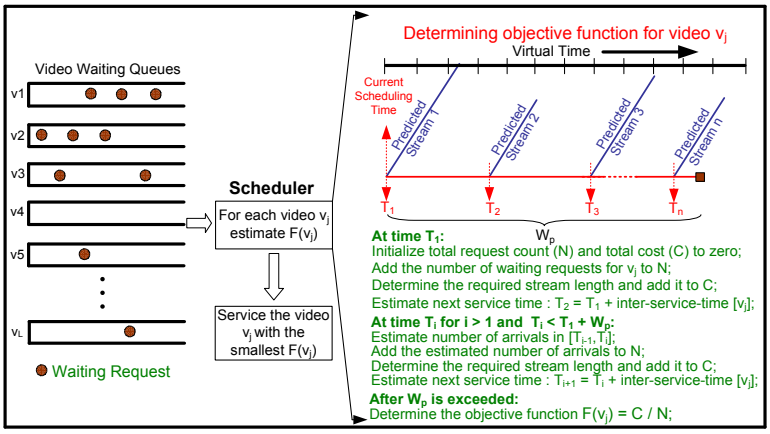

Figure 4.1: An Illustration of Lookahead Scheduling

considers any correlations on the cost among successive video selections. Figure 4.2 illustrates the operation of Combinational Scheduling. The best sequence is found by generating all possible sequences for the next n stream completion times during W_p, for only the n-best videos according to the MCF-P objective function. Note that stream completion times indicate when server channels become available for servicing new requests. The objective function of each sequence is then calculated. Consider the sequence $S_j = \{X_1, X_2, X_3, ..., X_n\}$, where X_i is the video selected to be serviced at the next i^{th} stream completion time. The objective function for this sequence is

$$F(S_j) = \frac{\sum_{i=1}^{n} C_{X_i}}{\sum_{i=1}^{n} N_{X_i}}, \tag{4.2}$$

where C_{X_i} is the cost required to service video X_i, and N_{X_i} is the number of waiting requests for that video. C_{X_i} is determined based on the used MCF-P variant. Combinational Scheduling chooses the sequence that is expected to lead to the least overall cost. Although many optimizations are possible to reduce the implementation complexity, we focus primarily on whether exploiting the correlations between successive video selections is indeed important in practical situations.

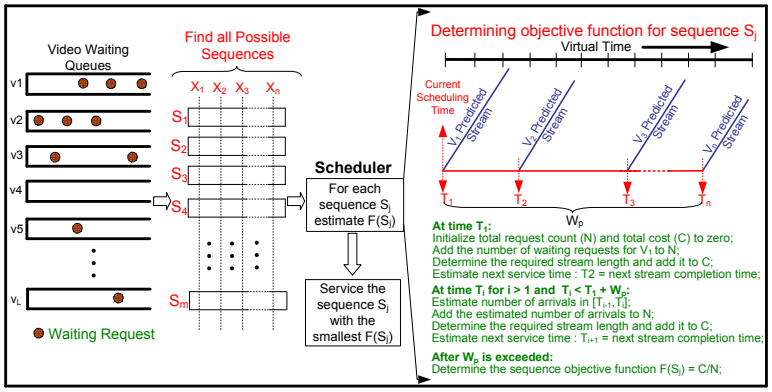

Figure 4.2: Illustration of Combinational Scheduling

4.3 Proposed Predictive Cost-Based Scheduling

The prediction of videos to be serviced and the prediction of waiting times for service have been proposed in Chapter 3. These prediction results, however, were not used to alter the scheduling decisions. In this study, we analyze the effectiveness of incorporating video prediction results into the scheduling decisions. We propose a scheduling policy, called *Predictive Cost-Based Scheduling* (PCS). PCS is based on MCF, but it predicts future system state and uses this prediction to possibly alter the scheduling decisions. The basic idea can be explained as follows. When a channel becomes available, PCS determines using the MCF-P objective function the video V_{Now} which is to be serviced tentatively at the current scheduling time (T_{Now}) and its associated delivery cost. To avoid unfairness against videos with high data rates, we use the required stream length for the cost [22]. Before actually servicing that video, PCS predicts the system state at the next scheduling time (T_{Next}) and estimates the delivery cost at that time assuming that video V_{Now} is not serviced at time T_{Now}. PCS does not service any request at time T_{Now} and thus postpone the service of video V_{Now} if the delivery cost at time T_{Next} is lower than that at time T_{Now}. Otherwise, video V_{Now} is serviced immediately.

To reduce possible server underutilization, PCS delays the service of streams only if the number of available server channels ($freeChannels$) is smaller than a certain threshold ($freeChannelThresh$).

Figure 4.3 shows a proposed algorithm to dynamically find the best value of $freeChannelThresh$. The algorithm changes the value of the threshold and observes its impact on customer defection probability over a certain time interval. The value of the threshold is then updated based on the trend in defection probability (increase or decrease) and the last action (increase or decrease) performed on the threshold. The algorithm is to be executed periodically but not frequently to ensure stable system behavior.

```
currDefectionRate = defectedCustomers/servedCustomers;
if (currDefectionRate < lastDefectionRate) {
   if (last action was decrement and freeChannelThresh > 2)
      freeChannelThresh − −;
   else if (last action was increment)
      freeChannelThresh + +;
} else if (currDefectionRate > lastDefectionRate){
   if (last action was increment and freeChannelThresh > 2)
      freeChannelThresh − −;
   else if (last action was decrement)
      freeChannelThresh + +;
}
lastDefectionRate = currDefectionRate;
```

Figure 4.3: Simplified Algorithm for Dynamically Computing *freeChannelThresh*

We present two alternative implementations of PCS: *PCS-V* and *PCS-L*. These two implementations differ in how to compute the delivery cost or required stream length at the next scheduling time. PCS-V predicts the video to be serviced at the next scheduling time and simply uses its required stream length. The video prediction is done by utilizing detailed information about the current state of the server in a manner similar to that of the waiting-time prediction approach in Chapter 3. This information includes the number of waiting requests for each video, the completion times of running streams, and statistics such as the average request arrival rate for each video (which is to be updated periodically). Figure 4.4 shows a simplified algorithm for PCS-V.

In contrast with PCS-V, PCS-L computes the expected required stream length at the next scheduling time based on the lengths of all possible video streams that may be required and their probabilities. A simplified algorithm for PCS-L is shown in Figure 4.5. The probability that a video is selected is equal to the probability that it has at least one waiting request at time T_{Next} times the probability that all video

```
V_Now = find the video that will tentatively be serviced at T_Now;
if ( freeChannels ≥ freeChannelThresh)
   Service the requests for V_Now;
else {
   currStreamLen = find required stream length to service V_Now at T_Now;
   V_Next = find the video that is expected to be serviced at T_Next;
   nextStreamLen = find required stream length to service V_Next at T_Next;
   if (currSreamLen ≤ nextStreamLen)
      Service the requests for V_Now;
}
```

Figure 4.4: Simplified Algorithm for PCS-V

streams with lower cost (i.e. shorter required streams) are not selected. The probability that video v has at least one arrival during duration $T_{Next} - T_{Now}$ can be found as one minus the probability of exactly zero arrivals:

$$1 - e^{-\lambda_v \times (T_{Next} - T_{Now})}, \tag{4.3}$$

where λ_i is the request arrival rate for video v and assuming a Poisson arrival process. If the video has already one waiting request, then this probability is 1. Sorting the videos according to the scheduling objective function is required to determine the probability that all videos with lower cost (or higher objective) are not selected.

As can be clearly seen from the algorithms, both PCS-V and PCS-L require a time overhead of $O(N_v)$, where N_v is the number of videos, assuming that that a priority queue structure is used to rank the videos according to the objective function.

4.4 Proposed Adaptive Regular Stream Triggering (ART)

As will be shown later, our analysis reveals a significant interaction between stream merging and scheduling decisions. One of the pertaining issues is how to best handle regular (i.e., full) streams. MCF-P (RAP) considers the cost of a regular stream as a patch and thus treats it in a differentiated manner. The question arises as to whether it is worthwhile, however, to delay regular streams in certain situations. Guided by analysis, we propose a technique, called *Adaptive Regular Stream Triggering*

```
V_Now = find the video that will tentatively be serviced at T_Now;
if ( freeChannels ≥ freeChannelThresh)
   Service the requests for V_Now;
else {
   currStreamLen = find required stream length to service V_Now at T_Now;
   Calculate objective function for each video at T_Next;
   Sort videos from best to worst according to objective function;
   expectedStreamLen = 0; // initialization
   // loop to find expected stream length at T_Next
   for (v = 0; v < N_v ; v++){ // for each video
      nextStreamLen = find required stream length to service v at T_Next;
      Prob(video v is selected) = Prob(no other video with better objective is selected)
            * Prob(video v has at least one arrival);
      expectedStreamLen +=Prob(video v is selected ) * nextStreamLen;
   }
   if (currSreamLen ≤ expectedStreamLen)
      Service the requests for V_Now;
}
```

Figure 4.5: Simplified Algorithm for PCS-L

(ART). A possible implementation is shown in Figure 4.6. The basic idea here is to delay regular streams as long as the number of free channels is below a certain threshold, which is to be computed dynamically based on the current workload and system state. ART uses the same algorithm (shown in Figure 4.3) to dynamically find the best value of $freeChannelThresh$ as that of PCS.

```
V_Now = find the video that will be serviced at T_Now;
if ( freeChannels ≥ freeChannelThresh)
     Service the requests for V_Now;
else {
     currStreamLen = find the required stream length to serve V_Now at T_Now;
     if (currStreamLen < movieLen) // not a full stream
          Service the requests for V_Now;
     else //full stream
          Postpone the requests for V_Now;
}
```

Figure 4.6: Simplified Implementation of ART

To further demonstrate the main idea of ART, Figure 4.7 plots the ERMT merge tree without and with ART, respectively. The solid lines show the initial stream lengths and the dotted lines show later extensions. The circles identify successive extensions. With ART, there is a gap before a regular stream

is initiated because of the postponement. We also observe that ART enhances the stream merging decisions of ERMT. The number of initial regular streams (called *I Streams* in this study) in the merge tree is relatively much smaller with ART. For example, there is only one *I Stream* in the merge tree with ART while there are many more *I Streams* in the merge tree without ART.

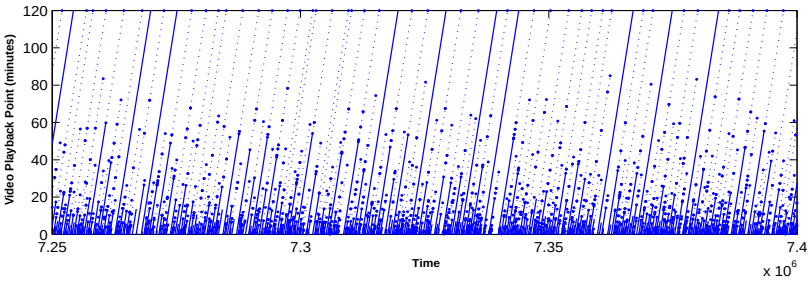

(a) MCF-P without ART

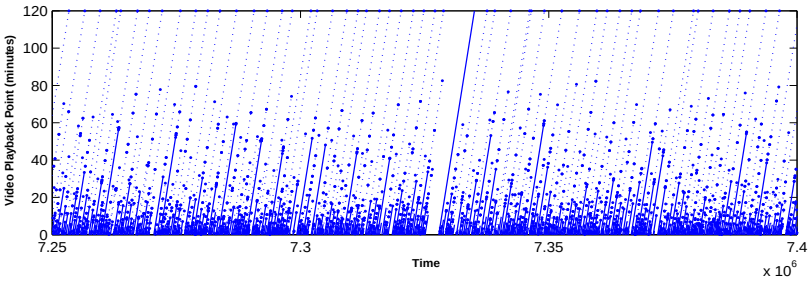

(b) MCF-P with ART

Figure 4.7: Impact of ART on ERMT Stream Merge Tree [*Video 11, MCF-P, Server Capacity = 450*]

As can be seen form the ART algorithm in Figure 4.6, ART requires a time overhead of $O(1)$ in addition to the time overhead of the base scheduling policy used.

In principle, ART can be used with any scheduling policy, including PCS, although some negative interference happens when it is combined with PCS, as will be shown in Section 4.6.

4.5 Evaluation Methodology

We study the effectiveness of the proposed policies through simulation. The simulation, written in C, stops after a steady state analysis with 95% confidence interval is reached.

4.5.1 Workload Characteristics

Table 4.1 summarizes the workload characteristics used. Like most prior studies, we generally

Table 4.1: Summary of Workload Characteristics

Parameter	**Model/Value(s)**
Request Arrival	Poisson Process (default) Weibull Distribution with shape $k = 0.6$ to 0.9
Request Arrival Rate	Variable, Default is 40 Req./min
Server Capacity	200 to 750 channels
Video Access	Zipf-Like
Video Skew (θ)	0.1 to 0.6, Default = 0.271
Number of Videos	Variable, Default is 120
Video Length	Fixed-Length Video Workload (Default) with length of 60 to 180 min (same for all videos), Default = 120 min Variable-Length Video Workload: with lengths randomly in the range: 60 to 180 min
Waiting Tolerance Model	A, B, C, Default is A
Waiting Tolerance Mean (μ_{tol})	Variable, Default is 30 sec
Flash Crowds	The peak arrival rate is 40 times the normal rate for a period of two movie lengths and flash crowds arrival rate is variable. Default: no flash crowds

assume that the arrival of the requests to the server follows a Poisson Process with an average arrival rate λ. We also experiment with the Weibull distribution with two parameters: shape and scale [68]. We analyze the impact of the shape (k), while adjusting the scale so that the desired average request arrival rate is reached. Additionally, we assume that the access to videos is highly localized and follows a Zipf-like distribution. With this distribution, the probability of choosing the nth most popular video is $C/n^{1-\theta}$ with a parameter θ and a normalized constant C. The parameter θ controls the skew of video access. Note that the skew reaches its peak when $\theta = 0$, and that the access becomes uniformly distributed when $\theta = 1$. We analyze the impact of this parameter, but we generally assume a value of 0.271 [66, 65].

We characterize the waiting tolerance of customers by three models. In *Model A*, the waiting tolerance follows an exponential distribution with mean μ_{tol} [66, 65]. In *Model B*, users with expected waiting times less than μ_{tol} will wait and the others will have the same waiting tolerance as Model A [66, 65]. We use *Model C* from Chapter 3 to capture situations in which users either wait or defect

immediately depending on the expected waiting times. The user waits if the expected waiting time is less than μ_{tol} and defects immediately if the waiting time is greater than $2\mu_{tol}$. Otherwise, the defection probability increases linearly from 0 to 1 for the expected waiting times between μ_{tol} and $2\mu_{tol}$.

As in most previous studies, we generally study a server with 120 videos, each of which is 120 minutes long. We examine the server at different loads by fixing the request arrival rate at 40 requests per minute and varying the number of channels (server capacity) generally from 200 to 750. In addition to the fixed-length video workload (in which all videos have the same length), we experiment with a variable-length video workload. Moreover, we study the impacts of arrival rate, user's waiting tolerance, number of videos, and video length (in the fixed-length workload).

Flash crowds workload characteristics were adopted from [69].

4.5.2 Considered Performance Metrics

To evaluate the effectiveness of the proposed schemes, we consider the main performance metrics discussed in Section 2.1. In addition, we analyze waiting-time predictability by two metrics: waiting-time prediction accuracy and the percentage of clients receiving expected waiting times. The waiting-time prediction accuracy is determined by the average deviation between the expected and actual waiting times. For waiting-time prediction, we use the algorithm in Chapter 3. Note that this algorithm may not provide an expected waiting time to each client because the prediction may not always be performed accurately.

4.6 Result Presentation and Analysis

4.6.1 Comparing the Effectiveness of Different Cost-Computation Alternatives

Let us start by studying the effectiveness of Lookahead and Combinational Scheduling. Interestingly, there is no clear benefit for computing the cost over a future period of time. In some cases, as shown in Figure 4.8, the performance in term of customer defection and average waiting time may be worse than

those when computing the cost at the current scheduling time with MCF-P. The results of Lookahead Scheduling are shown for two different prediction window values. Only the results with future stream extensions are shown. The results without extensions are almost the same.

Although computing the cost over a time interval seems intuitively to be an excellent choice, it interferes negatively with stream merging. Later in this study, we discuss how the interaction between stream merging and scheduling can be utilized by using the proposed ART technique, which can be used with any scheduling policy. Based on these results, we only consider next computing the cost at the current scheduling time.

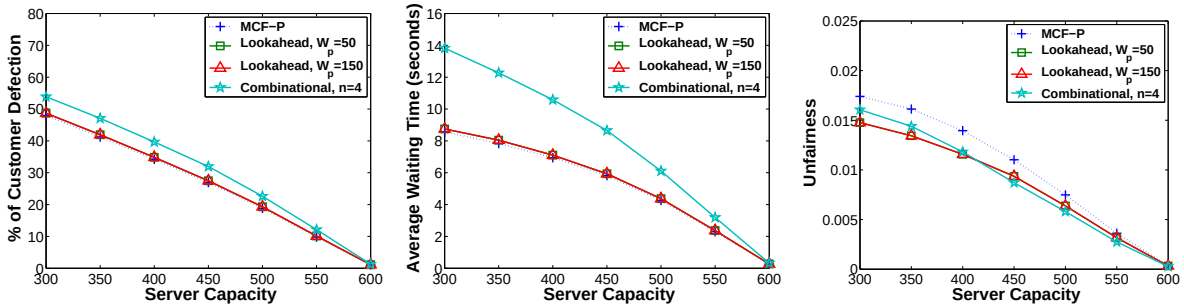

(a) Defection Rate (b) Average Waiting Time (c) Unfairness

Figure 4.8: Effectiveness of Lookahead and Combinational Scheduling [*ERMT*]

4.6.2 Effectiveness of the Proposed PCS Policy

Figures 4.9, 4.10, and 4.11 demonstrate the effectiveness of the two implementations of PCS when applied with ERMT, Transition Patching, and Patching, respectively, in terms of the customer defection probability, average waiting time, and unfairness. The figures shows that PCS outperforms MCF-P and MQL in terms of both the two most important performance metrics (defection probability and average waiting time), whereas MCF-P is fairer towards unpopular videos. The two implementations of PCS perform nearly the same and thus PCS-V is preferred because of its simplicity. From this point on, we consider only the PCS-V implementation.

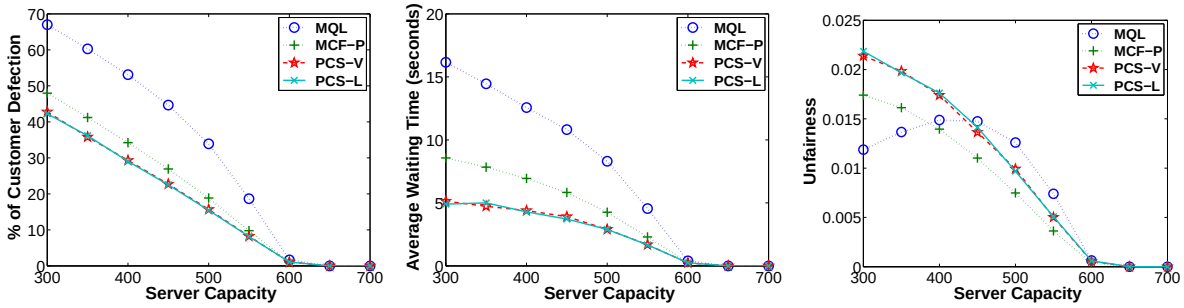

(a) Defection Rate (b) Average Waiting Time (c) Unfairness

Figure 4.9: Effectiveness of PCS [*ERMT*]

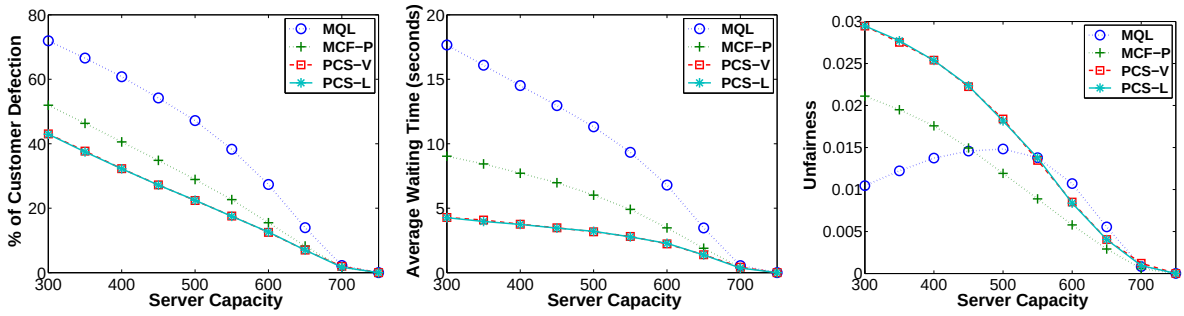

(a) Defection Rate (b) Average Waiting Time (c) Unfairness

Figure 4.10: Effectiveness of PCS [*Transition Patching*]

4.6.3 Effectiveness of the Proposed ART Enhancement

Figure 4.12 shows the effectiveness of the proposed ART technique when ERMT is used. With MCF-P, ART reduces the customer defection probability and average waiting time by up to 25% and 80%, respectively. It also yields significant improvements when used with MQL. Unfairness, the least important metric, is a little larger with ART because of its nature in favoring videos with shorter streams, but it is still acceptable compared with MQL.

Figure 4.13 depicts the impact of ART on regular streams in ERMT. We observe that when ART postpones regular streams, it forces ERMT to make more merges, which in turn, increases system utilization. We also observe that the number of regular streams does not decrease significantly despite of postponing these streams. In contrast, Figure 4.13(a) indicates that the average time between two

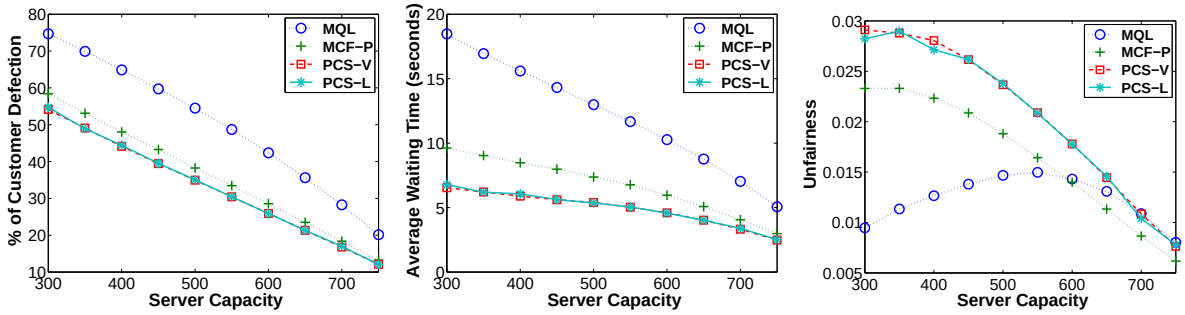

(a) Defection Rate (b) Average Waiting Time (c) Unfairness

Figure 4.11: Effectiveness of PCS [*Patching*]

successive regular streams for popular videos is even smaller with ART than that without it. This is because ERMT keeps extending streams, which eventually become regular streams. Figures 4.13(b) and 4.13(c) compare the percentage of initial regular streams (I Streams) and extended regular streams (E Streams) without and with ART, respectively. We can see that the percentage of extended regular streams with ART is much higher. This supports the fact that the number of regular streams is not reduced by postponing. In summary, we can say that ART improves ERMT by replacing many *I Streams* with *E Streams*.

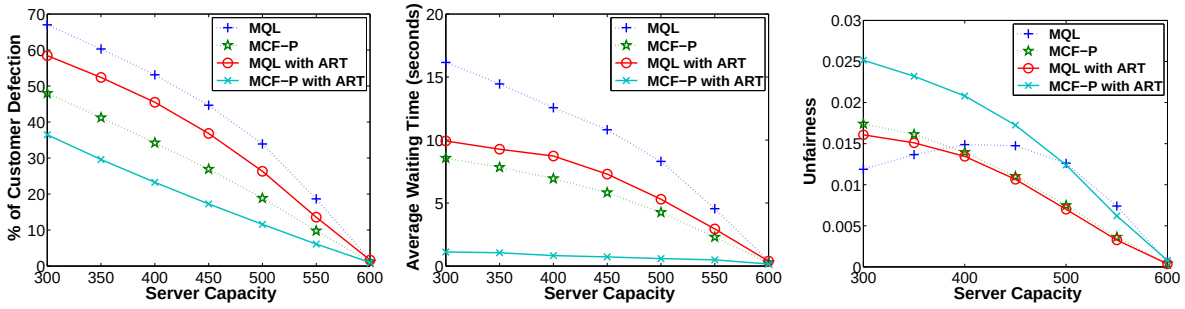

(a) Defection Rate (b) Average Waiting Time (c) Unfairness

Figure 4.12: Effectiveness of ART [*ERMT*]

Let us now discuss the impact of ART when Transition Patching and Patching are used. Transition Patching results are presented in Figure 4.14 and Patching results are presented in Figure 4.15. As with ERMT, ART reduces significantly the customer defection probability and the average waiting time

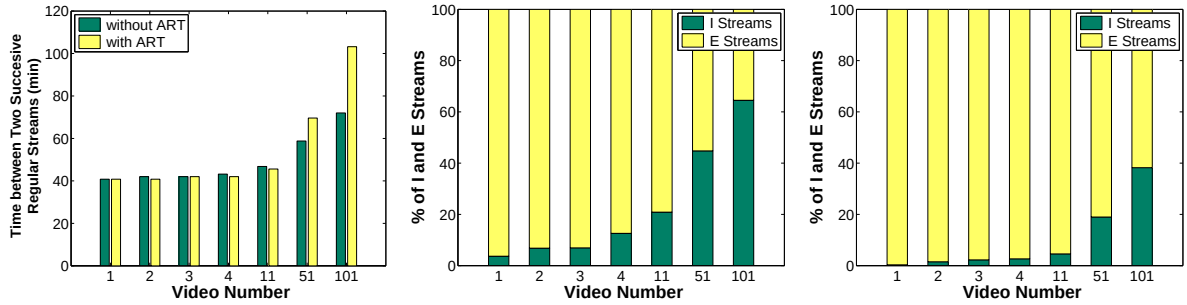

(a) Avg. Time between Two Regular Streams (b) Initial and Extended Regular Streams without ART (c) Initial and Extended Regular Streams with ART

Figure 4.13: Impact of ART on Regular Streams [*ERMT, MCF-P, Server Capacity = 450*]

when it is combined with MCF-P and MQL. Unfairness with ART is a little larger but still acceptable compared with that of MQL for medium and high server capacities.

Interestingly, ART improves Transition Patching and Patching despite that their best scheduling policy, MCF-P (RAP), depends on a conflicting principle. As discussed earlier, MCF-P (RAP) gives preference to regular streams while ART postpones them in certain situations. As illustrated in Figure 4.16, the main impact of ART is dynamically optimizing Wr, which is larger than that of MCF-P (RAP) and smaller than that of MCF-P (RAF) for popular videos, and even greater than that of MCF-P (RAF) for unpopular videos. The horizontal line in the figure marks the equation-based value of Wr [70]. (Note that the equation does not yield optimum values because it is based on important simplifying assumptions.)

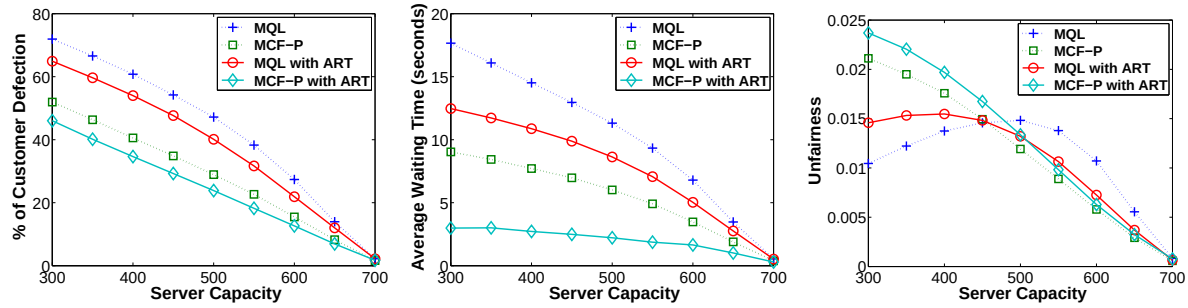

(a) Defection Rate (b) Average Waiting Time (c) Unfairness

Figure 4.14: Effectiveness of ART [*Transition Patching*]

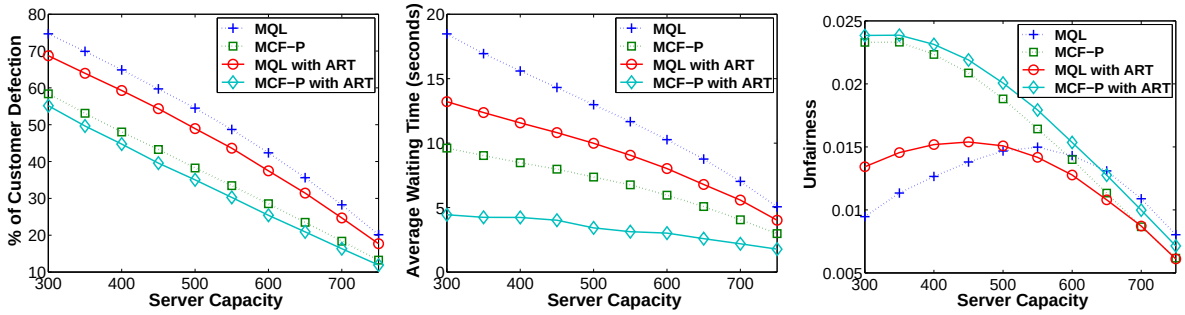

(a) Defection Rate (b) Average Waiting Time (c) Unfairness

Figure 4.15: Effectiveness of ART [*Patching*]

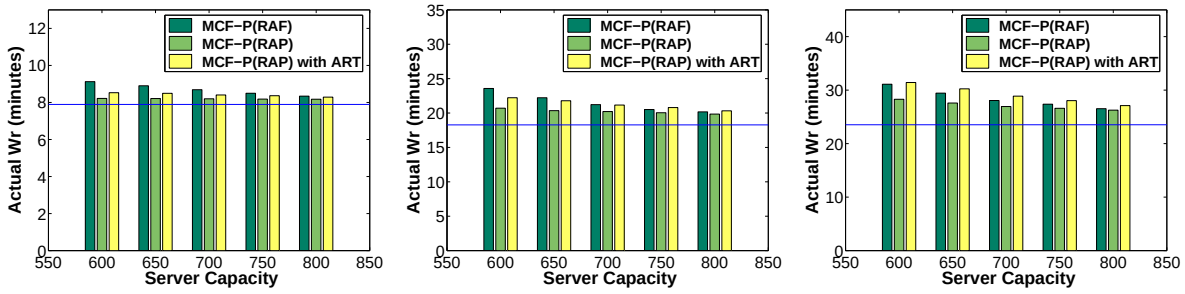

(a) Video 1 (b) Video 10 (c) Video 20

Figure 4.16: Comparing Actual *Wr* in MCF-P (RAF), MCF-P (RAP), and MCFP(RAP) with ART [*Patching*]

4.6.4 Comparing the Effectiveness of PCS and ART

Although ART can be applied with any scheduling policy, including PCS, for the time being, we consider it as an alternative to PCS because of negative interference between the two, as will be shown in Subsection 4.6.8. In this subsection, we compare the effectiveness of PCS-V and ART in terms of customer defection probability, average waiting time, unfairness against unpopular videos, and cost per request. Figures 4.17, 4.18, and 4.19 shows the results of ERMT, Transition Patching, and Patching respectively.

With ERMT, MCF-P when combined with ART performs better than PCS-V in terms of the customer defection probability and average waiting time. The results when Transition Patching and Patching are used exhibit different behavior than those with ERMT. MCF-P combined with ART gives almost the

same results as PCS-V in terms of customer defection probability, but it reduces the average waiting time significantly. Unfairness of PCS-V is less than that with ART in all stream merging techniques because ART favors videos with shorter streams more than PCS-V. These results indicate that MCF-P when combined with ART is the best overall performer.

To further support the fact that more customers are served with only one stream when using ART, Figure 4.20 demonstrates the impact of ART on the cost per request. We can see that the cost per request with ART is the lowest for different server capacities.

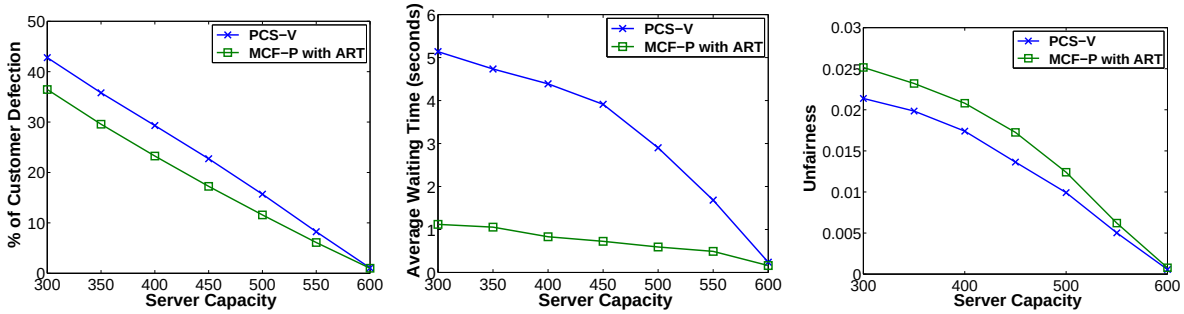

(a) Defection Rate (b) Average Waiting Time (c) Unfairness

Figure 4.17: Comparing the Effectiveness of PCS and ART [*ERMT*]

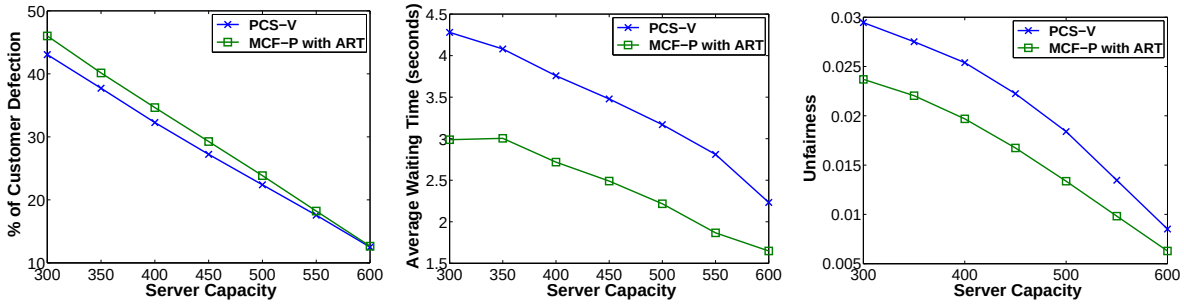

(a) Defection Rate (b) Average Waiting Time (c) Unfairness

Figure 4.18: Comparing the Effectiveness of PCS and ART [*Transition Patching*]

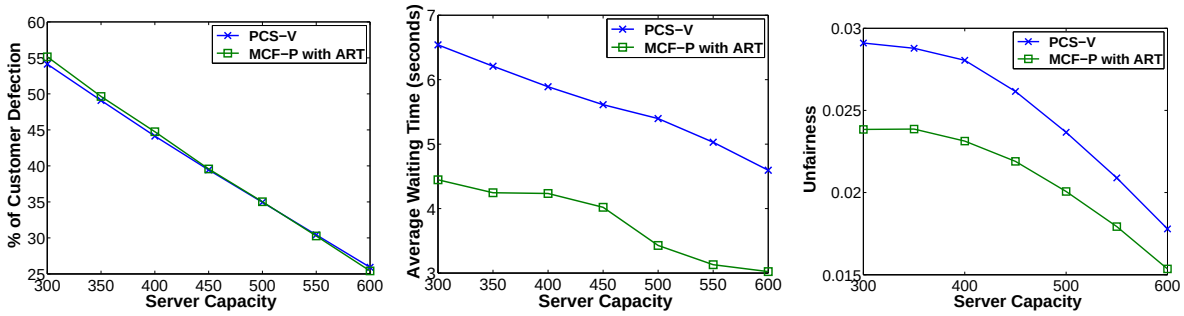

(a) Defection Rate (b) Average Waiting Time (c) Unfairness

Figure 4.19: Comparing the Effectiveness of PCS and ART [*Patching*]

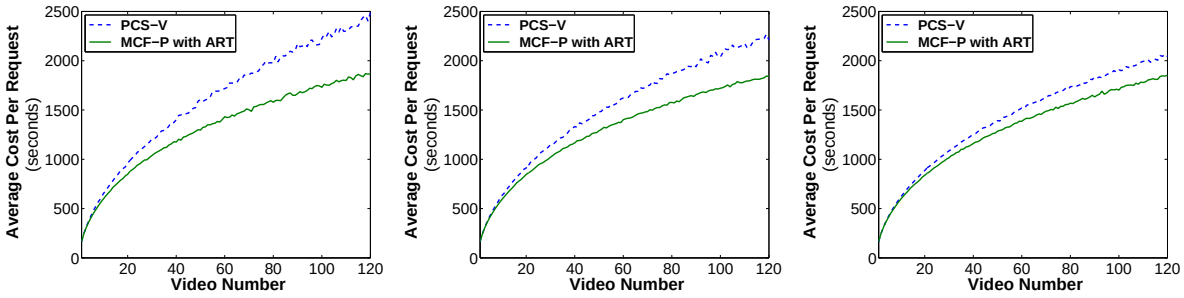

(a) 300 channel (b) 400 channel (c) 500 channel

Figure 4.20: Comparing the Impacts of PCS and ART on Cost per Request [*ERMT, MCF-P*]

4.6.5 Impact of Workload Parameters on the Effectiveness of PCS and ART

Figures 4.21, 4.22, 4.23, and 4.24 illustrate the impact of the request arrival rate, customer waiting tolerance, number of videos and video length on the effectiveness of PCS-V and ART. The results for both Patching and ERMT are shown. The results demonstrate that ART always achieves smaller customer defection probability and average waiting time than PCS-V in the case of ERMT. In Patching, the same trend is observed for the average waiting time, but PCS-V and "MCF-P combined with ART" perform nearly the same in terms of customer defection probability, especially when the server is highly loaded.

Figure 4.25 shows that the skew in video access has significant impacts on the customer defection probability, average waiting time and unfairness. Recall that as θ increases, the skew in video access

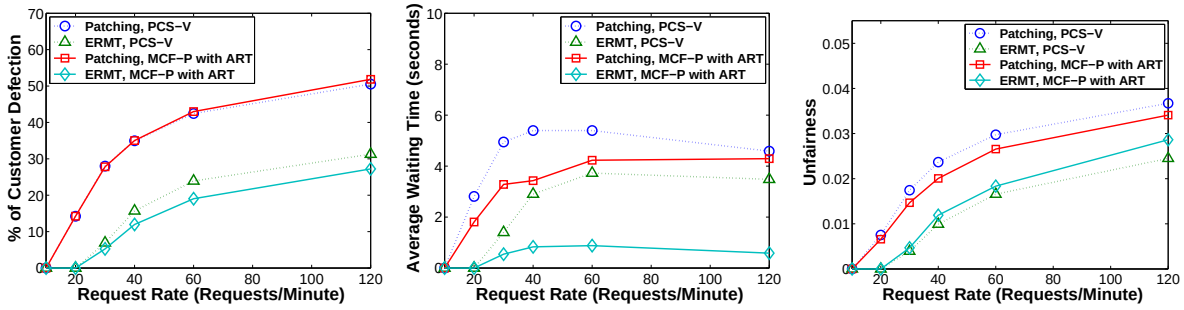

(a) Defection Rate (b) Average Waiting Time (c) Unfairness

Figure 4.21: Impact of Request Arrival Rate [*Server Capacity = 500*]

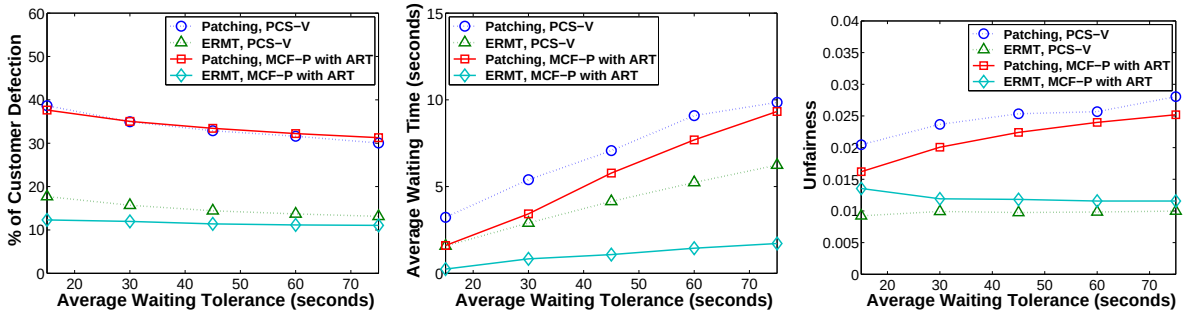

(a) Defection Rate (b) Average Waiting Time (c) Unfairness

Figure 4.22: Impact of Customer Waiting Tolerance [*Server Capacity = 500*]

decreases. Both the defection probability and average waiting time are worsen by the reduction in the skew. This is because cost-based scheduling policies favor popular videos by nature. When θ increases, the deference in video popularity decreases which in turn make the scheduling decision harder to make. Unfairness decreases by increasing θ which is as expected. Again, "MCF-P combined with ART" is the best policy in term of all performance metrics, except unfairness.

The results so far are for a video workload of a fixed video length. Figure 4.26 shows the customer defection probability, average waiting time and unfairness results for a variable-length video workload. The workload is comprised of videos with lengths in the range of 60 to 180 minutes. The length of each video is generated randomly within the specified range. The results for the workload are obtained by averaging the values of four runs. The PCS-V and ART algorithms also work well in this workload.

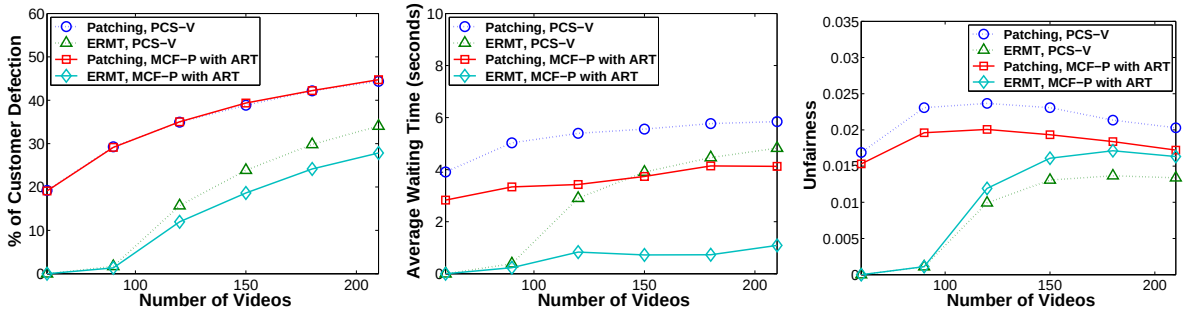

(a) Defection Rate (b) Average Waiting Time (c) Unfairness

Figure 4.23: Impact of Number of Videos [*Server Capacity = 500*]

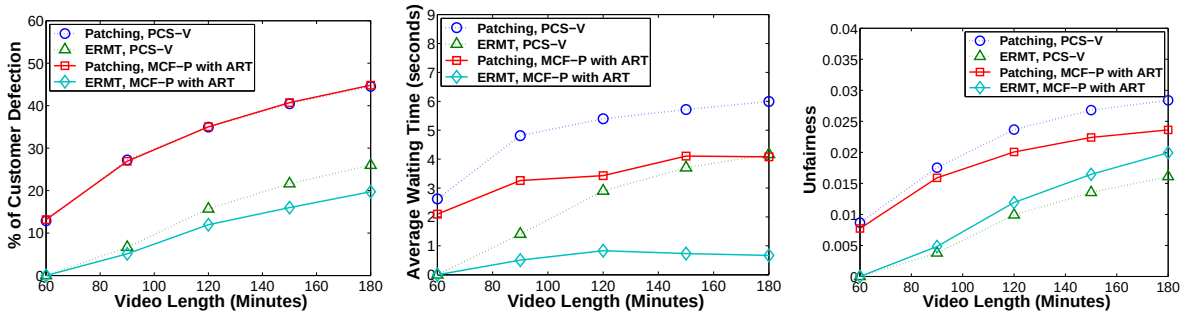

(a) Defection Rate (b) Average Waiting Time (c) Unfairness

Figure 4.24: Impact of Video Length [*Server Capacity = 500*]

"MCF-P combined with ART" as in most cases performs better than all other policies. Moreover, we can see that the fairness of ART and PCS-V is better than that of MCF-P with variable-length video workload.

The results so far assume a Poisson request arrival process. Let us now examine the behavior under Weibull distribution with different shape (k) values. Figure 4.27 demonstrates that the shape has a little impact, especially when the server capacity is larger than 500 channels. Figure 4.28 compares MCF-P, PCS-V, and MCF-P with ART under Weibull Arrival Distribution with the same shape. The results with other shape parameters have the same trend and thus are not shown. We can see clearly that PCS-V and "MCF-P combined with ART" sill perform better than MCF-P. We can see also that MCF-P with ART is the best policy.

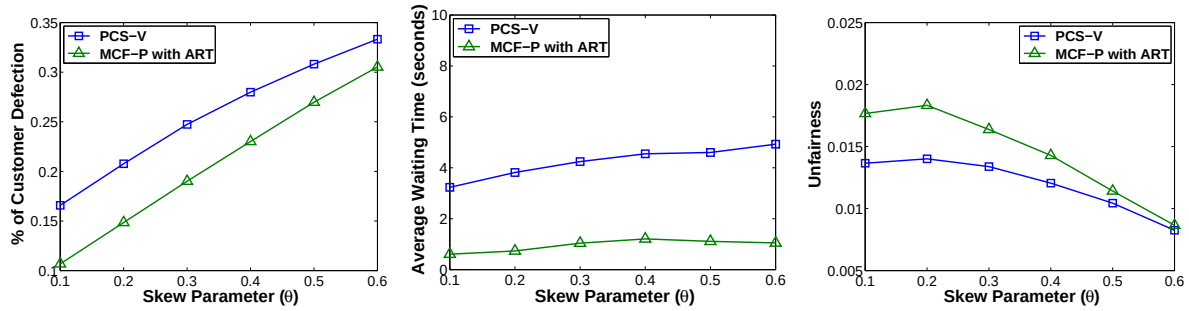

(a) Defection Rate (b) Average Waiting Time (c) Unfairness

Figure 4.25: Impact of Skew in Video Access [*ERMT, Server Capacity = 450*]

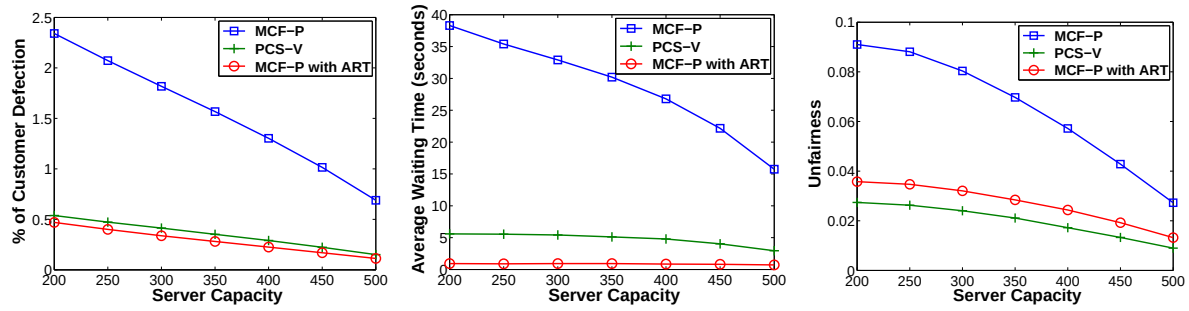

(a) Defection Rate (b) Average Waiting Time (c) Unfairness

Figure 4.26: Comparing the Effectiveness of MCF-P, PCS, and ART under a Variable-Length Video Workload [*ERMT, 60 to 180 minutes Video Length Range*]

4.6.6 Comparing Waiting-Time Predictability with PCS and ART

Figure 4.29 compares the predictability of MCF-P, PCS-V, and "MCF-P combined with ART" in terms of the average deviation and percentage of clients receiving expected time of service (PCRE) under waiting tolerance Model B. The results with Model C are similar and thus are not shown. The results demonstrate that ART significantly improves the predictability of MCF-P. PCS-V is also more predictable than MCF-P. In particular, ART reduces the average deviation by up to 30% and 75% for models B and C, respectively. It also increases the number of clients receiving expected times by up to 35%. Moreover, "MCF-P combined with ART" gives more customers expected times than PCS-V with a relatively less significant increase in the average deviation.

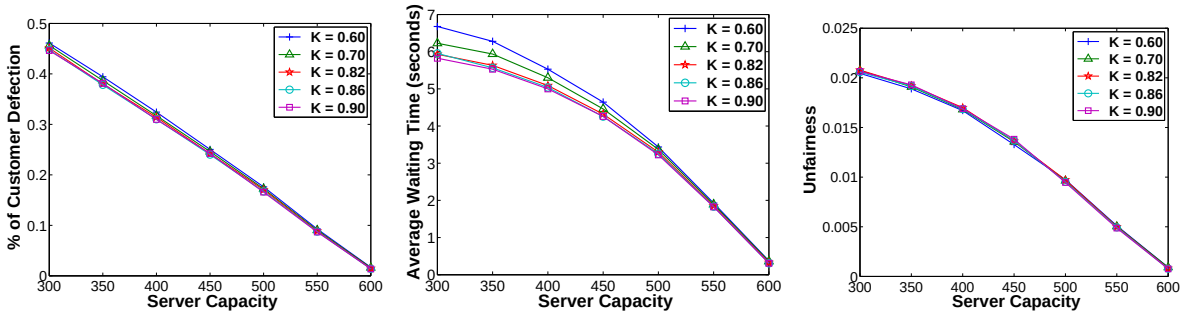

(a) Defection Rate (b) Average Waiting Time (c) Unfairness

Figure 4.27: Impact of the Shape Parameter of Weibull Arrival Distribution [*ERMT, PCS-V*]

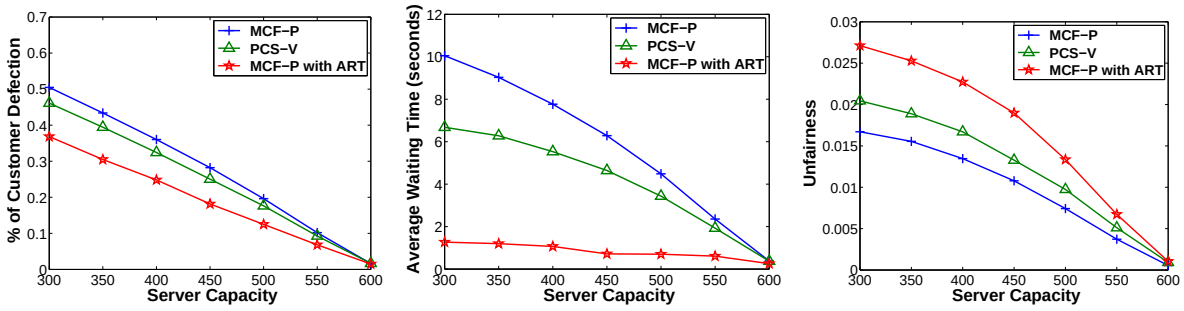

(a) Defection Rate (b) Average Waiting Time (c) Unfairness

Figure 4.28: Comparing MCF-P, PCS-V, and MCF-P with ART under Weibull Arrival Distribution [*ERMT, K = 0.6*]

4.6.7 Impact of Flash Crowds on the Effectiveness of PCS and ART

Let us now discuss the impact of flash crowds on the effectiveness of PCS-V and ART. Figure 4.30 demonstrates the impact of flash crowds inter-arrival time on MCF-P, PCS-V, and "MCF-P combined with ART". The results show that MCF-P when combined with ART handles the flash crowds more efficiently than the other policies. In particular, it achieves the best customer defection probability and average waiting time under all flash crowds inter-arrival times. PCS-V achieves better results than MCF-P, but it is improvement is less than that of ART. Figure 4.31 confirms that ART enhances the efficiency of stream handling even with flash crowds. It is clearly evident that "MCF-P combined with ART" achieves the lowest cost per request for all videos.

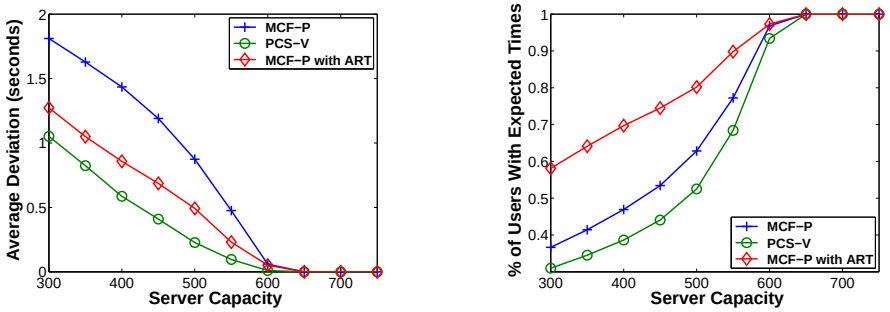

(a) Average Deviation (b) Customer With Expected Time

Figure 4.29: Waiting-Time Predictability of MCF-P, MCF-P with ART, and PCS-V [*ERMT*, $W_p = 0.5\mu_{tol}$, *Model B*]

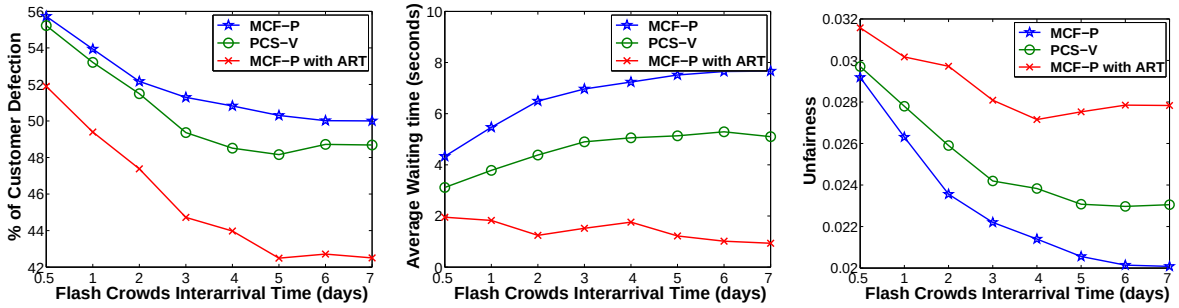

(a) Customer Defection (b) Waiting Time (c) Unfairness

Figure 4.30: Impact of Flash Crowds on MCF-P, PCS-V, and ART as a Function of Flash Crowds Inerarrival Time [*ERMT, Server capacity = 300*]

4.6.8 Effectiveness of Combining ART with PCS

Let us now look at the results of combining PCS-V with ART. We show the results under ERMT and Patching in Figures 4.32 and 4.33, respectively. Transition Patching has the same trend as Patching and therefore its results are not shown. These results indicate that "MCF-P combined with ART" performs the best among all variations, and that PCS-V performs better than "PCS-V with ART". From these figures, we conclude that negative interference occurs when ART is combined with PCS-V. Removing this interference by modifying these two strategies is a challenging task and left for a future study.

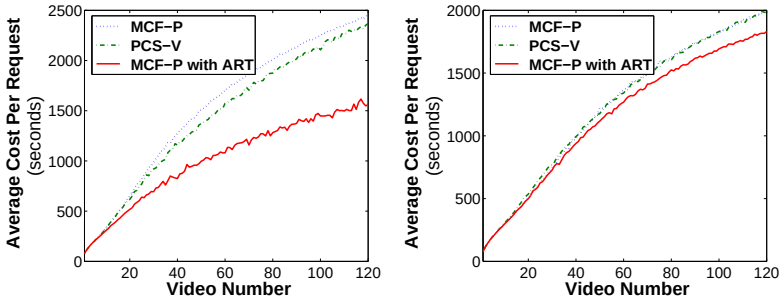

(a) 300 (b) 500

Figure 4.31: Comparing MCF-P, PCS-V, and MCF-P with ART with Flash Crowds in Average Cost per Request [*ERMT, Flash Crowds Arrival Rate = 1/day*]

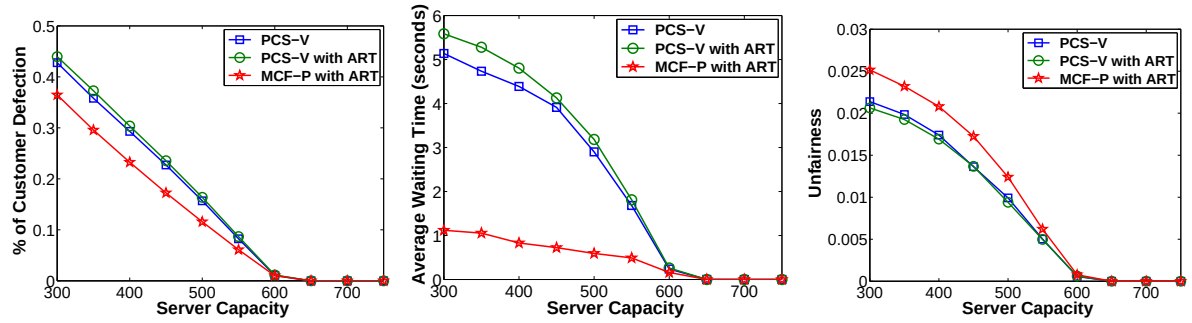

(a) Defection Rate (b) Average Waiting Time (c) Unfairness

Figure 4.32: Effectiveness of Combining Art with PCS [*ERMT*]

4.7 Conclusions

We have analyzed in detail cost-based scheduling for on-demand video streaming and proposed new strategies: *Predictive Cost-Based Scheduling* (PCS) and *Adaptive Regular Stream Triggering* (ART). The main results can be summarized as follows.

- There is no clear advantage of computing the cost over a future time window, compared with computing the cost only at the next scheduling time.

- The proposed PCS scheduling policy outperforms the best existing policy (MCF-P) in terms of customer defection probability and average waiting time. The waiting times can also be predicted more accurately with PCS. The two variations of PCS (PCS-V and PCS-L) perform nearly the same and thus the simpler variant (PCS-V) is preferred because of its lower implementation com-

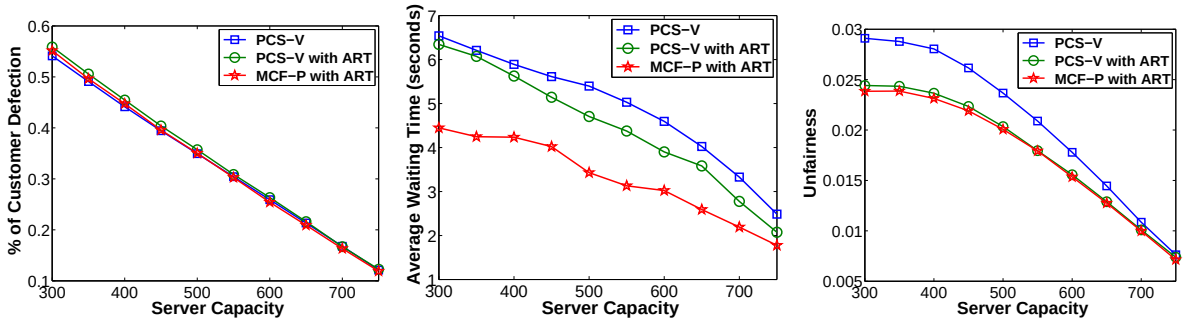

(a) Defection Rate (b) Average Waiting Time (c) Unfairness

Figure 4.33: Effectiveness of Combining PCS-V and ART [*Patching*]

plexity.

- By enhancing stream merging behavior, the proposed ART technique substantially improves both the customer defection probability and the average waiting time.

- Although ART in principle can be applied with any scheduling policy, including PCS, negative interference exists between ART and PCS, and thus their combination generally achieves worse than any of them applied individually. Removing this interference by modifying these two strategies is a challenging task and left for a future study.

- The best overall performer is “MCF-P combined with ART”, followed by PCS. With ART, significantly more clients can receive expected waiting times for service than PCS, but at a somewhat lower waiting time accuracy.

CHAPTER 5

DISTORTION-BASED CROSS-LAYER OPTIMIZATION FOR WIRELESS VIDEO STREAMING

5.1 Introduction

In this study, we consider video streaming from multiple video sources (or stations) to a central station over a single-hop IEEE 802.11 wireless LAN (WLAN) network. This application is typical in Automated Video Surveillance (AVS) systems. As shown in Figure 1.2, the wireless video sources (video cameras or sensors) share the same medium and can be either battery-powered or outlet-powered. The central proxy station is connected with a high-bandwidth link to the access point, and thus this link is not deemed as a bottleneck in the system. Large systems may be composed of multiple such systems or cells.

The main challenge in the considered system is that the wireless network has limited available bandwidth, which should be estimated accurately and distributed efficiently among various video sources. Our ultimate goal in this study is to build a cross-layer framework for maximizing the network bandwidth utilization. This cross-layer approach, clarified in Figure 5.1, utilizes and may adapt parameters from the application, link, and physical layers of the network layer stack. The problem is to be formulated using the AVS intuitive rate-accuracy function. The objective of the optimization will be to maximize the sum of the weighted accuracy of vision algorithms running in the system, where the weights are the importance factors of the video sources in the system.

Distortion-based bandwidth optimization in such systems has been addressed in only few studies [43, 44] by using cross-layer optimization and as discussed in Section 2.5, these solutions are highly limited. For this reason and for comparative purposes, we propose a distortion-based cross-layer framework that dynamically manages the available network bandwidth in such a way that minimizes the overall distortion. The proposed cross-layer framework utilizes an online approach for estimating the effective

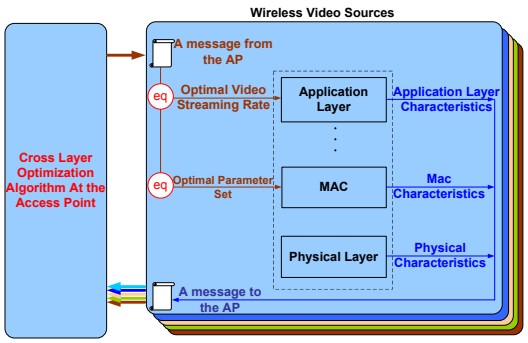

Figure 5.1: Cross Layer Framework Clarification

airtime of the network. To yield an accurate estimation, the proposed approach computes the effective airtime when the packet loss is below a specified threshold.

We evaluate the proposed solution by streaming real video frames (and not just an abstract bit stream) over a simulated network. The simulations are conducted using OPNET. Since the sent video packets may be lost, we implement an error concealment algorithm [71] at the proxy station to mitigate the impact of packet loss on perceptual video quality. We also study the performance of the proposed framework with the existence of other interfering/cross traffic in the network.

The main contributions of this part of the dissertation can be summarized as follows. (1) We propose a complete cross-layer optimization framework, including a new online and dynamic approach for estimating the effective airtime of the network. (2) We develop a new and accurate model that characterizes the relationship between the video data rate and the distortion. (3) We propose an enhanced online and dynamic approach for estimating the effective airtime of the network. (4) We develop a new model for adapting the link layer parameters in the video sources. (5) We test our framework by streaming real video frames over a simulated network and incorporating an error concealment algorithm to mitigate the impact of video packet loss. (6) We study the impact of interfering/cross traffic on the performance of the proposes framework.

The results show that the proposed framework enhances substantially the perceptual quality of re-

ceived video streams and that the proposed effective airtime estimation algorithm is accurate and converges quickly. The proposed framework also results in much less power consumption, compared with existing solutions. This behavior is due to sending and dropping much less data. Power consumption is a primary concern, especially when the video sources are battery-powered. Moreover, results shows that the proposed framework is highly adaptable for any interfering traffic in the network.

The rest of this chapter is organized as follows. Table 5.1 summarizes the notations that are used in this study and their definitions. Section 5.2 presents the proposed cross-layer optimization framework. Subsequently, Section 5.3 discusses the performance evaluation methodology. Finally, Section 5.4 presents and analyzes the main results.

Table 5.1: Notations Summary

Notation	**Definition**
CW_{min}	Minimum Contention Window
CW_{max}	Maximum Contention Window
AP	Access Point
AC	Access Category
AIFS	Arbitration Inter Frame Space
TXOP	Transmission Opportunity Time
S	Number of video sources
r_s	Rate of the encoded video sent by source s
y_s	Source s physical rate
A_{eff}	the effective airtime of the medium
f_s	Airtime fraction of source s
τ	Frame rate
Z	Video frame size
t_s	Throughput of source s video stream as received by the application layer of the proxy station
d_s	source s data dropping rate
A_Δ	The overall average dropping ratio, $A_\Delta = \sum_{s=1}^{S} d_s/y_s$.
A_{thresh}	A threshold that controls the allowable dropping in the network
λ	Lagrangian constant
a_s, b_s, c_s	Distortion curve constants
x_s	Optimized TXOP limit
R_s	Maximum load rate measured by the MAC layer at source s
L_s	Maximum video frame size at source s
N_s	Number of MAC layer data frames per maximum video frame at source s
l_s	Average data load per MAC layer data frame at source s
O_s	Average MAC and physical layers overhead at source s
t_s	Short Interframe Space (SIFS) time
t_a	Time required to send an acknowledgment

5.2 Proposed Cross-Layer Optimization Framework

This study considers a system of video streaming from multiple video sources (or stations) to a central station over a single-hop IEEE 802.11 WLAN network in EDCA mode. As shown in Figure 1.2, the system has $S \geq 1$ video sources and each source s streams a different encoded video at rate R_s. Each video source s may have a different physical rate (y_s).

The ultimate goal of this study is to provide an optimal solution that dynamically distributes and allocates the available network bandwidth among various video sources. This solution should consider all system, video, network, and environmental aspects, which may change dynamically. Therefore, the proposed cross-layer optimization solution utilizes and dynamically controls parameters in three layers in the network stack: Application, Link, and Physical.

5.2.1 Cross-Layer Optimization Problem Formulation

As in [44], we formulate the problem as a cross-layer optimization problem of the sum of the distortion of all video streams received by the central proxy station. We follow the formulation in [44], but adapt it to include the packetization overhead of the transport and application layers. Since all video sources share the same medium, the bandwidth allocation solution should determine the fraction of airtime that each video source receives in the system. Obviously, the total airtime cannot exceed the effective airtime of the medium. Specifically, the problem is formulated as: find the optimal fraction of the airtime allocation $F^* = \{f_s^* | s = 1, 2, 3, ..., S\}$ for various video sources that minimizes the total distortion ($\sum_{s=1}^{S} Distortion_s(r_s)$), where r_s is the application layer transfer rate for video source s, and S is the number of video sources. This optimization is subject to the following constraints. (1) The total airtime of all video sources is less than the effective airtime of the medium (A_{eff}). (2) The application layer transfer rate of source s is the product of the its airtime (f_s) and the physical layer transfer rate (y_s) for video source s. (3) The airtime of each source is between 0 and 1 (inclusive).

Mathematically, the problem can be stated as follows:

$$Find \quad F^* = \arg\min_{F} \sum_{s=1}^{S} Distortion(r_s) \tag{5.1a}$$

$$s.t. \quad \sum_{s=1}^{S} f_s = A_{eff} \tag{5.1b}$$

$$r_s = f_s \times y_s \tag{5.1c}$$

$$0 \leq f_s \leq 1 \tag{5.1d}$$

$$s = 1, 2, 3, ..., S, \tag{5.1e}$$

where F^* is the set of optimal fractions (f_s^*) of the airtime of all sources, r_s^* is the optimal application-layer rate of video source s, y_s is the physical-layer rate of video source s, and A_{eff} is the total effective airtime.

To solve the problem formulated in Equation (5.1), we need to characterize the distortion function and assess the effective airtime of the network.

5.2.2 Distortion Function Characterization

We seek to find a model of the relationship between the size of a JPEG snapshot (or alternatively the rate of an MJPEG video) and the distortion of the snapshot. We determine the size-distortion relationship based on the following image data sets: CMU/MIT [72], Georgia Tech [73], FERET [74], and SCFace [75]. We also use these image sets in our experiments to assemble the MJPEG video streams using the streamer discussed in Section 5.3 to load the network with video traffic. For fair evaluations of bandwidth allocation solutions, each video source should be able to stream the video at a bitrate that matches that of the optimization solution. The Georgia Tech image set produces a highly limited range of bitrates for the studied network. To produce a better variety, we generate another image set from the original Georgia Tech image set by changing the resolution of each image in the set to 50% of the

original resolution. The new image set have a resolution of 320 × 240. For each image set, we use the IJG JPEG library to compress each picture in the set with quality factors from 1 to 100, with 1 being the lowest, and then assess the distortion of each image against the original image using the Root Mean Square Error (RMSE) metric. Finally, we find the average size and the average distortion of all images with the same quality factor. The results are shown in Figure 5.2. These results indicate that the model formulated in [76] (identified as "Existing Model") is not accurate. We determine that the distortion can be better characterized as follows:

$$Distortion(RMSE) = a \times Z^b + c, \tag{5.2}$$

where Z is the image size and a, b, c are constants. This model is referred to as "New Model" in Figure 6.1. For MJPEG videos, image size Z can be calculated as $Z = R/\tau$, where R is the video playback rate and τ is the video frame rate.

5.2.3 Effective Airtime Estimation

As finding an accurate value for the effective airtime of the medium is necessary for solving the formulated optimization problem, we propose a novel online and dynamic effective airtime estimation algorithm for wireless networks in infrastructure configuration. In contrast with existing analytical models, the algorithm uses complete information about the network and involves the cooperation of the access point and all video sources as well as various layers in each source. The algorithm does not incur additional network traffic and can be executed only when significant changes in the network (such as variations in the physical rates) happen.

As shown in Figure 5.3, the algorithm proceeds as follows. First, for each video source s, it finds the throughput (t_s) of its video stream as received by the application layer of the proxy station, when all sources stream videos, each at a rate that is equal to the maximum physical rate of the network

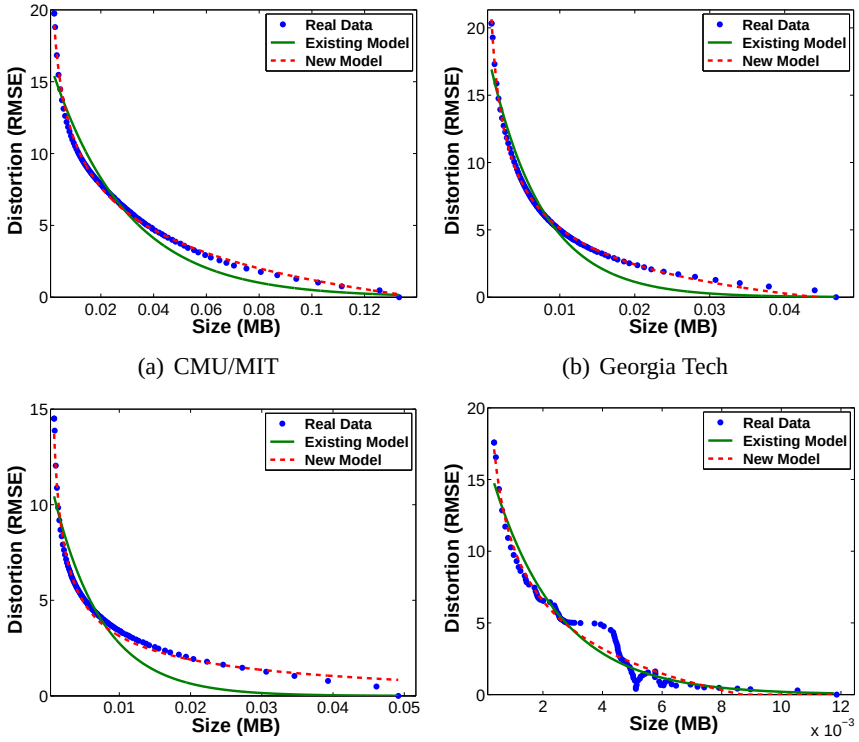

(a) CMU/MIT (b) Georgia Tech

(c) FERET (d) SCFace

Figure 5.2: Size-Distortion Models

divided by the number of sources [77]. The algorithm then uses this throughput to determine the initial value of the effective airtime (A_{eff}) as follows: $A_{eff} = \sum_{s=1}^{S} t_s/y_s$. Our experiments indicate that this initial value significantly overestimates the effective airtime, causing the actual received video rates to not conform to the cross-layer optimization solution because of the high level of packet packet dropping in the network. Thus, this value has to be adjusted based on the experienced level of packet dropping. Subsequently, during a period of time, called estimation period, each video source s assesses its own data dropping rate (d_s) while sending its video stream, and then sends this information to the access point (AP). Meanwhile, the AP determines the overall average dropping ratio as follows: $A_\Delta = \sum_{s=1}^{S} d_s/y_s$. A_Δ is used to adjust the current value of A_{eff} at the end of the current estimation period. If A_Δ is greater than some threshold A_{thresh}, the AP reduces A_{eff} by $A_\Delta - A_{thresh}$. A_{thresh} controls the allowable dropping in the network. If A_Δ, however, is less than A_{thresh}, the AP increases A_{eff} by a value I, which

set as half the last increment or decrement value, depending on whether the last operation is increment or decrement, respectively. Guided by extensive experiments, we set I to half the last decrement/increment to ensure better convergence and stability. The algorithm terminates when the increments become less than a threshold I_{thresh}. The estimation period and I_{thresh} should be chosen based on the best tradeoff between convergence and stability.

if this is the first time to run the algorithm
  $A_{eff} = \sum_{s=1}^{S} t_s/y_s$;
At the end of each estimation period{
  $A_\Delta = \sum_{s=1}^{S} d_s/y_s$;
  if ($A_\Delta < A_{thresh}$){
    if (last operation was decrement){
      $I = 0.5 * lastDecrement$;
      $A_{eff} = A_{eff} + I$;}
    else if (last operation was increment){
      $I = 0.5 * I$;
      $A_{eff} = A_{eff} + I$;}
    else //no decrements happened before
      //keep increasing A_{eff} to cause the first decrement
      $A_{eff} = A_{eff}$+ 0.05 ;
    if ($lastIncrement < I_{thresh}$)
      Stop the estimation algorithm;
  }
  else if ($A_\Delta \geq A_{thresh}$){
    $A_{eff} = A_{eff} - (A_\Delta - A_{thresh})$;
    $lastDecrement = A_\Delta - A_{thresh}$;}
}

Figure 5.3: The Algorithm for Dynamically Estimating the Effective Airtime

5.2.4 Enhanced Effective Airtime Estimation

By studying the online estimation algorithm proposed in the previous section in details, we have found some options for further enhancements. One of these enhancements is to eliminate the initial period that the algorithm spend to find an initial value for A_{eff} to start with. We find that starting with a moderate initial value such as 0.5 is sufficient. The other enhancement that can be done is to make the incrementing step of the algorithm directly dependent on the desired A_{thresh}. By doing this, the algorithm become more stable and converges to a more accurate effective airtime value. By employing

these enhancements, the resulting algorithm came out to be much simpler, easier to calibrate, and uses less design parameters. Figure 5.4 shows the enhanced algorithm.

The algorithm starts with initializing A_{eff} with 0.5. This statement is only executed once when the system start running. Next, as in the algorithm in the previous section, during a period of time called estimation period, each video source s assesses its own data dropping rate (d_s) while sending its video stream, and then sends this information to the access point (AP). Meanwhile, the AP determines the overall average dropping ratio as follows: $A_\Delta = \sum_{s=1}^{S} d_s/y_s$. A_Δ is then used to adjust the current value of A_{eff} at the end of the current estimation period. If A_Δ came out to be zero, A_{eff} is incremented by A_{thresh}. If A_Δ is greater than the threshold A_{thresh}, the AP reduces A_{eff} by $C*(A_\Delta - A_{thresh})$ where C is a positive constant. If A_Δ, however, is less than A_{thresh}, the AP increases A_{eff} by $C*(A_{thresh} - A_\Delta)$. The estimation period and the constant C should be chosen based on the best tradeoff between convergence and stability.

```
Initialize A_eff with 0.5
At the end of each estimation period{
   A_Δ = Σ_{s=1}^{S} d_s/y_s;
   if (A_Δ == 0)
      A_eff = A_eff + A_thresh;
   else if (A_Δ < A_thresh)
      A_eff = A_eff + C * (A_thresh − A_Δ);
   else if (A_Δ > A_thresh)
      A_eff = A_eff − C * (A_Δ − A_thresh);
}
```

Figure 5.4: Enhanced Effective Airtime Estimation Algorithm

5.2.5 Cross-Layer Optimization Solution

Now that we have a distortion function and a value for the effective airtime, we can solve the problem formulated in Equation (5.1). The problem solution can be summarized as follows:

Step 1: We first prove that the formulated problem is a convex programming problem by determining that all constraints ((6.1b)-(6.1e)) in the problem are linear and thus convex and that the optimization

function ($\sum_{s=1}^{S}(a_s(f_s y_s/\tau_s)^{b_s}+c_s)$) is also convex. The latter is valid since the derivative of the sum term is monotonically non-decreasing and convex.

Step 2: Since the problem is a budget constrained convex programming problem, it can be solved using the Lagrangian relaxation technique [78]. Thus, we can write the following Lagrangian-relaxed formula:

$$L(F^*,\lambda)=\sum_{s=1}^{S}(a_s(f_s y_s/\tau_s)^{b_s}+c_s)+\lambda(\sum_{s=1}^{S}f_s-A_{eff}), \tag{5.3}$$

where $0 \leq f_s \leq 1$, and $s = 1, 2, 3, ..., S$. Next, the Lagrangian conditions are formulated as follows:

$$\frac{\partial L}{\partial f_s}=0 \text{ and } \frac{\partial L}{\partial \lambda}=0. \tag{5.4}$$

Assuming that all video sources have the same b_s, which is empirically valid, solving these two equations yields the following solution:

$$f_s^*=(\frac{-\lambda^*\tau_s}{a_s b_s y_s (y_s/\tau_s)^{(b_s-1)}})^{(1/(b_s-1))}, \tag{5.5}$$

where

$$\lambda^*=(\frac{A_{eff}}{\sum_{s=1}^{S}(\frac{-\tau_s}{a_s b_s y_s (y_s/\tau_s)^{(b_s-1)}})^{(1/(b_s-1))}})^{(b_s-1)}. \tag{5.6}$$

5.2.6 Enforcing the Optimization Results

With the aforementioned solution, the AP determines λ^* and then each video source s determines its fraction of the airtime f_s^* after receiving λ^* from the AP. Subsequently, each video source s should change the application data rate, which is the video encoding rate in this case, as follows: $r_s^* = f_s^* \times y_s$. Finally, the link-layer parameters are determined based on the allocated airtime for each source. The link-layer parameters can either be the transmission opportunity duration limit (TXOP limit) or alternatively the frequency of the transmission opportunity. The control of the TXOP limit is more

preferred since it is only one parameter, whereas the transmission frequency involves three parameters (AIFS, CW_{min}, and CW_{max}), which complicates the control process design.

In [44], the TXOP limit (x_s^*) for source s is determined as the time required to transmit the number of MAC data frames that source s can transmit during one beacon interval time (t_b). As discussed in Section 5.4.3, our results show that choosing intervals other the beacon interval can achieve better performance. In particular, the received video quality improves with the chosen time interval up to a certain point, and then it starts to worsen. In addition, the time interval that achieves the best results varies with the network size. Furthermore, the model in [44] does not incorporate the packetization overhead of the transport and application layers.

In our framework, we address these problems as follows. Each video source determines its TXOP limit as the time required to transmit the packets that belong to a single video frame along with all associated overhead. Because of the cross-layer approach, the MAC layer in source s can know the frame rate τ_s of the video sent by the application layer in that source. The MAC layer can also determine the maximum load rate R_s coming from the source's upper layers. Using this information, we can determine the maximum video frame size L_s (with overhead) as R_s/τ_s and the number of MAC layer data frames per maximum video frame N_s as L_s/l_s, where l_s is the average data load per MAC layer data frame. Given that O_s is the average MAC and physical layers overhead, t_s is *Short Interframe Space (SIFS)* time, and t_a is the time required to send an acknowledgment, TXOP limit can be found as follows:

$$x_s^* = [\frac{L_s}{y_s}] + [\frac{O_s N_s}{y_s}] + [(2N_s - 1)t_s] + [N_s t_a], \tag{5.7}$$

where $\frac{L_s}{y_s}$ is the time required for transmitting the data of a single video frame and the overhead of the upper layers associated with that video frame, $\frac{O_s N_s}{y_s}$ is the time required for transmitting the associated MAC and physical layers overhead, $(2Ns - 1)t_s$ is the sum of the *SIFS* periods needed for transmitting all the packets of the video frame, and $N_s t_a$ is the time required for receiving all the acknowledgment

packets of the video frame packets.

5.3 Performance Evaluation Methodology

We use the OPNET simulator to conduct various experiments. In contrast with prior studies, which deal with video streams as abstract data streams with certain bitrates, we implement a traffic source in OPNET that streams MJPEG videos as Real-time Transport Protocol (RTP) packets. Moreover, we implement a realistic video streaming client at the application layer of the proxy station. This client receives and reassembles the RTP packets from various video streams, and then carries out error concealment to mitigate the impact of packet loss. The use of MJPEG enables the use of standard image data sets that are suitable for surveillance applications because the MJPEG video stream is a set of JPEG images. We use the the following image sets to assemble the video streams: CMU/MIT [72], Georgia Tech [73], and FERET [74]. The streamer at each source takes a bitrate, a frame rate, and an image set as inputs and produces a corresponding MJPEG video stream.

As shown in Figure 5.1, the implementation of the proposed framework is distributed between the video sources and the AP. Each video source send its state information (physical rate, data dropping rate, and Rate-Distortion curve characteristics) to the AP periodically using a new management packet. This packet can be called *state report* [44]. The AP can than calculate λ^* using Equation 5.6 and distribute it using the beacon packet. Each video source s than uses λ^* from the received beacon packet to calculate f_s^* according to Equation 5.5 that is used eventually by source s to calculate its optimal application rate according to Equation 5.1c and its optimal TXOP limit time using Equation 5.7.

For comparative purposes, we implement the cross-layer algorithm proposed in [44], referred to here as *Distortion Optimization (DO)*. Our proposed solution is referred to as *Enhanced Distortion Optimization (EDO)*. We also compare the results with standard EDCA. In addition, we implement a variation of the standard EDCA, called *Adaptive EDCA*, in which the application layer in each video source adapts its video rate according to the physical rate of that source, and thus the rate is set as y_s/S.

We analyze the following *performance metrics*.

- *Perceptual Video Quality* - It is the main metric and is measured in the overall Peak Signal to Noise Ratio (PSNR). We set the PSNR of missed frames to 0.
- *Average video packet delay* - The average time needed for the access point to receive a video data packet sent by a video source. The average video packet delay is an essential metric due to the real-time playback requirement.
- *Average percentage of received complete video frames*.
- *Average percentage of received incomplete video frames*.
- *Average percentage of missed video frames*.
- *Overall network load* - It is defined as the total load sent from the application layers of all sources.
- *Overall dropping rate due to buffer overflow*.
- *Overall dropping rate due to reaching the retransmission limit*.
- *Power Consumption* - It is the average power consumption of the wireless interfaces of the video sources and is determined by using the power consumption model proposed in [79] for MJPEG video streaming.

Since the proposed cross-layer framework utilizes a dynamic and online effective airtime estimator that estimates the useful fraction of the airtime that can be used for surveillance traffic, the framework adapts the sending rates of the video sources to achieve the best performance with the existence of any other interfering/cross data traffic in the network. To show the impact of this interfering/cross traffic on the performance of the proposed framework, we conduct various experiments with 8 none-video sources that are sharing the same wireless medium of the surveillance system. These none-video sources send best effort traffic to the access point all with the same pr-specified rate. We perform experiments with three packet rates of cross traffic. Cross traffic 1 sources send packets with 0.005 seconds inter-arrival time. In cross traffic 2 sources, we set the inter-arrival time to 0.003 second while we set the inter-arrival

time to 0.001 seconds in cross traffic 3 sources.

Table 5.2 summarizes the main simulation parameters.

Table 5.2: Summary of Simulation Parameters

Parameter	**Model/Value(s)**
Number of video sources	10-44
Simulation Time	10 min
Packet Size	1024 bytes
Application Rate	Optimized, Default = Max Physical Rate / No. of Sources
Video Frame Rate	20 frames/sec
Physical characteristics	Extended Rate (802.11g)
Physical Data Rate	Random from {12Mb/s, 18Mb/s, 24Mb/s, 36Mb/s, 48Mb/s, 54Mb/s}
Weight	One of five levels between [0 1] chosen randomly
Buffer size	256 Kb
Video TXOP limit	Optimized, Default = 3008μs
Video CW_{min}	15
Video CW_{max}	31
Video AIFS	2
Short Retry Limit	7
Long Retry Limit	4
Beacon Interval	0.02 second
State Report Interval	1 second

5.4 Results Presentation and Analysis

5.4.1 Effectiveness of Using the Cross-Layer Approach in Bandwidth Allocation

Let us start by demonstrating the benefits of utilizing information from different network layers in bandwidth allocation. Figure 5.5 compares standard EDCA and adaptive EDCA in terms of PSNR.These results indicate that adapting the application rate according to the physical rate in each video source (as done in Adaptive EDCA) improves the PSNR by at least 50%!

5.4.2 Analysis of the Enhanced Effective Airtime Estimation Algorithm

Extensive analysis of the design parameters of the enhanced effective airtime estimation algorithm indicates that their values are best set as follows to enhance the performance in terms of stability and convergence: $A_{thresh} = 0.0075$, $C = 0.2$, and *Estimation Period* $= 5$ seconds. Figure 5.6 shows the effective airtime over the whole time of running the EDO solution using FERET image sets. Results

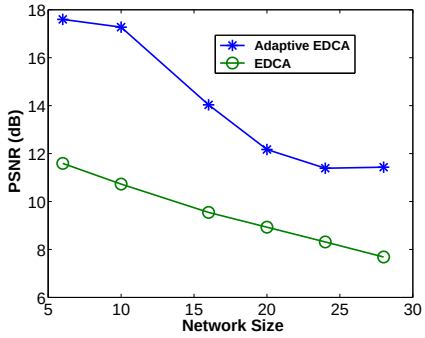

Figure 5.5: Comparing EDCA with Adaptive EDCA [CMU/MIT Image set]

for other image sets follow the same trend and thus are not shown. The figure shows that the algorithm converges quickly in all studied network sizes.

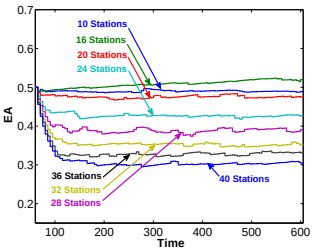

Figure 5.6: Enhanced Effective Airtime Estimation Progress [FERET Image Set]

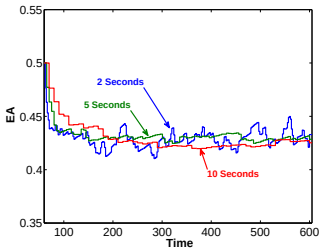

Figure 5.7: Calculation Period Impact on the Progress of the Enhanced Effective Airtime Estimation Algorithm [Georgia Tech Image Set At 50% Resolution, 24 Stations]

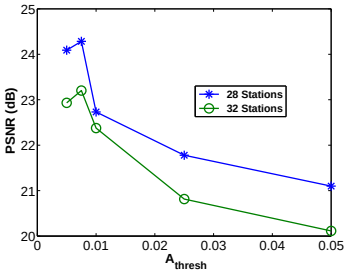

Figure 5.8: Effect of A_{thresh} on PSNR [EDO, CMU/MIT Image set]

Figure 5.7 shows the impact of calculation period on the convergence and the stability of the enhanced effective airtime estimation algorithm. The figure shows the effective airtime values over the whole time of running the EDO solution using Georgia Tech at 50% resolution with three different values of calculation period: 2, 5 ,and 10 seconds. As expected, the estimation algorithm with 10 seconds calculation period achieves the best stability and the longest convergence time while the run with 2 seconds calculation period achieves the fastest convergence and the worst stability. In this study, we choose

5 seconds as our calculation period because it achieves very good trade-off between the convergence and the stability of the estimation algorithm.

Impact of A_{thresh}, which determines the allowable dropping in the network, on perceptual video quality is shown in Figure 5.8. This figure depicts the results of running the proposed EDO solution for two different network sizes: 28 and 32 stations. The results show that the quality of the received video streams improves with A_{thresh} up to a point and then the quality starts to worsen. The peak happens when A_{thresh} is smaller than 0.01, suggesting that that optimal perceptual video quality is achieved when the dropping is very small.

5.4.3 Analysis of Link-Layer Adaptation

As discussed in Subsection 6.2.5, study [44] determines the TXOP limit (x_s^*) for source *s* as the time required to transmit the number of MAC data frames that source *s* can transmit during one beacon interval time (t_b). Let us know discuss the impact of choosing time intervals other than the beacon interval. Table 5.3 shows the PSNR when running the solution proposed in [44] (DO) for different time intervals and network sizes. These results indicate that perceptual video quality improves with increasing the chosen time interval until a peak is reached, and then it starts to worsen. Furthermore, the best value of the time interval varies with the network size.

Table 5.3: Impact of the Time Interval Selected to Determine TXOP Limit on Perceptual Video Quality [PSNR (dB)]

Time Interval \ Network Size	**10**	**16**	**20**	**24**
0.02	19.15	12.30	10.25	8.81
0.5	24.46	18.77	16.17	15.69
1	24.46	19.00	16.40	15.66
2	24.46	19.00	16.46	15.66
3	24.46	19.00	16.46	15.65

5.4.4 *Comparing Various Bandwidth Allocation Solutions*

Figure 5.9 compares the performance of various solutions (EDCA, DO, EDO) in terms of (*a*) perceptual video quality, (*b*) average video packet delay, (*d*) percentage of received complete video frames, (*e*) percentage of received incomplete video frames, (*f*) percentage of missed video frames, (*g*) overall network load, and (*h*) overall dropping rate due to buffer overflow, and (*i*) overall dropping rate due to reaching the retransmission limit. This figure shows the results when using the CMU/MIT image set. Figures 5.10 and 5.11 show the same results when using Georgia Tech. at 50% resolution and FERET image sets respectively.

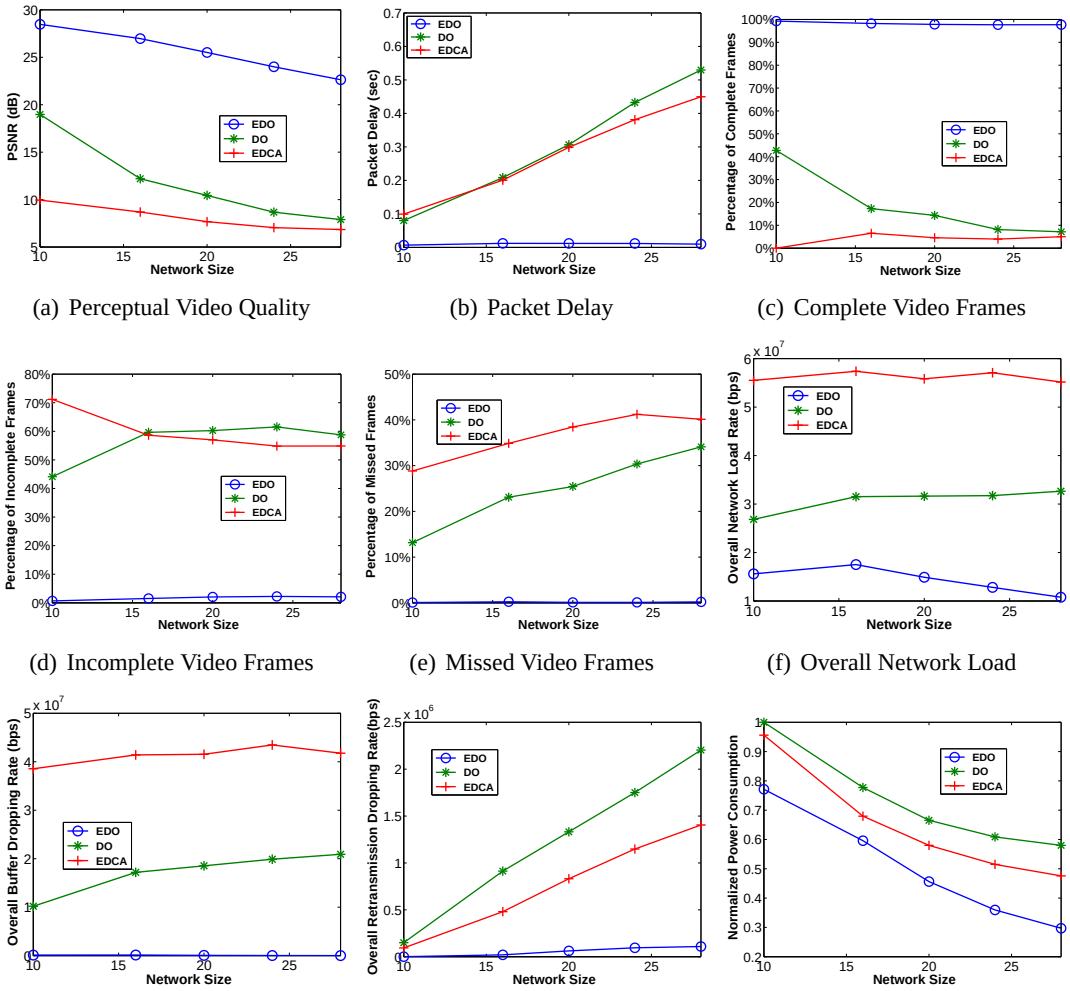

(a) Perceptual Video Quality (b) Packet Delay (c) Complete Video Frames

(d) Incomplete Video Frames (e) Missed Video Frames (f) Overall Network Load

(g) Overall Buffer Dropping Rate (h) Overall Retransmission Dropping Rate (i) Normalized Power Consumption

Figure 5.9: Comparing Various Bandwidth Allocation Solutions [CMU/MIT Image Set]

The results show that EDO significantly outperforms other studied solutions. In particular, it improves PSNR by more than 100% compared with standard EDCA and by 20% to 100% compared with DO. In addition to that, we can see clearly that EDO almost eliminates video packet delay. Moreover, EDO yields the highest percentage of completely received video frames and the lowest percentage of incomplete and missed frames. This behavior is due to the effective airtime estimation algorithm, which minimizes packet dropping and to the effective link-layer adaptation model used. Accordingly, EDO reduces significantly the following three metrics: overall network load, buffer dropping rate , and retransmission dropping rate. These results indicate that EDO consumes much less processing power by sending and dropping much less data. Finally, the results show that EDO significantly enhances the wireless interface power consumption at the video sources. It reduces the power consumption on average by 20%.

5.4.5 Impact of Interfering Traffic on the Performance of the Proposed Bandwidth Allocation Solution

In this subsection, we analyze the impact of cross traffic with different data rates on the performance of the studied bandwidth allocation solutions. Figures 5.12 and 5.13 show the results in terms of PSNR, Packet Delay, and Normalized Power Consumption with Georgia Tech at 50% resolution and FERET image sets respectively when using EDO solution. We show only the results in terms of these three metrics because they summarize all other performance metrics. The results show that the proposed framework is highly adaptable to cross traffic in the network. In particular, the degradation of PSNR and average packet delay is almost negligible even with the highest data rate cross traffic (cross traffic 3). Power consumption is less with cross traffic because the proposed framework adapts the video sources and make them send video streams with lower rates.

Figures 5.14 and 5.15 compare EDO, DO, and EDCA all with cross traffic 2 in terms of PSNR, Packet Delay, and Normalized Power Consumption when using Georgia Tech at 50% resolution and FERET image sets respectively. Figures 5.16 and 5.17 show the same results with cross traffic 3. Re-

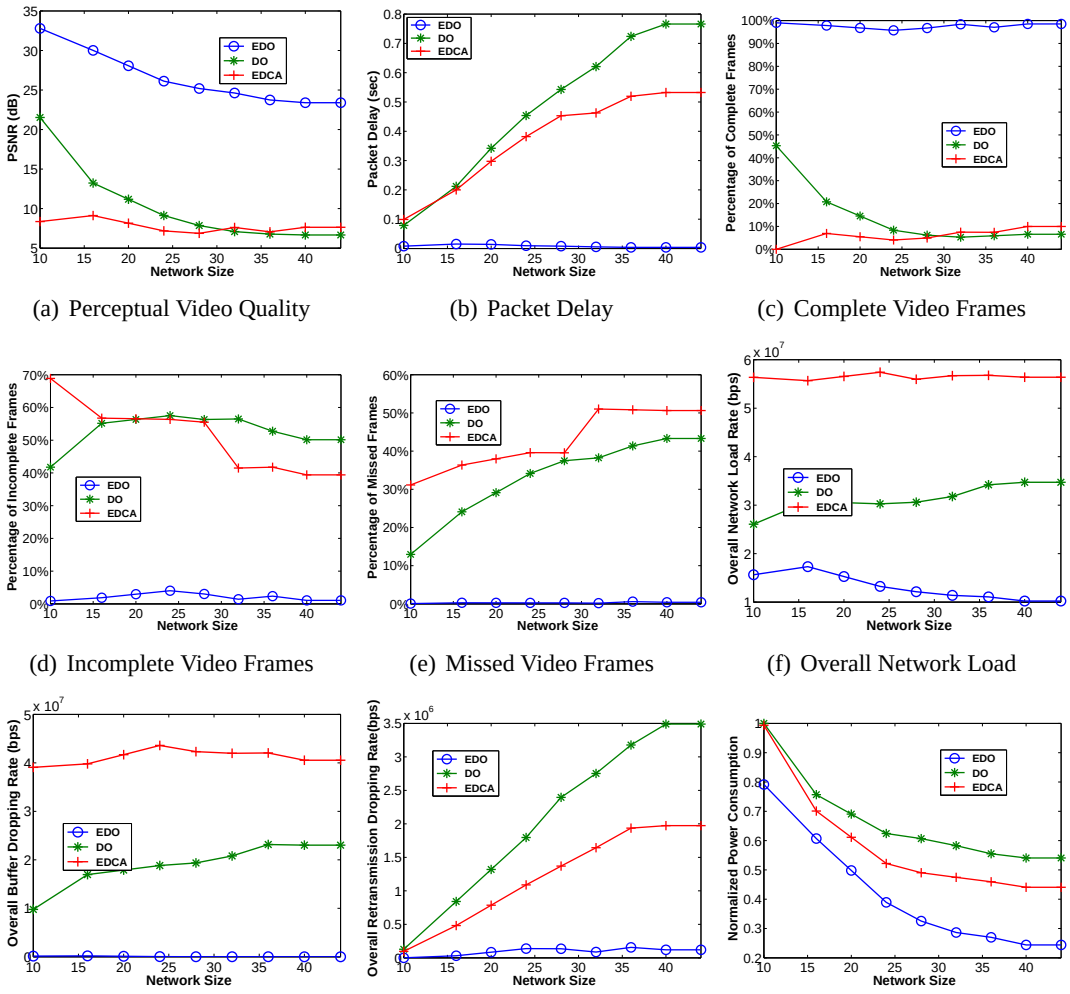

(a) Perceptual Video Quality (b) Packet Delay (c) Complete Video Frames

(d) Incomplete Video Frames (e) Missed Video Frames (f) Overall Network Load

(g) Overall Buffer Dropping Rate (h) Overall Retransmission Dropping Rate (i) Normalized Power Consumption

Figure 5.10: Comparing Various Bandwidth Allocation Solutions [Georgia Tech Image Set At 50% Resolution]

sults show that even with cross traffic, EDO outperform DO and EDCA significantly in terms of all performance metrics.

Figures 5.18 and 5.19 compare EDO with cross traffic 3, DO and EDCA without any cross traffic in terms of PSNR, Packet Delay, and Normalized Power Consumption when Georgia Tech at 50% resolution and FERET image sets are used respectively. Despite the fact that EDO was running with the highest data rate cross traffic and other solutions are running without any cross traffic, results show that EDO still outperforms DO and EDCA significantly in terms of all studied performance metrics.

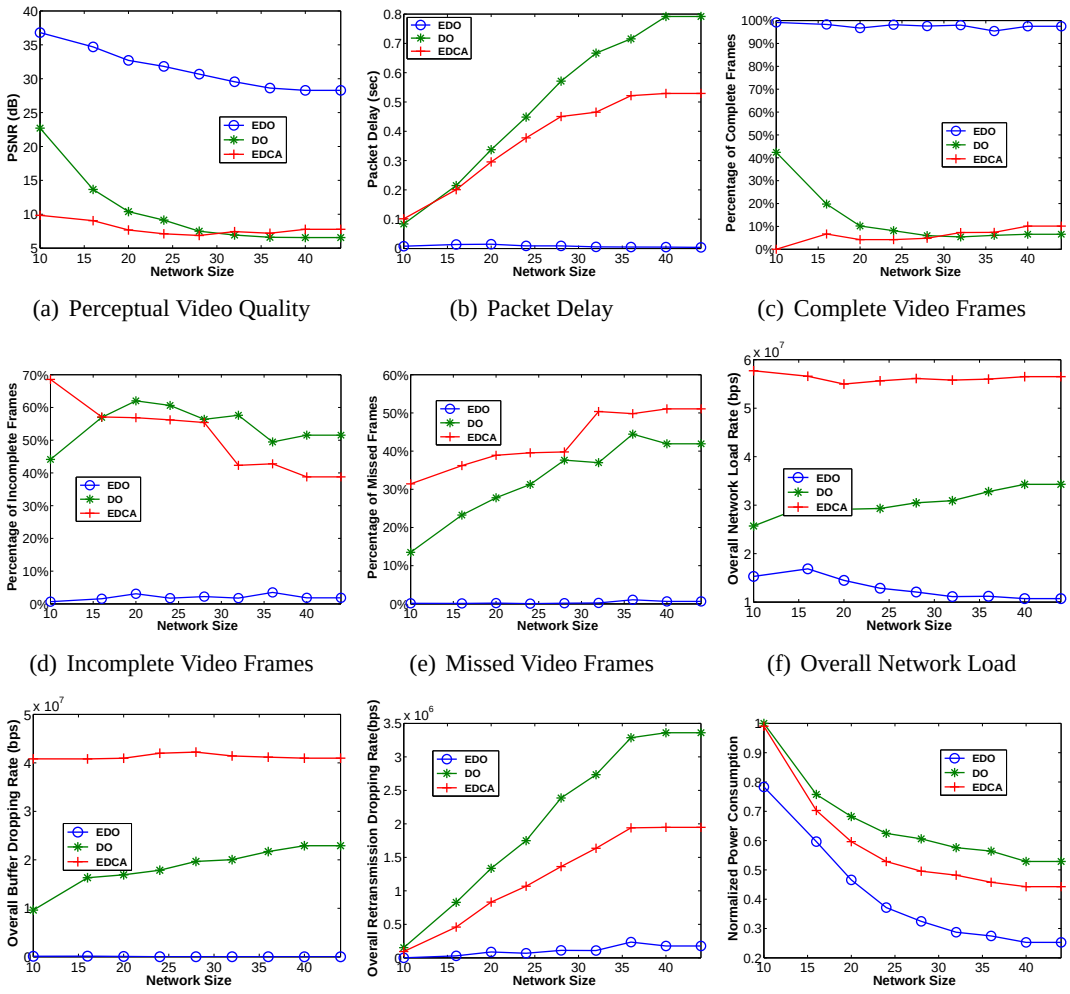

(a) Perceptual Video Quality (b) Packet Delay (c) Complete Video Frames

(d) Incomplete Video Frames (e) Missed Video Frames (f) Overall Network Load

(g) Overall Buffer Dropping Rate (h) Overall Retransmission Dropping Rate (i) Normalized Power Consumption

Figure 5.11: Comparing Various Bandwidth Allocation Solutions [FERET Image Set]

5.5 Conclusions

We have proposed a cross-layer video optimization framework that manages the network bandwidth to minimize the total distortion in video streams. The proposed framework utilizes a new online network effective airtime estimation algorithm. Moreover, we have developed a new and accurate model for characterizing the video data rate and distortion relationship as well as a new model for adapting the link-layer parameters. We have evaluated our framework by streaming real video frames over an OPNET-simulated wireless network.

The main results can be summarized as follows. (1) The proposed framework enhances substan-

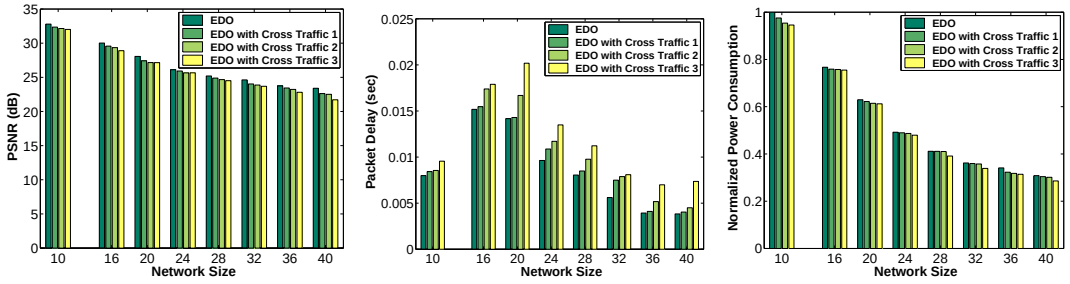

(a) Perceptual Video Quality (b) Packet Delay (c) Normalized Power Consumption

Figure 5.12: Impact of Cross traffic on EDO [Georgia Tech Image Set At 50% Resolution]

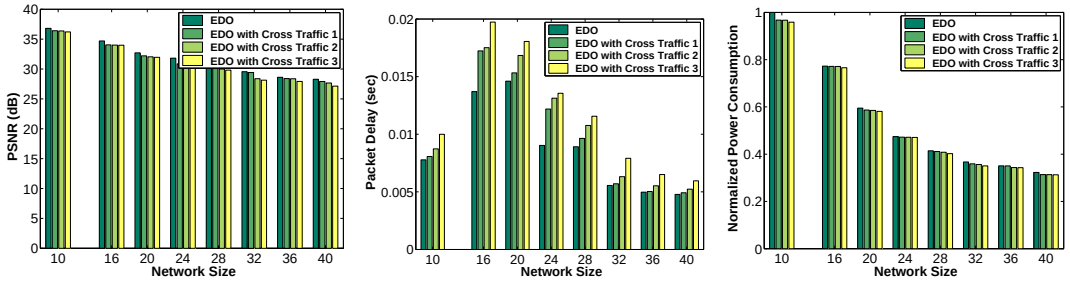

(a) Perceptual Video Quality (b) Packet Delay (c) Normalized Power Consumption

Figure 5.13: Impact of Cross traffic on EDO [FERET Image Set]

tially the perceptual quality of received video streams. (2) The proposed effective airtime estimation algorithm is accurate and converges quickly. (3) Optimal perceptual video quality is achieved when the packet dropping is very small. (4) The transmission opportunity adaptation model works effectively. (5) The proposed framework results in much less processing power consumption and the wireless interface power consumption, compared with existing solutions. This behavior is due to sending and dropping much less data. Power consumption is a primary concern, especially when the video sources are battery-powered. (6) The proposed framework is highly adaptable to the existence of any other interfering traffic in the network.

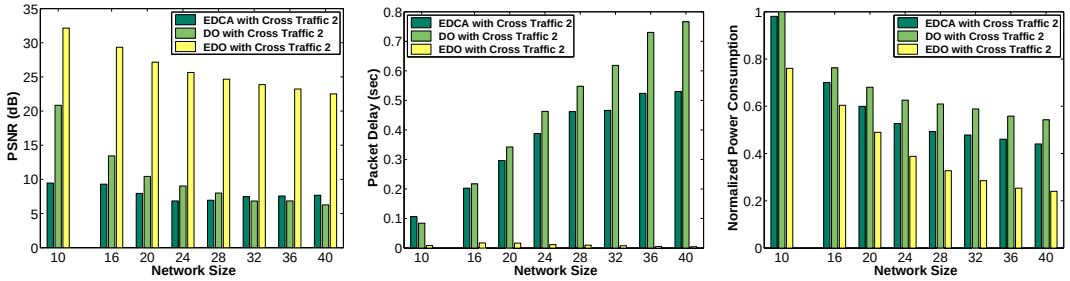

(a) Perceptual Video Quality (b) Packet Delay (c) Normalized Power Consumption

Figure 5.14: Comparing EDCA, DO, and EDO all with cross traffic 2 [Georgia Tech Image Set At 50% Resolution]

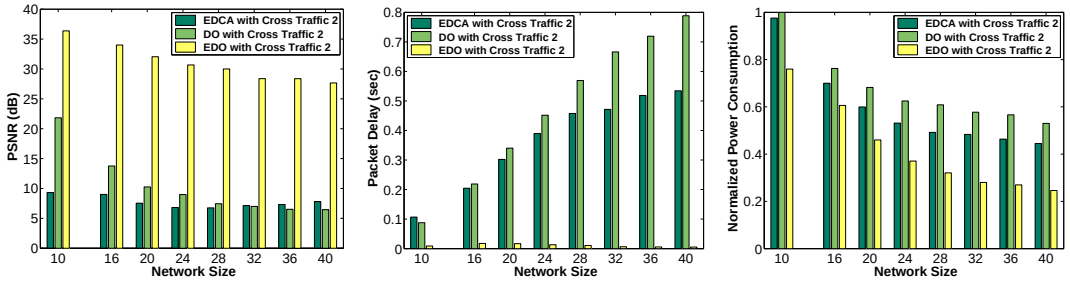

(a) Perceptual Video Quality (b) Packet Delay (c) Normalized Power Consumption

Figure 5.15: Comparing EDCA, DO, and EDO all with cross traffic 2 [FERET Image Set]

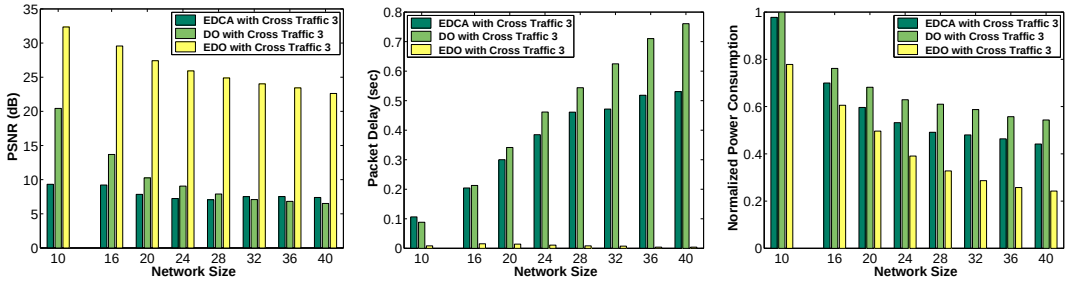

(a) Perceptual Video Quality (b) Packet Delay (c) Normalized Power Consumption

Figure 5.16: Comparing EDCA, DO, and EDO all with cross traffic 3 [Georgia Tech Image Set At 50% Resolution]

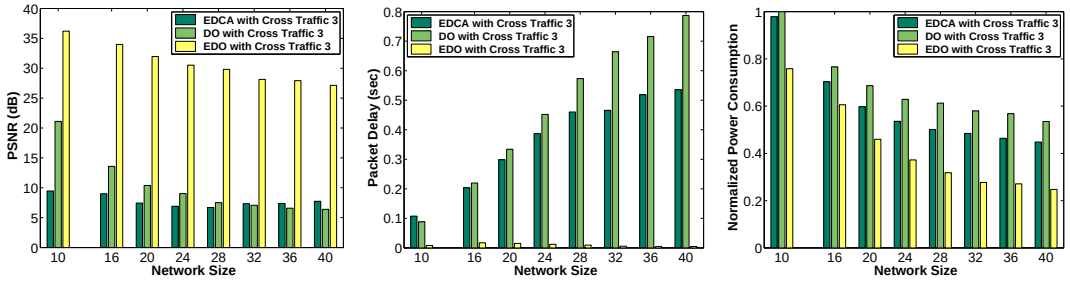

(a) Perceptual Video Quality (b) Packet Delay (c) Normalized Power Consumption

Figure 5.17: Comparing EDCA, DO, and EDO all with cross traffic 3 [FERET Image Set]

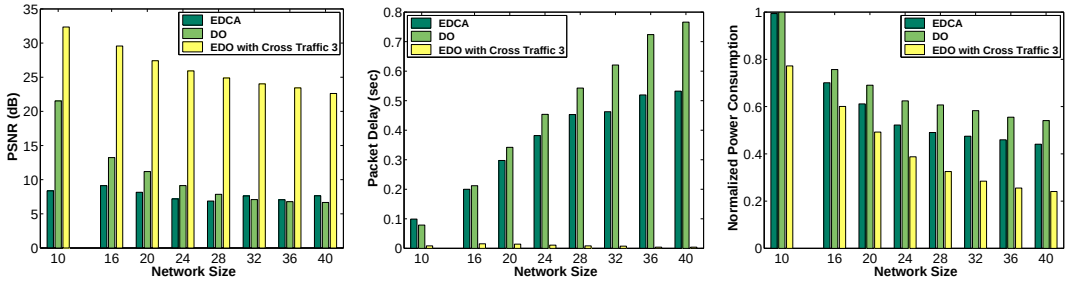

(a) Perceptual Video Quality (b) Packet Delay (c) Normalized Power Consumption

Figure 5.18: Comparing EDCA, DO, and EDO with cross traffic 3 [Georgia Tech Image Set At 50% Resolution]

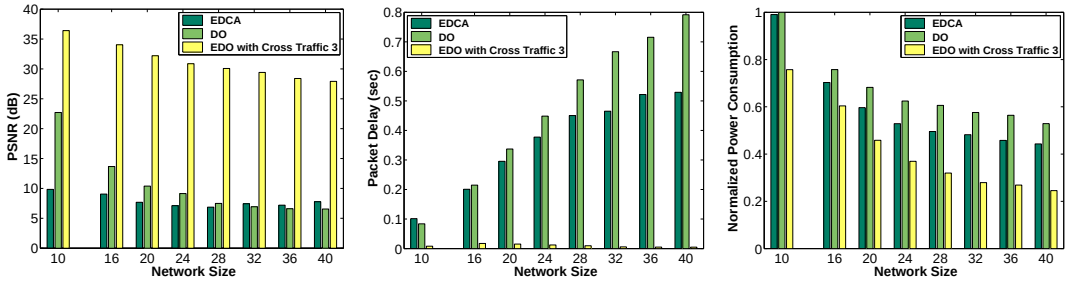

(a) Perceptual Video Quality (b) Packet Delay (c) Normalized Power Consumption

Figure 5.19: Comparing EDCA, DO, and EDO with cross traffic 3 [FERET Image Set]

CHAPTER 6

ACCURACY-BASED CROSS-LAYER OPTIMIZATION FOR AUTOMATED VIDEO SURVEILLANCE

6.1 Introduction

In this chapter, the main idea is to formulate the bandwidth allocation problem as a cross-layer optimization problem of the sum of the weighted event detection accuracy (or alternatively the sum of the weighted detection error), subject to the constraint in the total available bandwidth. The weights can be assigned based on many factors, including the potential threat level, placement of video sources, and location importance. Therefore, the weights represent the importance levels of various video sources at the current time. With this formulation, we show that the problem can be solved using Lagrangian relaxation techniques. The solution employs rate-accuracy curves (i.e. accuracy functions of the rate or bandwidth), which are best to be generated for each video source in its designated location. The proposed solution considers three layers: Application, Link, and Physical.

The main contributions of this part of the dissertation can be summarized as follows. (1) We propose a complete accuracy-based cross-layer optimization solution. Up to our knowledge, this is the first cross-layer solution that optimizes the detection accuracy in AVS systems. (2) The proposed solution utilizes a novel *Proportional Integral Differential* (PID) controller algorithm for estimating the effective airtime of the wireless medium. (3) We develop an accurate model that characterizes the relationship between the video data rate and the face detection accuracy error. (4) We propose a bandwidth pruning mechanism that can be used to achieve the desired power consumption and detection accuracy tradeoff.

We evaluate the proposed solution by streaming real MJPEG video frames (and not just an abstract bit stream) and MPEG-4 video streams over a simulated network. The simulations are conducted using OPNET. Since the sent video packets may be lost, we implement an error concealment algorithm [71] at the proxy station to mitigate the impact of packet loss on video quality. The results show that the

proposed framework enhances the accuracy of face detection applied on the received video streams and yields a significant power reduction and that the new proposed effective airtime estimation algorithm is accurate and converges quickly.

The rest of this chapter is organized as follows. Section 6.2 presents the proposed accuracy-based cross-layer optimization framework. Section 6.3 discusses the performance evaluation methodology. Finally, Section 6.4 presents and analyzes the main results.

6.2 Proposed Accuracy-Based Cross-Layer Optimization Framework

In this study, we consider an automated video surveillance (AVS) system, in which multiple video sources/stations (cameras and/or sensors) stream videos to a central station over a single-hop IEEE 802.11 WLAN network in the EDCA mode. The main two challenges in the considered system can be summarized as follows. (1) The wireless network has limited available bandwidth, which should be estimated accurately and distributed efficiently among various video sources to maximize the detection accuracy of the computer vision algorithm(s) running on the proxy station. (2) Providing differential bandwidth assignment to different sources is required because various sources in the network have different characteristics, including channel conditions, power constraints, and lighting conditions. In addition, different sources may have different importance levels. As shown in Figure 1.2, the system has $S \geq 1$ video sources and each source s streams a different encoded video at rate R_s. Each video source s may have a different physical rate (y_s) and importance level or weight (ω_s). The weight represents the importance level of a video source at the current time and depends on many factors, including the potential threat level, placement of video sources, and location importance. In this study, we assume that the weights are already predetermined.

The ultimate objective of this study is to provide an optimal solution that dynamically distributes and allocates the available network bandwidth among various video sources. This solution should consider all system, video, network, and environmental aspects, which may change dynamically. Therefore, the

proposed cross-layer optimization solution utilizes and dynamically controls parameters in three layers in the network stack: Application, Link, and Physical.

6.2.1 Optimization Problem Formulation

We formulate the problem as a cross-layer optimization problem of the summation of the weighted detection accuracy error of the computer vision algorithm running at the central proxy station. As in Chapter 5 and [44], since all video sources share the same medium, the bandwidth allocation solution should determine the fraction of airtime that each video source receives in the system. Obviously, the total airtime cannot exceed the effective airtime of the medium. Specifically, the problem is formulated as: find the optimal fraction of the airtime allocation $F^* = \{f_s^* | s = 1, 2, 3, ..., S\}$ for various video sources that minimizes the summation of the weighted detection accuracy error. ($\sum_{s=1}^{S} w_s * accuracyError_s(r_s)$), where w_s is the importance factor of video source s, r_s is the application layer transfer rate for video source s, and S is the number of video sources. This optimization is subject to the following constraints. (1) The total airtime of all video sources is less than the effective airtime of the medium (A_{eff}). (2) The application layer transfer rate of source s is the product of the its airtime (f_s) and the physical layer transfer rate (y_s) for video source s. (3) The airtime of each source is between 0 and 1 (inclusive).

Mathematically, the problem can be stated as follows:

$$Find \quad F^* = \arg\min_{F} \sum_{s=1}^{S} w_s * accuracyError_s(r_s) \tag{6.1a}$$

$$s.t. \quad \sum_{s=1}^{S} f_s = A_{eff} \tag{6.1b}$$

$$r_s = f_s \times y_s \tag{6.1c}$$

$$0 \leq f_s \leq 1 \tag{6.1d}$$

$$s = 1, 2, 3, ..., S, \tag{6.1e}$$

where F^* is the set of optimal fractions (f_s^*) of the airtime of all sources, r_s^* is the optimal application-layer rate of video source s, y_s is the physical-layer rate of video source s, and A_{eff} is the total effective airtime.

To solve the problem formulated in Equation (6.1), we need to characterize the accuracy error function and assess the effective airtime of the network.

6.2.2 Rate-Accuracy Characterization

We seek to find a model of the relationship between the playback rate of a video and the accuracy error of a computer vision algorithm applied to the video. To keep the study focused, we analyze only the face detection algorithm. Experimenting with other computer vision algorithms is left for another study. We use the Viola-Jones algorithm for face detection as implemented in OpenCV. In this study, we characterize the rate-accuracy relationship of two video compression standards: MJPEG and MPEG-4.

MJPEG Rate-Accuracy Characterization

We determine the MJPEG size-accuracy error relationship based on the following image datasets: CMU/MIT [72], Georgia Tech [73], and SCFace [75]. We use these image sets in our experiments to assemble the MJPEG video streams using the streamer discussed in Section 6.3 to load the network with video traffic. For fair evaluations of bandwidth allocation solutions, each video source should be able to stream the video at a bitrate that matches that of the optimization solution. The Georgia Tech image set produces a highly limited range of bitrates for the studied network. To produce a better variety, we generate two image sets from the original Georgia Tech image set by changing the resolution of each image in the set to 30% and 50% of the original resolution, respectively. The new image sets have resolutions of 192×144 and 320×240, respectively. Using these sets, the video sources can achieve the rates produced by the optimization more accurately. In SCFace, the images are taken by three cameras at three different distances from the subjects. Effectively, the cameras capture different resolutions of

the subjects. We refer to these image sets in decreasing order of the distance as *SCFace at Distance 1*, *SCFace at Distance 2*, and *SCFace at Distance 3*.

For each image set, we use the IJG JPEG library to compress each picture in the set with quality factors from 1 to 100, with 1 being the lowest, and then apply the computer vision algorithm on each image to calculate the accuracy using a predefined ground truth about the location of the faces in the image. We use two metrics for the detection accuracy: *positive index* and *negative index*. The positive index is determined as x/y, assuming the image contains y faces and the algorithm detects x faces correctly. In contrast, the negative index is determined as z/y, where z faces are detected but do not exist in the image. We can then find the average size, the average positive index, and the average negative index of all images with the same quality factor and then the accuracy error can be calculated as the sum of the total error: $accuracyError = (1 - positiveIndex) + negativeIndex$. The results are shown in Figure 6.1. By curve fitting the results, we determine that the accuracy error can be characterized as follows:

$$accuracyError = a \times Z^b + c, \tag{6.2}$$

where Z is the image size and a,b, and c are constants. This model is referred to as "Model" in Figure 6.1. For MJPEG videos, image size Z can be calculated as $Z = R/\tau$, where R is the video playback rate and τ is the video frame rate.

MPEG-4 Rate-Accuracy Characterization

We use the *YUV Video Sequences* from [80] to characterize the MPEG-4 Rate-Accuracy relationship. In particular, we use the video sequences Akiyo, Carphone, Claire, Foreman, Grandma, Miss America, Mother and Daughter, News, Salesman, Silent, and Suzie for QCIF resolution characterization and we use Foreman, Mother and Daughter, News, and Silent video sequences for CIF resolution characterization. We started by generating a ground truth for the position of the faces in each frame

of each video sequence. After that, we use *FFmpeg* library and the option *-qscale* to compress each video with quality scales from 2 to 31, with 2 being the highest quality, and then apply the computer vision algorithm on each video frame to calculate the accuracy using the ground truth that we generated initially. We use two metrics for the detection accuracy: *positive index* and *negative index*. The positive index is determined as x/y, assuming the video contains y faces and the algorithm detects x faces correctly. In contrast, the negative index is determined as z/y, where z faces are detected but do not exist in the video. We can then find the average frame size per video sequence and then we can find the average frame size, the average positive index, and the average negative index of all videos with the same quality factor and resolution and then the accuracy error can be calculated as the sum of the total error: $accuracyError = (1 - positiveIndex) + negativeIndex$.

For comparative purposes, we also perform rate-distortion characterization on the MPEG-4 sequences. We followed the same approach as with rate-accuracy characterization. We assess the distortion of each video frame against the uncompressed video frame using the Root Mean Square Error (RMSE) metric. The video distortion can then be calculated as the average frame distortion of all the frames in the video.

The results are shown in Figure 6.2. By curve fitting the results, we determine that the MPEG-4 accuracy error and distortion can be characterized using the following model:

$$Model = a \times Z^b + c, \tag{6.3}$$

where Z is the average video frame size and a,b, and c are constants. For any MPEG-4 videos, average frame size Z can be calculated as $Z = R/\tau$, where R is the video playback rate and τ is the video frame rate. This model is referred to as “Model” in Figure 6.2.

6.2.3 Effective Airtime Estimation

As finding an accurate value for the effective airtime of the medium is necessary for solving the formulated optimization problem, we propose a new online and dynamic effective airtime estimation algorithm for wireless networks in infrastructure configuration. In contrast with existing analytical models, the online approach uses complete information about the network and involves the cooperation of the access point and all video sources as well as various layers in each source. To yield an accurate estimation, the proposed approach computes the effective airtime when the packet loss in the network is below a specified threshold.

The proposed algorithm is based on the approach that we proposed in Chapter 5 but uses a *Proportional Integral Differential* (PID) controller for adjusting the currently estimated value of the effective airtime in order to achieve a faster, more stable, and more accurate estimation. As depicted in Figure 6.3, the PID controller adjusts the current effective airtime value based on the history and the rate of change of the error. The error depends on the dropping rate in the network. The PID controller has three components: *proportional*, *integral*, and *differential*. These components are weighted by constants K_P, K_I and K_D, respectively. The proportional component changes the effective airtime based on the immediate value of the error. The integral component considers the past values of the error, whereas the differential component anticipates the future, and thus they help reduce the steady state error and the overshoot, respectively.

As shown in Figure 6.4, the new estimation algorithm proceeds as follows. First, for each video source s, it finds the throughput (t_s) of its video stream as received by the application layer of the proxy station, when all sources stream videos, each at a rate that is equal to the maximum physical rate of the network divided by the number of sources [77]. The algorithm then uses these throughput values to determine the initial value of the effective airtime (A_{eff}) as follows: $A_{eff} = \sum_{s=1}^{S} t_s/y_s$. Our experiments indicate that this initial value significantly overestimates the effective airtime, causing the

actual received video rates to not conform to the cross-layer optimization solution because of the high level of packet dropping in the network. Thus, this value has to be adjusted based on the experienced level of packet dropping. Subsequently, during a period of time, called estimation period, each video source s assesses its own data dropping rate (d_s) while sending its video stream, and then sends this information to the access point (AP). Meanwhile, the AP determines the overall average dropping ratio as follows: $A_\Delta = \sum_{s=1}^{S} d_s/y_s$. The PID error is than calculated as $A_{thresh} - A_\Delta$ and A_{eff} is adjusted by the PID controller to eliminate the error as illustrated in Figure 6.3.

We use the following well-established procedure in control theory to tune the three PID parameters. (1) Set K_I and K_D to zeros and increase K_P until the output oscillates, and then set K_P to half of that value. (2) Increase K_I until any offset is corrected in adequate time. (3) Increase K_D until the reference can be reached quickly after load disturbance.

6.2.4 Optimization Solution

Now that we have an accuracy error function (which is the same for both MJPEG and MPEG-4) and a value for the effective airtime, we can solve the problem formulated in Equation (6.1). The problem solution can be summarized as follows:

Step 1: We first prove that the formulated problem is a convex programming problem by determining that all constraints ((6.1b)-(6.1e)) in the problem are linear and thus convex and that the optimization function $\sum_{s=1}^{S}(w_s(a_s(f_s y_s/\tau)^{b_s} + c_s))$ is also convex. The latter is valid since the derivative of the sum term is monotonically non-decreasing and convex.

Step 2: Since the problem is a budget constrained convex programming problem, it can be solved using the Lagrangian relaxation technique [78]. Thus, we can write the following Lagrangian-relaxed formula:

$$L(F^*, \lambda) = \sum_{s=1}^{S}(w_s(a_s(f_s y_s/\tau_s)^{b_s} + c_s)) + \lambda(\sum_{s=1}^{S} f_s - A_{eff}), \tag{6.4}$$

where $0 \leq f_s \leq 1$, and $s = 1, 2, 3, ..., S$. Next, the Lagrangian conditions are formulated as follows:

$$\frac{\partial L}{\partial f_s} = 0 \text{ and } \frac{\partial L}{\partial \lambda} = 0. \tag{6.5}$$

Assuming that all video sources have the same b_s, which is empirically valid, solving these two equations yields the following solution:

$$f_s^* = \left(\frac{-\lambda^* \tau_s}{w_s a_s b_s y_s (y_s/\tau_s)^{(b_s-1)}}\right)^{(1/(b_s-1))}, \tag{6.6}$$

where

$$\lambda^* = \left(\frac{A_{eff}}{\sum_{s=1}^{S} \left(\frac{-\tau_s}{w_S a_s b_s y_s (y_s/\tau_s)^{(b_s-1)}}\right)^{(1/(b_s-1))}}\right)^{(b_s-1)}. \tag{6.7}$$

6.2.5 The Allocation Algorithm

With the aforementioned solution, the access point (AP) determines λ^* and sends it to all video sources in the network using the beacon packet. When a video source s receives λ^*, it determines its fraction of the airtime f_s^* and it changes the application data rate, which is the video encoding rate in this case, according to the equation: $r_s^* = f_s^* \times y_s$. Finally, the link-layer parameters are determined based on the allocated airtime for each source. The link-layer parameters can either be the transmission opportunity duration limit (TXOP limit) or alternatively the frequency of the transmission opportunity. The control of the TXOP limit is more preferred since it is only one parameter, whereas the transmission frequency involves three parameters (AIFS, CW_{min}, and CW_{max}), which complicates the control process design. We used the model proposed in Chapter 5 to determine the TXOP limit.

6.2.6 Proposed Bandwidth Pruning Mechanism

As discussed earlier, with the optimization solution, each video source can determine its sending application rate. The results in Figure 6.1 suggest that the detection accuracy increases only slightly with the video rate (application rate) after a certain point. (That point varies based on the system, network, and environmental conditions.) Therefore, we propose a *bandwidth pruning* mechanism to achieve any desired tradeoff between the detection accuracy and power consumption. With this mechanism, each video source adjusts (reduces) its application rate if the anticipated loss in the detection accuracy is below a certain threshold. The threshold can be simply a fixed percentage or a function of the remaining battery energy in the video source and its importance. The pruning mechanism is of significant importance, especially when the sources are battery operated.

In this study, we experiment with 4 levels of bandwidth pruning: 95%, 90%, 80%, and 70%. Each level specifies the percentage of the original accuracy that will be achieved after the pruning mechanism is applied. Level 95%, for example, means that the achieved detection accuracy for each video source after pruning will be 95% of that produced by the optimization solution. In other words, a 5% reduction in the accuracy will be experienced by each source. Obviously, with higher reductions in the bandwidth, greater savings in power consumption will be achieved.

6.3 Performance Evaluation Methodology

We use OPNET to evaluate the effectiveness of the proposed optimization solution, including the effective airtime estimation algorithm and the bandwidth pruning mechanism.

We use two types of video traffic in our evaluation: MJPEG and MPEG-4. For MJPEG, we use the video streamer described in Section 5.3. In the case of MPEG-4, we implemented a video streamer that takes a video playback rate and a frame rate and produces raw video packets to simulate a video stream. We experimented with QCIF as well as CIF video resolutions.

We also used similar experiment setups as in Section 5.3 and Table 6.1 summarizes the main simulation parameters.

Table 6.1: Summary of Simulation Parameters

Parameter	**Model/Value(s)**
Number of video sources	4-68
Simulation Time	10 min
Packet Size	1024 bytes
Application Rate	Optimized, Default = Max Physical Rate / No. of Sources
Video Frame Rate	20 frames/sec
Physical characteristics	Extended Rate (802.11g)
Physical Data Rate	Random from {12Mb/s, 18Mb/s, 24Mb/s, 36Mb/s, 48Mb/s, 54Mb/s}
Weight	One of five levels between [0 1] chosen randomly
Buffer size	256 Kb
Video TXOP limit	Optimized, Default = 3008μs
Video CW_{min}	15
Video CW_{max}	31
Video AIFS	2
Short Retry Limit	7
Long Retry Limit	4
Beacon Interval	0.02 second
State Report Interval	1 second

We compare the proposed accuracy-based optimization solution, referred to in the results as *Weighted Accuracy Optimization* (WAO), with the following two solutions.

- The cross-layer solution in Chapter 5, called *Enhanced Distortion Optimization* (EDO).
- A new version of EDO that uses weights for various video sources, which is referred to here as *Weighted Distortion Optimization* (WDO).

We analyze the following *performance metrics*.

- *Weighted Accuracy* - It is the sum of the weighted detection accuracy of each video source. The accuracy for each source is found as the average accuracy of the received frames sent by that source. The accuracy of a dropped video frame is assumed to be 0.
- *Overall Network Load* - It is defined as the total load sent by the application layers of all video sources.
- *Power Consumption* - It is the average power consumption of the wireless interfaces of the video

sources and is determined by using the power consumption model in [79].

6.4 Result Presentation and Analysis

Using the aforementioned manual tuning method and extensive experimentation, we observe that the best values for the PID parameters depend on the workload and the desired value of A_{thresh}. Table 6.2 summarizes these results.

Table 6.2: Summary of PID Parameter Tuning

Workload	A_{thresh}	K_P	K_I	K_D
Georgia Tech at 30% Resolution	0.001	1	0.25	0.25
Georgia Tech at 30% Resolution	0.005	1.5	0.25	0.25
Georgia Tech at 50% Resolution	0.001	0.5	0.25	0.25
Georgia Tech at 50% Resolution	0.005	1.5	0.25	0.25
CMU/MIT	0.005	0.5	0.25	0.25
MPEG-4 QCIF Resolution	0.005	1.5	0.25	0.25
MPEG-4 CIF Resolution	0.005	1.5	0.25	0.25

6.4.1 Effectiveness of the Proposed Effective Airtime Estimation

Let us start by showing the effectiveness of the proposed effective airtime estimation algorithm utilizing the PID controller in terms of convergence time and stability. Figure 6.5 shows the output effective airtime values over time for Georgia Tech at 30% and 50% of the original resolution. The results demonstrate that the PID estimator is fast to converge to a stable state and has very small overshooting and undershooting.

Figure 6.6 shows the average effective airtime versus the number of video sources for the three bandwidth allocation solutions. These results show that the effective airtime increases with the network size up to a point and then starts to decrease. The peak happens when the proper balance between node contention and network utilization is reached. The peak point in the figure is when the network size is 16, but this value varies with the total sending rate of the sources. In particular, the peak should happen at a smaller network size if the sources are more demanding for bandwidth and at a larger network size if the sources are less demanding. Note that the three solution yield close airtimes, especially for larger

networks.

Let us now discuss the impact of A_{thresh}, which determines the allowable packet dropping in the network, on the weighted accuracy metric and power consumption. Figure 6.7 shows the results of running the proposed WAO solution for two different network sizes. The results demonstrate that the weighted accuracy metric improves with A_{thresh} up to a point and then starts to worsen. The peak happens when A_{thresh} is smaller than 0.01, suggesting that that optimal accuracy is achieved when the dropping is very small. As expected, the power consumption increases with A_{thresh} because the sending rate increases with A_{thresh}. Therefore, A_{thresh} should be selected based on the proper tradeoff between accuracy and power consumption. According to the figure, the value that causes the peak in accuracy could be chosen.

6.4.2 Effectiveness of the Proposed Bandwidth Allocation Solution

Figures 6.8 and 6.9 compare the performance of various solutions (EDO, WAO, WDO) for A_{thresh} values of 0.001 and 0.005, respectively, when using Georgia Tech dataset at 30% resolution. Figure 6.10 shows the same results when A_{thresh} is equal to 0.005 and for Georgia Tech at 50% resolution. Furthermore, Figure 6.11 shows the results for CMU/MIT dataset and $A_{thresh} = 0.005$. Moreover, Figures 6.12 and 6.13 show the same results for MPEG-4 QCIF and CIF resolutions respectively when $A_{thresh} = 0.005$.

These results show that the proposed accuracy-based optimization solution (WAO) outperforms other solutions in all metrics. In particular, it improves both the weighted accuracy and power consumption by up to 10%. The improvement in power consumption is due to reducing the application rates (network loads) of various video sources. In addition, the results indicate that incorporating weights for various video sources with the distortion-based optimization has no noticeable improvement. On the contrary, it may worsen the weighted accuracy in some cases. By carefully analyzing these results, we noticed that applying these weights in WDO forces the video sources with low importance factors to send the video

streams at extremely low bitrates, and in some cases, it prevents these sources from sending any video, leading to an unacceptable levels of accuracy for these sources.

6.4.3 Effectiveness of the Proposed Bandwidth Pruning Mechanism

Figures 6.14-6.16 show the effectiveness of the bandwidth pruning mechanism in terms of weighted accuracy, overall network load, and power consumption for various image datasets and values of A_{thresh}. Furthermore, Figure 6.17 shows the same results for MPEG-4 CIF resolution when $A_{thresh} = 0.005$. Not all combinations are shown since the shown results are representative of the overall behavior. The results demonstrate that the effectiveness of pruning when the WAO solution is used. Four levels of pruning are analyzed: 95%, 90%, 80%, and 70%, with each level specifying the percentage of the original accuracy that will be achieved after the pruning mechanism is applied. The result shows that the pruning mechanism significantly reduces the overall network load and power consumption with much less reduction in the weighted detection accuracy. For example, with 95% pruning, we can save up to 45% in power consumption by scarifying only 5% in the accuracy.

Finally, let us discuss the effectiveness of the proposed WAO solution with the pruning mechanism, compared with the other two solutions (EDO and WDO). Figures 6.18 and 6.19 compare EDO, WDO, and WAO to WAO with 95% pruning in terms of weighted accuracy, overall network load, and power consumption for A_{thresh} of 0.005 and two different datasets. (The results for other datasets and values of A_{thresh} exhibit similar behavior.) The results demonstrate that while the WAO solution with 95% pruning achieves almost the same values of weighted accuracy as EDO and WDO, it yields up to 45% saving in power consumption and network load.

6.5 Conclusions

We have proposed an accuracy-based cross-layer video optimization framework for automated video surveillance systems that manages the network bandwidth to minimize the sum of the weighted detec-

tion accuracy in video streams. The proposed framework utilizes an enhanced effective airtime estimation algorithm utilizing a *Proportional Integral Differential* (PID) controller. Moreover, we have proposed a bandwidth pruning mechanism to achieve any desired tradeoff between detection accuracy and power consumption. Furthermore, we have developed an accurate model for characterizing the rate-accuracy relationship. We have evaluated our framework by streaming real video frames over an OPNET-simulated wireless network.

The main results can be summarized as follows. (1) The proposed framework significantly enhances both the detection accuracy and power consumption, compared to the distortion-based optimization. The reduction in power consumption is due to sending and dropping much less data. (2) The proposed PID-based effective airtime estimation algorithm is accurate, converges quickly, and more stable than the one proposed in Chapter 5. (3) With a 95% pruning level, the proposed bandwidth allocation solution achieves almost the same accuracy as the distortion-based optimization but reduces power consumption by up to 45%.

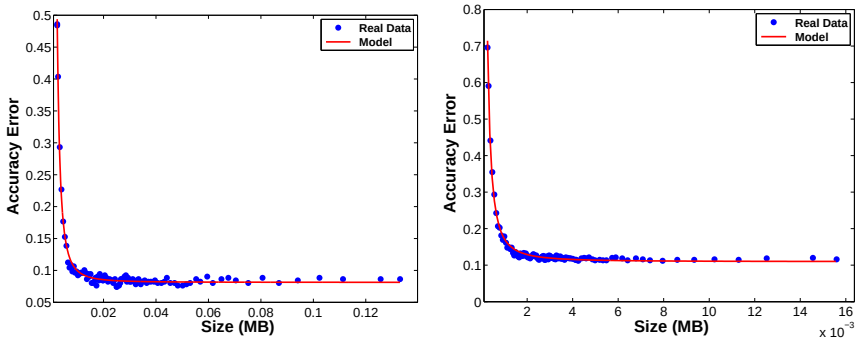

(a) CMU/MIT (b) Georgia Tech at 30% Resolution

(c) Georgia Tech at 50% Resolution (d) SCFace at Distance 1

(e) SCFace at Distance 2 (f) SCFace at Distance 3

Figure 6.1: MJPEG Rate-Accuracy Characterization

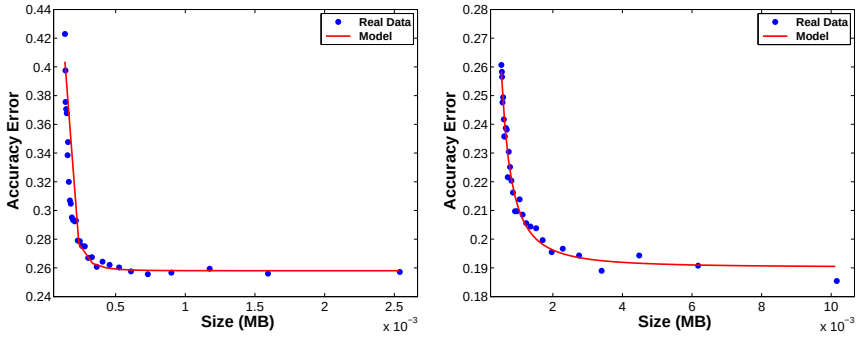

(a) Size-Accuracy, QCIF

(b) Size-Accuracy, CIF

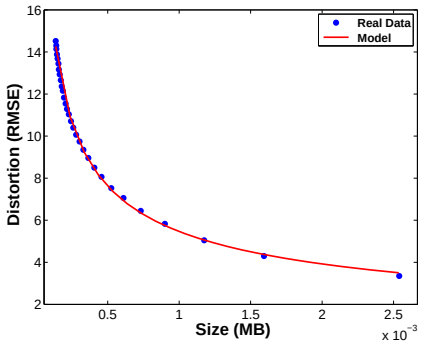

(c) Size-Distortion, QCIF

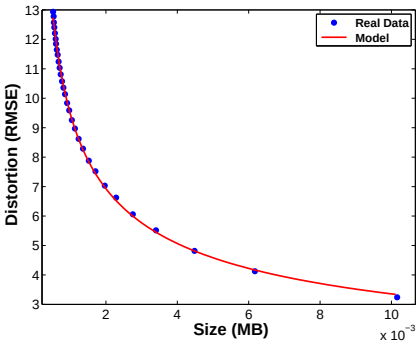

(d) Size-Distortion, CIF

Figure 6.2: MPEG-4 Rate-Accuracy and Rate-Distortion Characterization

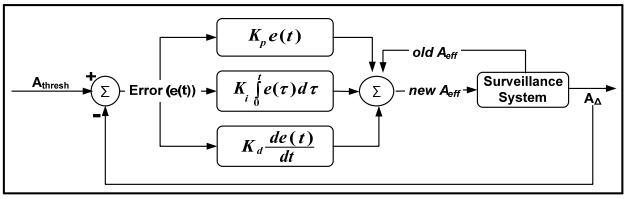

Figure 6.3: Simplified PID Controller for Effective Airtime Estimation

while initialization period is not expired
Force each source to send in a rate equals to the maximum physical rate divided by the number of sources;
Update t_s value for each source.
$A_{eff} = \sum_{s=1}^{S} t_s / y_s$;
At the end of each estimation period{
$A_\Delta = \sum_{s=1}^{S} d_s / y_s$;
BeforeLastError=LastError;
LastError=error;
error = $A_{thresh} - A_\Delta$;
$A_{eff} = A_{eff} + K_P \times error - K_I \times LastError + K_D \times BeforeLastError$;
}

Figure 6.4: Simplified PID Algorithm for Dynamically Estimating the Effective Airtime

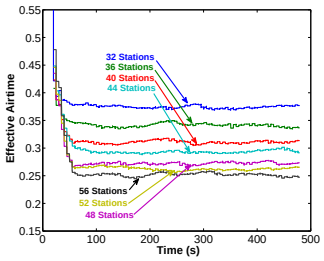

(a) Georgia Tech at 30% Resolution, $A_{thresh} = 0.005$

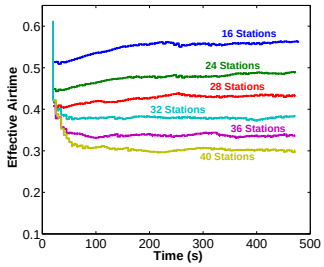

(b) Georgia Tech at 50% Resolution, $A_{thresh} = 0.005$

Figure 6.5: Effectiveness of Proposed PID-Based Estimation

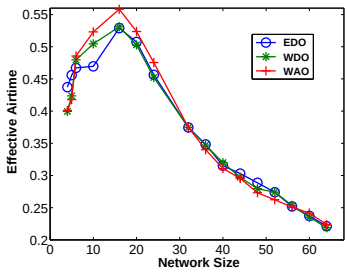

Figure 6.6: Comparing Various Bandwidth Allocation Solutions in Effective Airtime [Georgia Tech at 30% Resolution, $A_{thresh} = 0.005$]

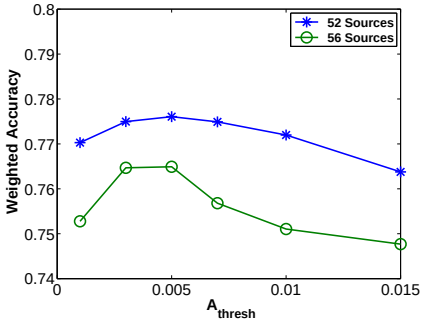

(a) Weighted Accuracy

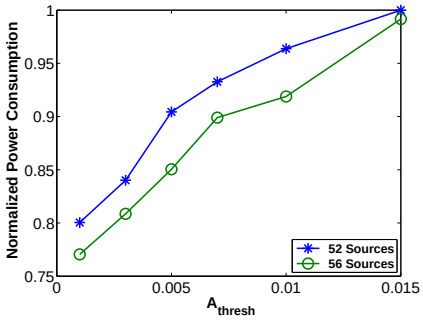

(b) Power Consumption

Figure 6.7: Impact of A_{thresh} with Proposed Weighted Accuracy Optimization [Georgia Tech at 30% Resolution]

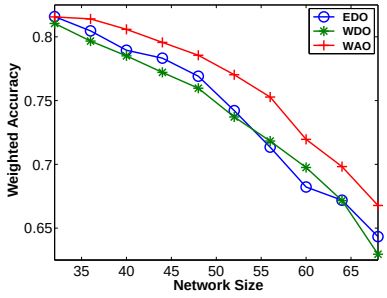

(a) Weighted Accuracy

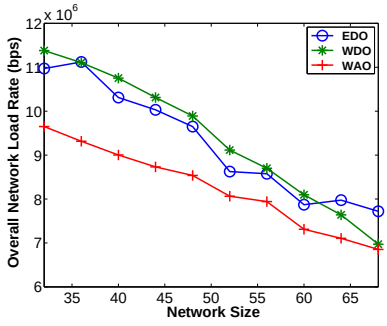

(b) Overall Network Load

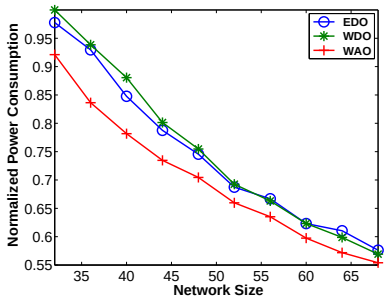

(c) Power Consumption

Figure 6.8: Comparing the Effectiveness of Various Bandwidth Allocation Solutions [Georgia Tech at 30% Resolution, $A_{thresh} = 0.001$]

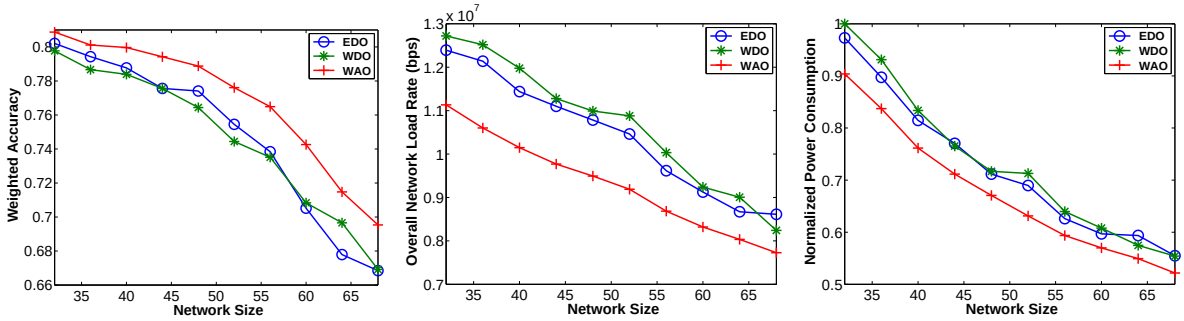

(a) Weighted Accuracy (b) Overall Network Load (c) Power Consumption

Figure 6.9: Comparing the Effectiveness of Various Bandwidth Allocation Solutions [Georgia Tech at 30% Resolution, $A_{thresh} = 0.005$]

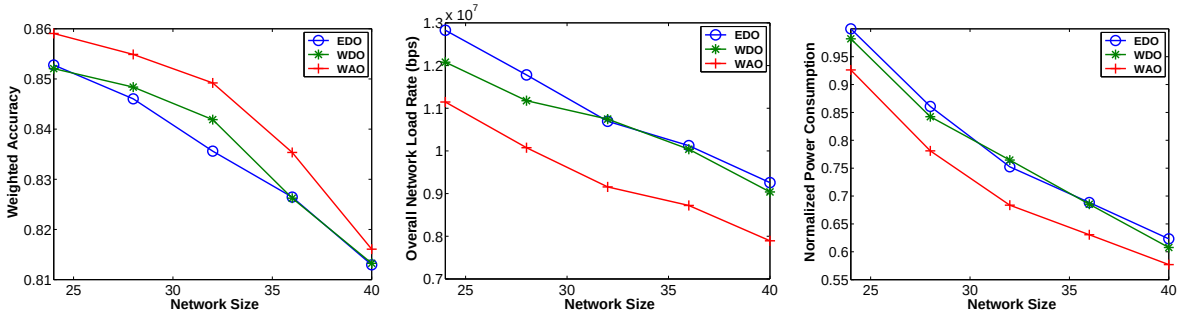

(a) Weighted Accuracy (b) Overall Network Load (c) Power Consumption

Figure 6.10: Comparing the Effectiveness of Various Bandwidth Allocation Solutions [Georgia Tech at 50% Resolution $A_{thresh} = 0.001$]

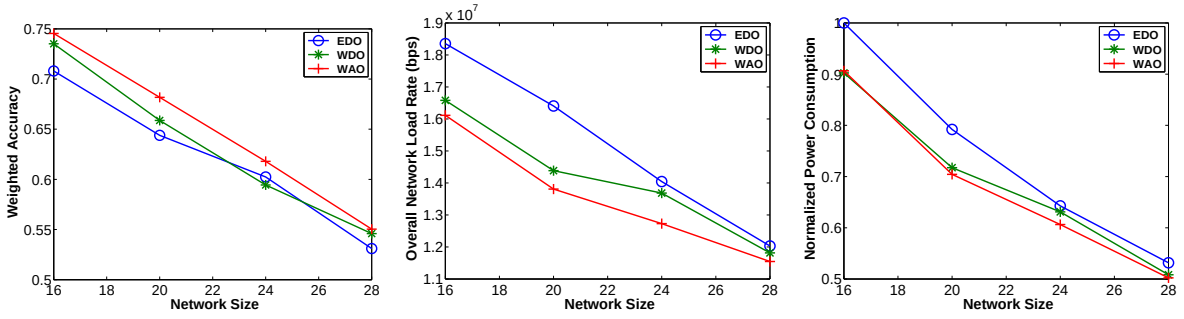

(a) Weighted Accuracy (b) Overall Network Load (c) Power Consumption

Figure 6.11: Comparing the Effectiveness of Various Bandwidth Allocation Solutions [CMU/MIT, $A_{thresh} = 0.005$]

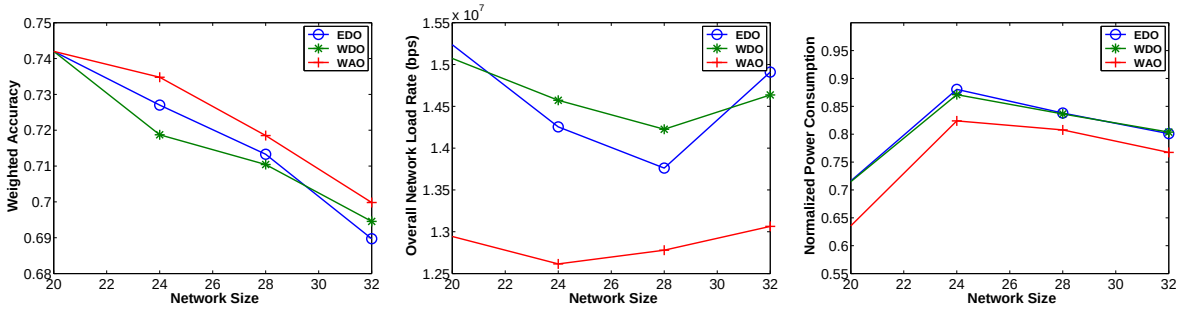

(a) Weighted Accuracy (b) Overall Network Load (c) Power Consumption

Figure 6.12: Comparing the Effectiveness of Various Bandwidth Allocation Solutions [MPEG-4 QCIF Resolution, $A_{thresh} = 0.005$]

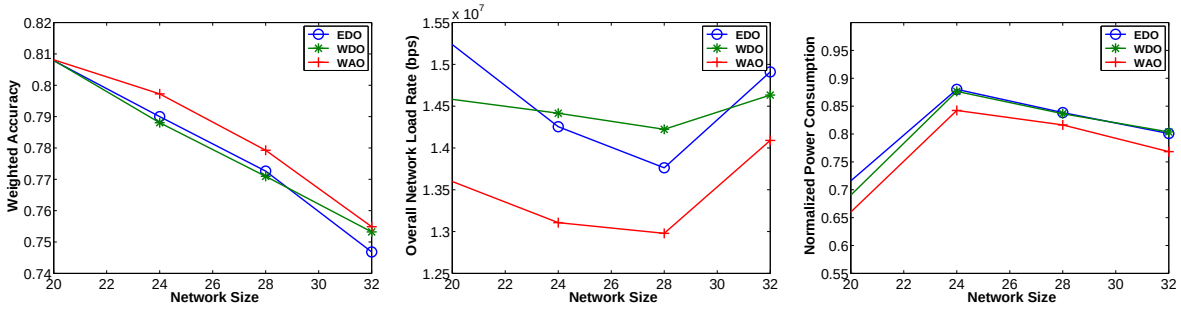

(a) Weighted Accuracy (b) Overall Network Load (c) Power Consumption

Figure 6.13: Comparing the Effectiveness of Various Bandwidth Allocation Solutions [MPEG-4 CIF Resolution, $A_{thresh} = 0.005$]

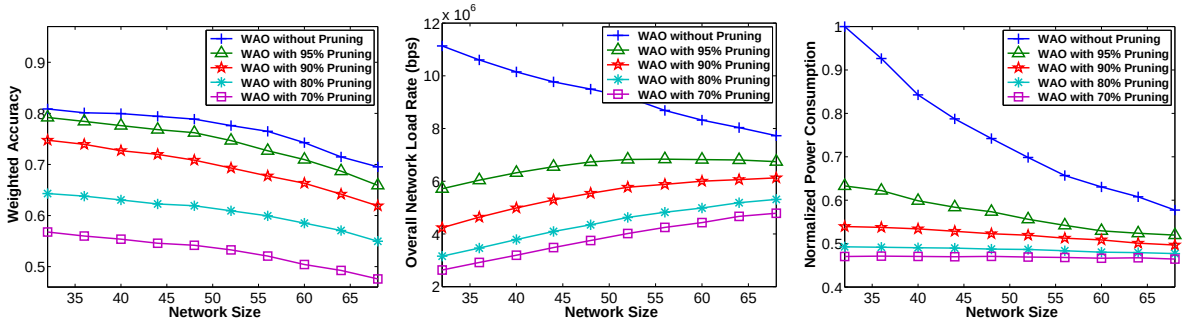

(a) Weighted Accuracy (b) Overall Network Load (c) Power Consumption

Figure 6.14: Effectiveness of Bandwidth Pruning Mechanism [WAO Solution, Georgia Tech at 30% Resolution, $A_{thresh} = 0.005$]

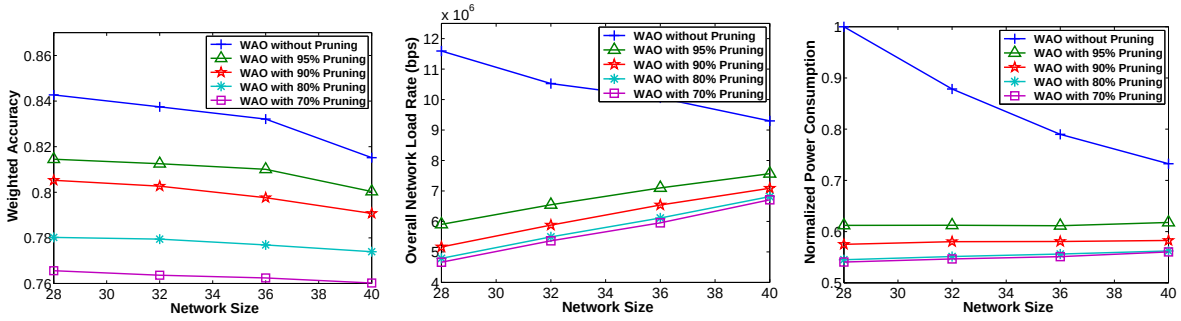

(a) Weighted Accuracy (b) Overall Network Load (c) Power Consumption

Figure 6.15: Effectiveness of Bandwidth Pruning Mechanism [WAO Solution, Georgia Tech at 50% Resolution, $A_{thresh} = 0.005$]

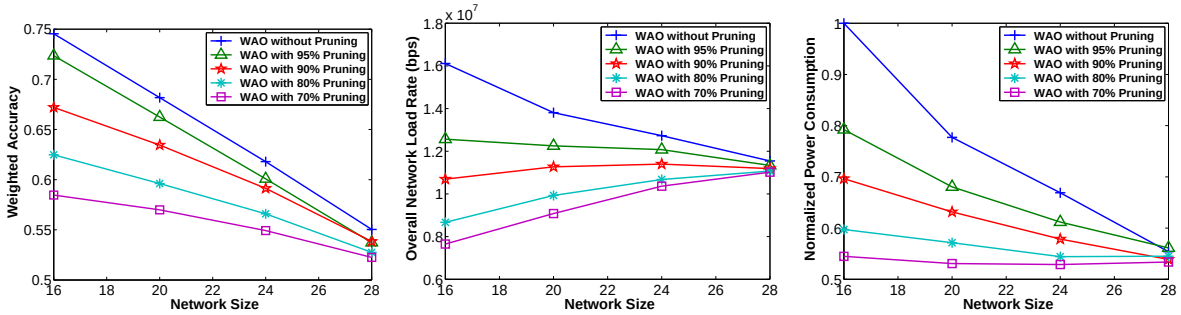

(a) Weighted Accuracy (b) Overall Network Load (c) Power Consumption

Figure 6.16: Effectiveness of Bandwidth Pruning Mechanism [WAO Solution, CMU/MIT, $A_{thresh} = 0.005$]

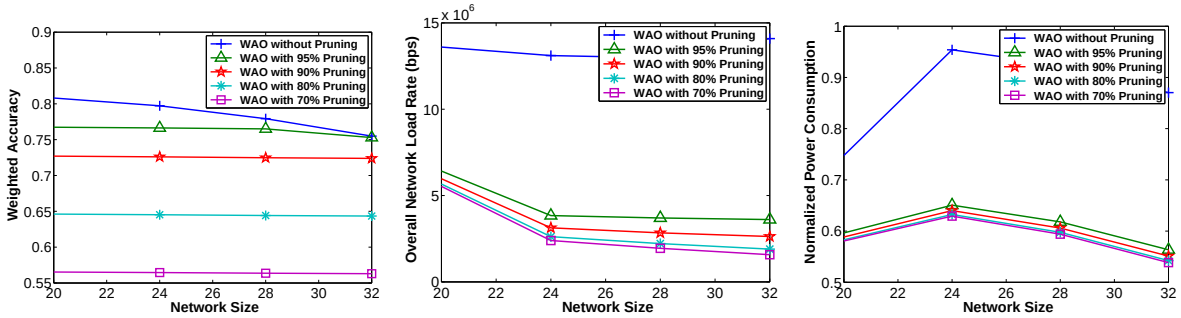

(a) Weighted Accuracy (b) Overall Network Load (c) Power Consumption

Figure 6.17: Effectiveness of Bandwidth Pruning Mechanism [WAO Solution, MPEG-4 CIF Resolution, $A_{thresh} = 0.005$]

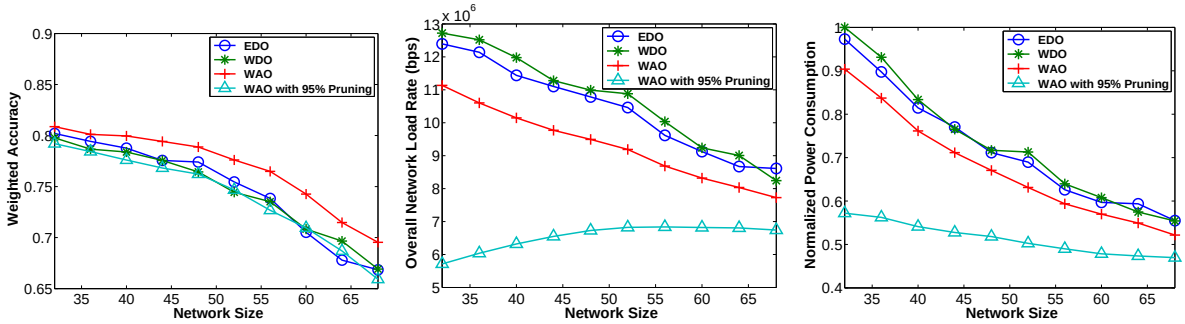

(a) Weighted Accuracy (b) Overall Network Load (c) Power Consumption

Figure 6.18: Effectiveness of the Proposed WAO Solution with the Pruning Mechanism [Georgia Tech at 30% Resolution, $A_{thresh} = 0.005$]

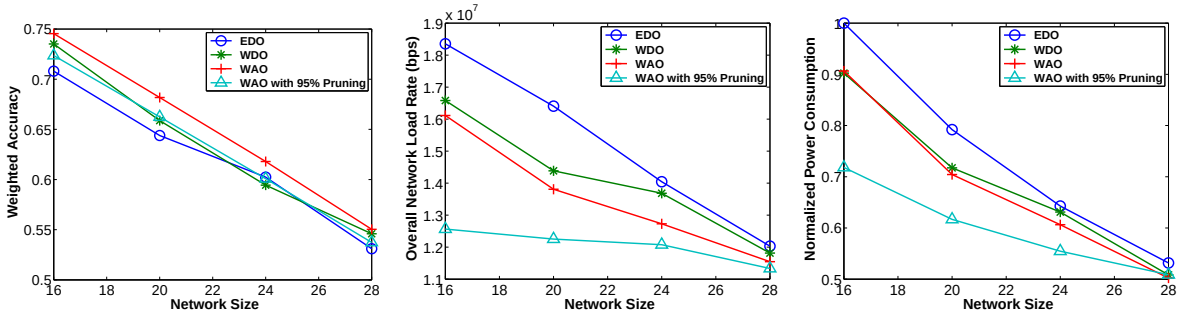

(a) Weighted Accuracy (b) Overall Network Load (c) Power Consumption

Figure 6.19: Effectiveness of the Proposed WAO Solution with the Pruning Mechanism [CMU/MIT, $A_{thresh} = 0.005$]

CHAPTER 7

SUMMARY AND FUTURE WORK

7.1 Summary

7.1.1 Waiting-time Predictability

We have analyzed the waiting-time predictability in scalable video streaming and have presented two prediction schemes: *Assign Expected Stream Completion Time* (AEC) and *Hybrid Prediction*. AEC utilizes detailed information about the server state and considers the applied scheduling policy to predict the future scheduling decisions over a certain period, called *prediction window*. This window introduces a tradeoff between the prediction accuracy and the number of users receiving expected waiting times. The hybrid scheme uses AEC and then assigns the average video waiting time for those requests that did not obtain a predicted time by AEC.

We have analyzed the effectiveness of the two prediction schemes when applied with various stream merging techniques and scheduling policies. We have also compared the effectiveness of the waiting-time prediction approach with the approach that provides time-of-service guarantees. The latter is represented by an extended policy, called *Generalized Next Schedule Time First* (GNSTF). In addition, we have studied the impacts of prediction window, server capacity, user's waiting tolerance, arrival rate, skew in video access, video length, and number of videos.

The main results can be summarized as follows.

- The waiting time can be predicted accurately, especially with AEC and when MCF-P is used. MCF-P is not only highly predictable (in terms of user waiting time) but also achieves the best performance in server throughput and average waiting time.
- In contrast with AEC, the hybrid prediction scheme provides expected times to each user but achieves lower accuracy and a longer confidence interval.

- Combining AEC or the hybrid scheme with MCF-P leads to outstanding performance benefits, compared with GNSTF.
- This combination, called *Predictive MCF-P*, can be applied with hierarchical stream merging techniques (such as ERMT) to improve performance further, whereas GNSTF cannot.

7.1.2 Scheduling

We have analyzed in detail cost-based scheduling for on-demand video streaming and proposed new strategies: *Predictive Cost-Based Scheduling* (PCS) and *Adaptive Regular Stream Triggering* (ART).

The main results can be summarized as follows.

- There is no clear advantage of computing the cost over a future time window, compared with computing the cost only at the next scheduling time.
- The proposed PCS scheduling policy outperforms the best existing policy (MCF-P) in terms of customer defection probability and average waiting time. The waiting times can also be predicted more accurately with PCS. The two variations of PCS (PCS-V and PCS-L) perform nearly the same and thus the simpler variant (PCS-V) is preferred because of its lower implementation complexity.
- By enhancing stream merging behavior, the proposed ART technique substantially improves both the customer defection probability and the average waiting time.
- The best overall performer is “MCF-P combined with ART”, followed by PCS. With ART, significantly more clients can receive expected waiting times for service than PCS, but at a somewhat lower waiting time accuracy.

7.1.3 Distortion-based Dynamic Bandwidth Allocation

We have proposed a cross-layer video optimization framework that manages the network bandwidth to minimize the total distortion in video streams. The proposed framework utilizes a new online network effective airtime estimation algorithm. Moreover, we have developed a new and accurate model for

characterizing the video data rate and distortion relationship as well as a new model for adapting the link-layer parameters. We have evaluated our framework by streaming real video frames over an OPNET-simulated wireless network.

The main results can be summarized as follows.

- The proposed framework enhances substantially the perceptual quality of received video streams.
- The proposed effective airtime estimation algorithm is accurate and converges quickly.
- Optimal perceptual video quality is achieved when the packet dropping is very small.
- The transmission opportunity adaptation model works effectively.
- The proposed framework results in much less power consumption, compared with existing solutions. This behavior is due to sending and dropping much less data. Power consumption is a primary concern, especially when the video sources are battery-powered.
- The proposed framework is highly adaptable to any interfering traffic in the network.

7.1.4 Accuracy-based Dynamic Bandwidth Allocation

We have proposed an accuracy-based cross-layer video optimization framework for automated video surveillance systems that manages the network bandwidth to minimize the sum of the weighted detection accuracy in video streams. The proposed framework utilizes an enhanced effective airtime estimation algorithm utilizing a *Proportional Integral Differential* (PID) controller. Moreover, we have proposed a bandwidth pruning mechanism to achieve any desired tradeoff between detection accuracy and power consumption. Furthermore, we have developed an accurate model for characterizing the rate-accuracy relationship. We have evaluated our framework by streaming real video frames over an OPNET-simulated wireless network.

The main results can be summarized as follows.

- The proposed framework significantly enhances both the detection accuracy and power consump-

tion, compared to the distortion-based optimization. The reduction in power consumption is due to sending and dropping much less data.

- The PID-based effective airtime estimation algorithm is accurate and more stable than the one proposed in Chapter 5.
- With pruning, the proposed bandwidth allocation solution achieves almost the same accuracy as the distortion-based optimization but reduces power consumption significantly.

7.2 Future Work

In future work, we plan to study the cross-layer framework with more computer vision algorithms, such as face recognition and object tracking. We also plan to study the framework with different video adaptation techniques, including resolution-based adaptation. Furthermore, we plan to perform study with different networks, such as WiMAX.

BIBLIOGRAPHY

[1] "Alexa The Web Information Company," http://www.alexa.com/topsites.

[2] Brandon C Welsh and David P Farrington, "Evidence-based crime prevention: The effectiveness of cctv," *Crime Prevention and Community Safety An International Journal*, vol. 6, no. 2, pp. 21–33, 2004.

[3] "CCTV Image 42: How many cameras are there in the UK?," http://www.securitynewsdesk.com/wp-content/uploads/2011/03/CCTV-Image-42-How-many-cameras-are-there-in-the-UK.pdf.

[4] "Chicago's video surveillance cameras: A pervasive and unregulated threat to our privacy," 2011, http://heartland.org/policy-documents/chicagos-video-surveillance-cameras-pervasive-and-unregulated-threat-our-privacy.

[5] Isaac Wang, "China video surveillance revenue to reach $9.5 billion by 2014," 2011, http://www.isuppli.com/China-Electronics-Supply-Chain/MarketWatch/Pages/China-Video-Surveillance-Revenue-to-Reach-$95-Billion-by-2014.aspx.

[6] Kien A. Hua, Ying Cai, and Simon Sheu, "Patching: A multicast technique for true Video-on-Demand services," in *Proc. of ACM Multimedia*, 1998, pp. 191–200.

[7] Ying Cai and Kien A. Hua, "An efficient bandwidth-sharing technique for true video on demand systems," in *Proc. of ACM Multimedia*, Oct. 1999, pp. 211–214.

[8] D. L. Eager, M. K. Vernon, and J. Zahorjan, "Optimal and efficient merging schedules for Video-on-Demand servers," in *Proc. of ACM Multimedia*, Oct. 1999, pp. 199–202.

[9] Marcus Rocha, Marcelo Maia, Italo Cunha, Jussara Almeida, and Sergio Campos, "Scalable media streaming to interactive users," in *Proc. of ACM Multimedia*, Nov. 2005, pp. 966–975.

[10] Huadong Ma, G. Kang Shin, and Weibiao Wu, "Best-effort patching for multicast true VoD service," *Multimedia Tools Appl.*, vol. 26, no. 1, pp. 101–122, 2005.

[11] Bashar Qudah and Nabil J. Sarhan, "Towards scalable delivery of video streams to heterogeneous receivers," in *Proc. of ACM Multimedia*, Oct. 2006, pp. 347–356.

[12] Musab Al-Hadrusi and Nabil J. Sarhan, "A scalable delivery framework and a pricing model for streaming media with advertisements," in *Proc. of SPIE/ACM Multimedia Computing and Networking Conference (MMCN)*, Januray 2008.

[13] K. A. Hua and S. Sheu, "Skyscraper broadcasting: A new broadcasting scheme for metropolitan Video-on-Demand system," in *Proc. of ACM SIGCOMM*, Sept. 1997, pp. 89–100.

[14] L. Juhn and L. Tseng, "Harmonic broadcasting for Video-on-Demand service," *IEEE Trans. on Broadcasting*, vol. 43, no. 3, pp. 268–271, Sept. 1997.

[15] J.-F. Pâris, S. W. Carter, and D. D. E. Long, "Efficient broadcasting protocols for video on demand," in *Proc. of the Int'l Symp. on Modeling, Analysis and Simulation of Computer and Telecommunication Systems (MASCOTS)*, July 1998, pp. 127–132.

[16] Cheng Huang, Ramaprabhu Janakiraman, and Lihao Xu, "Loss-resilient on-demand media streaming using priority encoding," in *Proc. of ACM Multimedia*, Oct. 2004, pp. 152–159.

[17] Liqi Shi, Phillipa Sessini, Anirban Mahanti, Zongpeng Li, and Derek L. Eager, "Scalable streaming for heterogeneous clients," in *Proc. of ACM Multimedia*, Oct. 2006, pp. 337–346.

[18] S. W. Carter and D. D. E. Long, "Improving Video-on-Demand server efficiency through stream tapping," in *the International Conference on Computer Communication and Networks (ICCCN)*, Sept. 1997, pp. 200–207.

[19] Y. Cai and Kien A. Hua, "Sharing multicast videos using patching streams," *Multimedia Tools and Applications journal*, vol. 21, no. 2, pp. 125–146, Nov. 2003.

[20] Y. Cai, W. Tavanapong, and Kien A. Hua, "Enhancing patching performance through double patching," in *Proc. of 9th Intl Conf. on Distributed Multimedia Systems*, Sept. 2003, pp. 72–77.

[21] D. L. Eager, M. K. Vernon, and J. Zahorjan, "Bandwidth skimming: A technique for cost-effective Video-on-Demand," in *Proc. of Multimedia Computing and Networking Conf. (MMCN)*, Jan. 2000, pp. 206–215.

[22] Nabil J. Sarhan and Bashar Qudah, "Efficient cost-based scheduling for scalable media streaming," in *Proc. of Multimedia Computing and Networking Conf. (MMCN)*, January 2007.

[23] Robert Collins, Alan Lipton, Takeo Kanade, Hironobu Fujiyoshi, David Duggins, Yanghai Tsin, David Tolliver, Nobuyoshi Enomoto, and Osamu Hasegawa, "A system for video surveillance and monitoring," Tech. Rep. CMU-RI-TR-00-12, Robotics Institute, Carnegie Mellon University, Pittsburgh, PA, May 2000.

[24] Omar Javed and Mubarak Shah, "Tracking and object classification for automated surveillance," in *Proceedings of the 7th European Conference on Computer Vision-Part IV*, 2002, pp. 343–357.

[25] Xiaojing Yuan, Zehang Sun, Yaakov Varol, and George Bebis, "A distributed visual surveillance system," in *Proceedings of the IEEE Conference on Advanced Video and Signal Based Surveillance (AVSS)*, 2003, p. 199.

[26] Lun Zhang, Stan Z. Li, Xiaotong Yuan, and Shiming Xiang, "Real-time object classification in video surveillance based on appearance learning," in *CVPR*, 2007.

[27] Artur oza, Lyudmila Mihaylova, David Bull, and Nishan Canagarajah, "Structural similarity-based object tracking in multimodality surveillance videos," *Mach. Vision Appl.*, vol. 20, no. 2, pp. 71–83, Jan. 2009.

[28] Yangqing Jia and Changshui Zhang, "Front-view vehicle detection by markov chain monte carlo method," *Pattern Recognition*, vol. 42, no. 3, pp. 313–321, 2009.

[29] Lubomir Bourdev, Subhransu Maji, and Jitendra Malik, "Describing people: Poselet-based attribute classification," in *International Conference on Computer Vision (ICCV)*, 2011.

[30] V. Nair and J. Clark, "Automated visual surveillance using hidden markov models," in *Proceedings of the 15th International Conference on Vision Interface (VI)*, May 2002, pp. 88–92.

[31] W. Niu and J. Long, "Human activity detection and recognition for video surveillance," in *Proceedings of the IEEE Multimedia and Expo Conference (ICME)*, June 2004, pp. 719–722.

[32] Yiğithan Dedeoğlu, B. Uğur Töreyin, Uğur Güdükbay, and A. Enis Çetin, "Silhouette-based method for object classification and human action recognition in video," in *Proceedings of the 2006 international conference on Computer Vision in Human-Computer Interaction*, Berlin, Heidelberg, 2006, ECCV'06, pp. 64–77, Springer-Verlag.

[33] Rajat Singh, Sarvesh Vishwakarma, Anupam Agrawal, and M. D. Tiwari, "Unusual activity detection for video surveillance," in *Proceedings of the First International Conference on Intelligent Interactive Technologies and Multimedia*, New York, NY, USA, 2010, IITM '10, pp. 297–305, ACM.

[34] Juan Carlos Niebles, Chih-Wei Chen, , and Li Fei-Fei, "Modeling temporal structure of decomposable motion segments for activity classification," in *Proceedings of the 12th European Conference of Computer Vision (ECCV)*, Crete, Greece, September 2010.

[35] L. Fei-Fei and L.-J. Li, "What, Where and Who? Telling the Story of an Image by Activity Classification, Scene Recognition and Object Categorization," *Studies in Computational Intelligence-Computer Vision*, pp. 157–171, 2010.

[36] Wu-Chi Feng, Ed Kaiser, Wu Chang Feng, and Mikael Le Baillif, "Panoptes: scalable low-power video sensor networking technologies," *ACM Trans. Multimedia Comput. Commun. Appl.*, vol. 1, no. 2, pp. 151–167, 2005.

[37] Xiaoan Lu, Elza Erkip, Yao Wang, and David Goodman, "Power efficient multimedia communication over wireless channels," *IEEE Journal on Selected Areas in Communications*, vol. 21, pp. 1738–1751, 2003.

[38] Zhihai He and Dapeng Wu, "Resource allocation and performance analysis of wireless video sensors," *IEEE Transactions on Circuits and Systems for Video Technology*, vol. 16, pp. 590–599, 2006.

[39] Y. Andreopoulos, N. Mastronarde, and M. van der Schaar, "Cross-Layer Optimized Video Streaming Over Wireless Multihop Mesh Networks," *Selected Areas in Communications, IEEE Journal on*, vol. 24, no. 11, pp. 2104–2115, 2006.

[40] S. Khan, J. Brehmer, W. Kellerer, W. Utschick, and E. Steinbach, "Application-driven cross-layer optimization for video streaming over wireless networks," *IEEE Communications Magazine*, vol. 44, pp. 122–130, 2006.

[41] Honghai Zhang, Yanyan Zheng, Mohammad Ali Khojastepour, and Sampath Rangarajan, "Cross-layer optimization for streaming scalable video over fading wireless networks," *IEEE Journal on Selected Areas in Communications*, vol. 28, no. 3, pp. 344–353, 2010.

[42] Mihaela van der Schaar, Yiannis Andreopoulos, and Zhiping Hu, "Optimized scalable video streaming over ieee 802.11a/e hcca wireless networks under delay constraints," *IEEE Transactions on Mobile Computing*, vol. 5, pp. 755–768, June 2006.

[43] Jian wei Huang, Zhu Li, Mung Chiang, and Aggelos K. Katsaggelos, "Pricing-based rate control and joint packet scheduling for multi-user wireless uplink video streaming," in *Proc. 15th International Packet Video Workshop (PV2006)*, 2006.

[44] Cheng-Hsin Hsu and Mohamed Hefeeda, "A framework for cross-layer optimization of video streaming in wireless networks," 2011.

[45] Pavel Korshunov and Wei Tsang Ooi, "Critical video quality for distributed automated video surveillance," in *Proceedings of the 13th annual ACM international conference on Multimedia*, 2005, pp. 151–160.

[46] Pavel Korshunov, "Rate-accuracy tradeoff in automated, distributed video surveillance systems," in *Proceedings of the 14th annual ACM international conference on Multimedia*, 2006, pp. 887–889.

[47] Pavel Korshunov and Wei Tsang Ooi, "Video quality for face detection, recognition, and tracking," *ACM Trans. Multimedia Comput. Commun. Appl.*, vol. 7, no. 3, pp. 14:1–14:21, Sept. 2011.

[48] D. L. Eager, M. K. Vernon, and J. Zahorjan, "Minimizing bandwidth requirements for on-demand data delivery," *IEEE Trans. on Knowledge and Data Engineering*, vol. 13, no. 5, pp. 742–757, Sept. 2001.

[49] A. Bar-Noy, G. Goshi, R.E. Ladner, and K. Tam, "Comparison of stream merging algorithms for Media-on-Demand," *Multimedia Systems Journal*, vol. 9, pp. 211–223, 2004.

[50] A. Dan, D. Sitaram, and P. Shahabuddin, "Scheduling policies for an on-demand video server with batching," in *Proc. of ACM Multimedia*, Oct. 1994, pp. 391–398.

[51] C. C. Aggarwal, J. L. Wolf, and P. S. Yu, "The maximum factor queue length batching scheme for Video-on-Demand systems," *IEEE Trans. on Computers*, vol. 50, no. 2, pp. 97–110, Feb. 2001.

[52] Nabil J. Sarhan and Chita R. Das, "A new class of scheduling policies for providing time of service guarantees in Video-On-Demand servers," in *Proc. of the 7th IFIP/IEEE Int'l Conf. on Management of Multimedia Networks and Services*, Oct. 2004, pp. 127–139.

[53] N.S. Shankar and M. van der Schaar, "Performance analysis of video transmission over ieee 802.11a/e wlans," *IEEE Transactions on Vehicular Technology*, vol. 56, no. 4, pp. 2346 –2362, july 2007.

[54] Ye Ge, Jennifer C. Hou, and Sunghyun Choi, "An analytic study of tuning systems parameters in ieee 802.11e enhanced distributed channel access," *Computer Networks*, vol. 51, no. 8, pp. 1955–1980, 2007.

[55] Chun-Ting Chou, S. N. Shankar, and Kang G. Shin, "Achieving per-stream qos with distributed airtime allocation and admission control in ieee 802.11e wireless lans," in *INFOCOM*, 2005, pp. 1584–1595.

[56] I. Pavlidis, V. Morellas, P. Tsiamyrtzis, and S. Harp, "Urban surveillance systems: From the laboratory to the commercial world," *IEEE Proceedings*, vol. 89, no. 10, pp. 1478–1497, October 2001.

[57] O. Javed, Z. Rasheed, O. Alatas, and M. Shah, "KNIGHT: A real-time surveillance system for multiple overlapping and non-overlapping cameras," in *Proceedings of IEEE International Conference on Multimedia and Expo (ICME)*, July 2003, pp. 649–652.

[58] R. Rangaswami, Z. Dimitrijevi, K. Kakligian, E. Chang, and Y. Wang, "The SfinX video surveillance system," in *Proceedings of the IEEE International Conference on Multimedia and Expo (ICME)*, June 2004.

[59] Jie Hui and M. Devetsikiotis, "A unified model for the performance analysis of IEEE 802.11e EDCA," *Communications, IEEE Transactions on*, vol. 53, no. 9, pp. 1498–1510, 2005.

[60] Lixiang Xiong and Guoqiang Mao, "Saturated throughput analysis of ieee 802.11e edca," *Computer Networks*, vol. 51, no. 11, pp. 3047–3068, 2007.

[61] Zhenyu Yang and Klara Nahrstedt, "A bandwidth management framework for wireless camera array," in *NOSSDAV*, 2005, pp. 147–152.

[62] Samarth H. Shah, Kai Chen, and Klara Nahrstedt, "Dynamic bandwidth management in single-hop ad hoc wireless networks," *MONET*, vol. 10, no. 1-2, pp. 199–217, 2005.

[63] Samarth H. Shah, Kai Chen, Klara Nahrstedt, and I. Introduction, "Available bandwidth estimation in ieee 802.11-based wireless networks," 2003.

[64] Cheikh Sarr, Claude Chaudet, Guillaume Chelius, and Isabelle Guerin Lassous, "Bandwidth estimation for ieee 802.11-based ad hoc networks," *IEEE Trans. Mob. Comput.*, vol. 7, no. 10, pp. 1228–1241, 2008.

[65] Nabil J. Sarhan and Chita R. Das, "A new class of scheduling policies for providing time of service guarantees in Video-On-Demand servers," in *Proc. of the 7th IFIP/IEEE Int'l Conf. on Management of Multimedia Networks and Services*, Oct. 2004, pp. 127–139.

[66] A. K. Tsiolis and M. K. Vernon., "Group-guaranteed channel capacity in multimedia storage servers.," in *Proc. of ACM SIGMETRICS*, June 1997, pp. 285–297.

[67] C. Costa, I. Cunha, A. Borges, C. Ramos, M. Rocha, J. Almeida, and B. Ribeiro-Neto, "Analyzing client interactivity in streaming media," in *Proc. of The World Wide Web Conf.*, May 2004, pp. 534–543.

[68] Cristiano Costa, Italo Cunha, Alex Borges, Claudiney Ramos, Marcus Rocha, Jussara Almeida, and Berthier Ribeiro-neto, "Analyzing client interactivity in streaming media," 2004.

[69] I. Ari, B. Hong, E. Miller, S. Brandt, and D. Long, "Managing flash crowds on the internet," in *Proc. of the 11th IEEE/ACM International Symposium on Modeling, Analysis, and Simulation of Computer and Telecommunication Systems (MASCOTS)*, Oct. 2003, pp. 246–249.

[70] Bashar Qudah and Nabil J. Sarhan, "Analysis of resource sharing and cache management techniques in scalable video-on-demand," in *Proc. of the 14th IEEE International Symposium on Modeling, Analysis, and Simulation of Computer and Telecommunication Systems (MASCOTS)*, Sept. 2006, pp. 327–334.

[71] Shahram Shirani, Faouzi Kossentini, Samir Kallel, and Rabab Ward, "Reconstruction of jpeg coded images in lossy packet networks," .

[72] "CMU/MIT image set," http://vasc.ri.cmu.edu/idb/html/face/frontal_images.

[73] "Georgia tech face database," http://www.anefian.com/research/face_reco.htm.

[74] P. Jonathon Phillips, Harry Wechsler, Jeffrey Huang, and Patrick J. Rauss, "The FERET database and evaluation procedure for face-recognition algorithms," *Image Vision Comput.*, vol. 16, no. 5, pp. 295–306, 1998.

[75] Mislav Grgic, Kresimir Delac, and Sonja Grgic, "Scface - surveillance cameras face database," *Multimedia Tools Appl.*, vol. 51, no. 3, pp. 863–879, 2011.

[76] Wenye Cheng, Xi Chen, and Zhihai He, "Doubling of the operational lifetime of portable video communication devices using power-rate-distortion analysis and control," in *ICIP*, 2006, pp. 2473–2476.

[77] Andrew Symington and Pieter S. Kritzinger, "A hardware test bed for measuring ieee 802.11g distribution coordination function performance," in *MASCOTS*, 2009, pp. 1–7.

[78] A Ortega and K Ramchandran, "Rate-distortion methods for image and video compression," *IEEE Signal Processing Magazine*, vol. 15, no. 6, pp. 23–50, 1998.

[79] Yousef Sharrab and Nabil J. Sarhan, "Aggregate power consumption modeling of live video streaming systems," in *ACM Multimedia Systems (MMSys 2013)*, Oslo, Norway, February 2013.

[80] "Yuv video sequences," http://trace.eas.asu.edu/yuv/index.html.

ABSTRACT

MAXIMIZING RESOURCE UTILIZATION IN VIDEO STREAMING SYSTEMS

by

MOHAMMAD ABDULLAH ALSMIRAT

May 2013

Advisor: Dr. Nabil Sarhan

Major: Computer Engineering

Degree: Doctor of Philosophy

Video streaming has recently grown dramatically in popularity over the Internet, Cable TV, and wireless networks. Because of the resource demanding nature of video streaming applications, maximizing resource utilization in any video streaming system is a key factor to increase the scalability and decrease the cost of the system. Resources to utilize include server bandwidth, network bandwidth, battery life in battery operated devices, and processing time in limited processing power devices. In this work, we propose new techniques to maximize the utilization of video-on-demand (VOD) server resources. In addition to that, we propose new framework to maximize the utilization of the network bandwidth in wireless video streaming systems.

Providing video streaming users in a VOD system with expected waiting times enhances their perceived quality-of-service (QoS) and encourages them to wait thereby increasing server utilization by increasing server throughput. In this work, we analyze waiting-time predictability in scalable video streaming. We also propose two prediction schemes and study their effectiveness when applied with various stream merging techniques and scheduling policies. The results demonstrate that the waiting time can be predicted accurately, especially when enhanced cost-based scheduling is applied. The combination of waiting-time prediction and cost-based scheduling leads to outstanding performance benefits. The achieved resource sharing by stream merging depends greatly on how the waiting requests are scheduled for service. Motivated by the development of cost-based scheduling, we investigate its effec-

tiveness in great detail and discuss opportunities for further tunings and enhancements. Additionally, we analyze the effectiveness of incorporating video prediction results into the scheduling decisions. We also study the interaction between scheduling policies and the stream merging techniques and explore new ways for enhancements.

The interest in video surveillance systems has grown dramatically during the last decade. Automated video surveillance (AVS) serves as an efficient approach for the realtime detection of threats and for monitoring their progress. Wireless networks in AVS systems have limited available bandwidth that have to be estimated accurately and distributed efficiently. In this research, we develop two cross-layer optimization frameworks that maximize the bandwidth optimization of 802.11 wireless network. We develop a distortion-based cross-layer optimization framework that manages bandwidth in the wireless network in such a way that minimizes the overall distortion. We also develop an accuracy-based cross-layer optimization framework in which the overall detection accuracy of the computer vision algorithm(s) running in the system is maximized. Both proposed frameworks manage the application rates and transmission opportunities of various video sources based on the dynamic network conditions to achieve their goals. Each framework utilizes a novel online approach for estimating the effective airtime of the network. Moreover, we propose a bandwidth pruning mechanism that can be used with the accuracy-based framework to achieve any desired tradeoff between detection accuracy and power consumption. We demonstrate the effectiveness of the proposed frameworks, including the effective airtime estimation algorithms and the bandwidth pruning mechanism, through extensive experiments using OPNET.

AUTOBIOGRAPHICAL STATEMENT

Mohammad Alsmirat received his Bachelor's degree in Computer Science in 2002 from Jordan University of Science and Technology and received his Master's degree in Computer Science from New York Institute of Technology in 2003. Mohammad joined the department of Electrical and Computer Engineering (ECE) at Wayne State University to pursue his PhD degree in Computer Engineering in January, 2007 and he is currently a PhD. candidate. He has previously worked as full time lecturer in the Computer Science department at Jordan University of Science and Technology from October, 2003 until December, 2006. In January, 2007, he started working as Graduate Research Assistant in the ECE department at Wayne State University and then he started to work as Graduate Teaching Assistant in the ECE department in August, 2007 until December 2012. Mohammad started to work at General Motors Research and Development center in January 2013 to do research in Vehicle to Vehicle Communication area.